Plate Based Fuel Processing System

Final Report
December 2005

Award Recipient: Catalytica Energy Systems, Inc.,
430 Ferguson Dr., Mountain View, CA 94043-5272

Award Number: DE-FC36-01AL67605
Project Period: October 1, 2001 to September 30, 2005

Project Cost:
Total: $10,002,747
DOE Share: $6,999,051
CESI Share: $3,003,696

Working Partners: None
Cost-Sharing Partners: None

Contact:
Principal Investigator: Ralph Dalla Betta
650-940-6310
RDallaBetta@CatalyticaEnergy.com

Contract Manager: Julie Messersmith
650-640-6322
JMessersmith@CatalyticaEnergy.com

Project Manager: David Yee
650-940-6321
DYee@CatalyticaEnergy.com

DOE Managers:
Program Manager: Donna Ho (202) 586-8000 Donna.Ho@EE.DOE.GOV
Field Project Officer: Reginald Tyler (303) 275-4929 reginald.tyler@go.doe.gov

ANL Technical Advisor:
Walt Podolski (630) 252-7558 Podolski@CMT.ANL.GOV

Subcontractors:

National Fuel Cell Research Center, Irvine, CA

Catalytica Energy Systems team members:

Carlos Faz
Helen Liu
Yafeng Liu
Tek Ho
Armando Jimenez
Jacques Nicole
Christopher Pickett
Valery Sokolovskii
Jeffrey Zalc

Executive Summary

Project Objective:
This project is focused on developing reactor designs and catalyst systems for the direct steam reforming of gasoline to PEM fuel cell quality hydrogen. Computer simulation models will be developed and used to predict and optimize reactor performance. 1 to 10 kW(e) scale prototypes will be built and tested to demonstrate that reactor performance meets DOE target specifications.

Background:
Current fuel processors are typically packed bed reactors. These fuel processors are not well suited for transportation applications because their high thermal mass would lead to long start-up times and slow transient response. In addition, the granular catalyst beads will likely abrade under the mechanical vibrations common in transportation applications.

Catalytica Energy Systems, Inc. (CESI) is addressing on-board fuel processor issues by designing a compact, low thermal mass plate reactor with rapid start-up and transient response capabilities. The plate-based reactor assembly process is illustrated in the figure below. In this steam reforming reactor illustration, each corrugated plate is coated with reforming catalyst on one side and combustion catalyst on the opposite side. Two plates are assembled together to form a single cell. When several cells are stacked together and assembled with the appropriate inlet and outlet manifolds, a plate-reactor is formed.

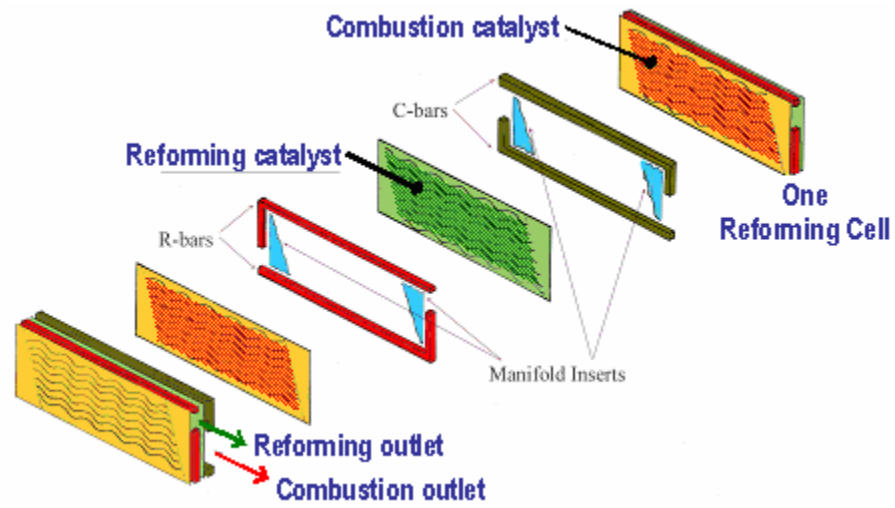

The separation of the reforming and combustion streams permits the reforming reaction to be conducted at a higher pressure than the combustion reaction, thereby avoiding costly gas compression for combustion. The separation of the two streams also prevents the dilution of the reformate stream by the combustion air.

The advantages of the plate reactor are not limited to steam reforming applications. In a WGS or PrOx reaction, the non-catalytic side of the plate would act as a heat exchanger to remove the heat generated by the exothermic WGS or PrOx reactions. This would maintain the catalyst under nearly isothermal conditions whereby the catalyst would operate at its optimal temperature.

Furthermore, the plate design approach results in a low pressure drop, rapid transient capable and attrition-resistant reactor. These qualities are valued in any application, be it on-board or stationary fuel processing, since they reduce parasitic losses, increase over-all system efficiency and help perpetuate catalyst durability.

Initial reactor design concepts were evaluated using thermal stress analysis and transient response modeling. Several mechanical designs were selected for prototype fabrication and testing.

In parallel to the prototype fabrication, CESI is developing the steam reforming, water gas shift and preferential oxidation catalysts. The catalysts are screened on specially designed coated-wall reactors that simulate the operating conditions found in a plate reactor. Catalyst development activities are focused on improving catalyst activity, selectivity and durability.

At the initiation of the program in 2001, CESI's goal was to design, fabricate and test a fully integrated 50 kW(e) plate-based gasoline fuel reforming system to demonstrate performance that meets or exceeds the DOE targets for on-board fuel reforming of PEM fuel cell powered vehicles. However, after the first program review with FreedomCAR, our goal was modified to design, fabricate and test the catalytic plate-based reactors (1 to 10 kW(e) scale) of a gasoline fuel reforming system to demonstrate performance that meets or exceeds the DOE targets for on-board fuel reforming for PEM fuel cell powered vehicles. Two years later, CESI's goal was changed yet again after the DOE's no-go decision for on-board fuel processing. The new goals were:

- To design, fabricate and test the catalytic steam reforming plate-based reactor (1 to 10 kW(e)) to demonstrate rapid start-up and transient performance advantages
- To demonstrate steam reforming, water-gas-shift and preferential oxidation catalyst durability through 1000 hour sub-scale testing

As we neared the contract expiration date, it became apparent that the sub-contracted vendors had underestimated the difficulties in fabricating and delivering the leak-free next generation steam reforming prototypes that were scheduled for testing. After reviewing the vendors' challenges and progress, CESI and DOE agreed that it was unlikely that the next generation prototypes could be fabricated and tested within the time and budget constraints of the contract. Therefore, it would be mutually beneficial to CESI and the DOE to forgo the next generation fabrication/testing and simply close-out the program within 90-days of the contract expiration date of September 30, 2005.

Accomplishments:
In this program, CESI took the initial steam reforming plate-reactor concept and advanced it towards an integrated fuel processing system. A substantial amount of modeling was performed to guide the catalyst development and prototype hardware design and fabrication efforts. The plate-reactor mechanical design was studied in detail to establish design guidelines which would help the plate reactor survive the stresses of repeated thermal cycles (from start-ups and shut-downs). Integrated system performance modeling was performed to predict system efficiencies and determine the parameters with the most significant impact on efficiency.

In conjunction with the modeling effort, a significant effort was directed towards catalyst development. CESI developed a highly active, sulfur tolerant, coke resistant, precious metal based reforming catalyst. CESI also developed its own non-precious metal based water-gas shift catalyst and demonstrated the catalyst's durability over several thousands of hours of testing. CESI also developed a unique preferential oxidation catalyst capable of reducing 1% CO to < 10 ppm CO over a 35°C operating window through a single pass plate-based reactor.

Finally, CESI combined the modeling results and steam reforming catalyst development efforts into prototype hardware. The first generation 3kW(e) prototype was fabricated from existing heat-exchanger plates to expedite the fabrication process. This prototype demonstrated steady state operation ranging from 5 to 100% load conditions. The prototype also demonstrated a 20:1 turndown ratio, 10:1 load transient operation and rapid start-up capability.

Table of Content

Status and Discussion

1. Reactor and System Modeling

In CESI's approach to research and development, modeling plays a key role. This section presents the various modeling efforts that have been initiated during this project. Three different areas are described here: the mechanical stress analysis of different plate reactor designs, the reactor design modeling and the fuel processor modeling.

1.1 Reactor Structural and Mechanical Design Modeling

The origin of the research proposal submitted to the DOE was the successful completion of a >400 h long methane steam reforming test using the original 1 kW(e) welded plate reactor. The original plate reactor (shown Figure 1.1.1) was built using 0.008" thick Fe-Cr-Al-Alloy and 3/32" thick 316 stainless steel frames. The frames form a channel between the flat foils and provide a manifold to flow reactants though the unit. The gap formed by the frame was filled with stainless steel (Type 316) spheres of 3/32" diameter, which also served as static mixers by inducing turbulence to the flow. Unfortunately, the frames and the spheres added an undesirable mass to the reactor and severely limited the reactor's thermal cycle durability. A series of stress analysis studies helped the team to design reactors that would be capable of maintaining mechanical durability through repeated thermal cycles.

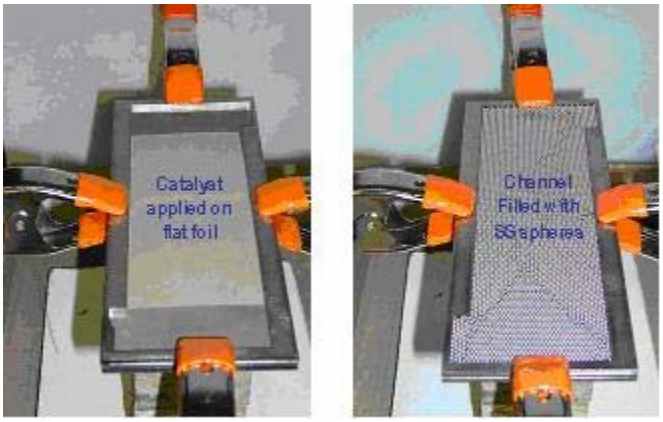

Figure 1.1.1. 1 kW(e) methane plate reformer.

As the primary application of the gasoline fuel processor was for on-board hydrogen generation, all the reactors of the processor system had to be built to sustain numerous and rapid heating-cooling cycles. It was estimated that a target life acceptable for the reactors was 250,000 thermal cycles. In order to obtain a reactor design capable to withstand the targeted cyclic life of 250,000 cycles, the local strain needed to be less than 0.25%.

To model the reactor's temperatures changes from room temperature to reforming temperature, a start-up cycle for the transient operation calculations was set as follows:

- 0-15 s Inlet gas temperature to reforming and combustion channels rises linearly from 20°C to 550°C.
- 15-75 s Temperature in combustion and reforming chambers is ramped from 550°C up to their peak values of 760°C. Combustion and reforming streams are ramped from 0% to 100% load values.
- 75 s Combustion and reforming streams flow rates are at steady sate.

A detailed finite element analysis (FEA) was conducted for four different designs of plate reactors, namely: flat plate, corrugated plate, circular-concave and race track designs. The first design, pictured in Figure 1.1.2 is simply a flat plate with frames, similar to the original methane reformer plate reactor design.

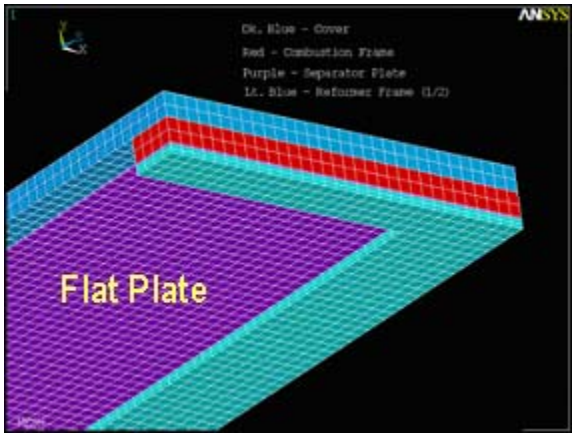

Figure 1.1.2. Modeled plate reactor design: flat plate.

The second plate reactor design (Figure 1.1.3) adds corrugations to the plate, primarily to increase the catalytic area per reactor volume:

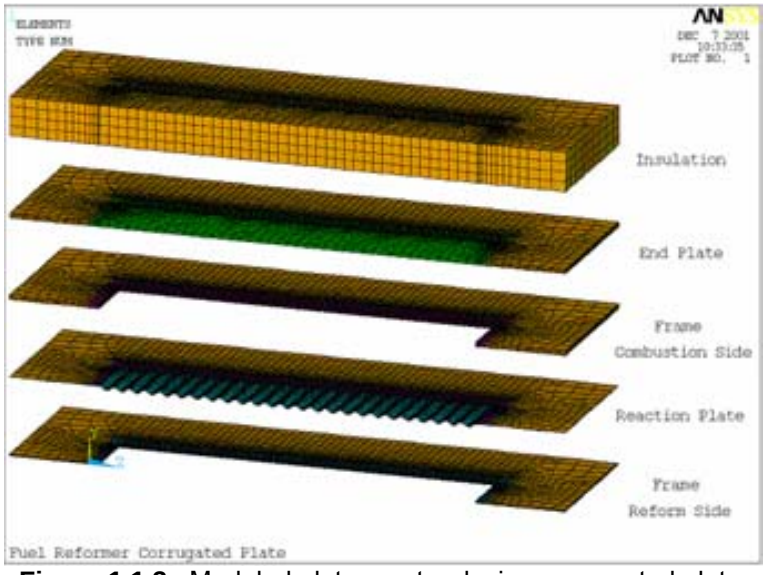

Figure 1.1.3. Modeled plate reactor design: corrugated plate.

The third design (Figure 1.1.4) is based on a circular concave geometry that could expand by growing its concavity without adding stress to the outer frame:

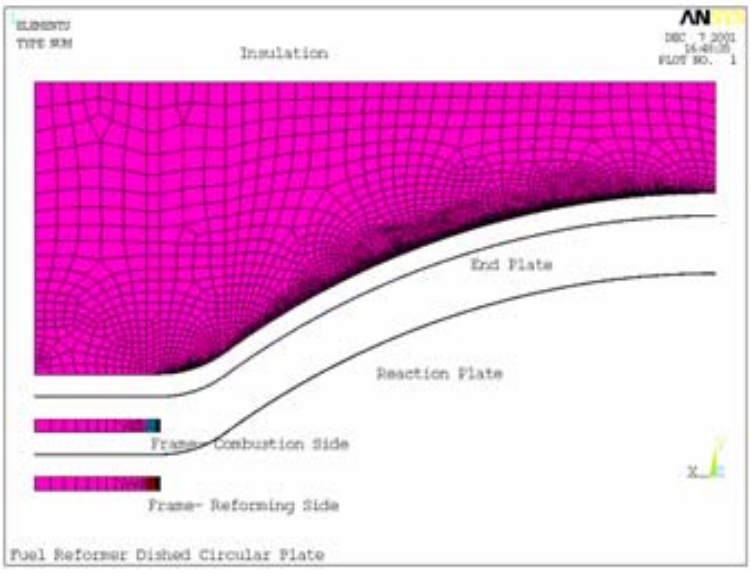

Figure 1.1.4. Modeled plate reactor design: concave plate.

The last design investigated (Figure 1.1.5) has the shape of a “race track” with concentric corrugations to minimize the concentrated stresses found in the rectangular corrugated design.

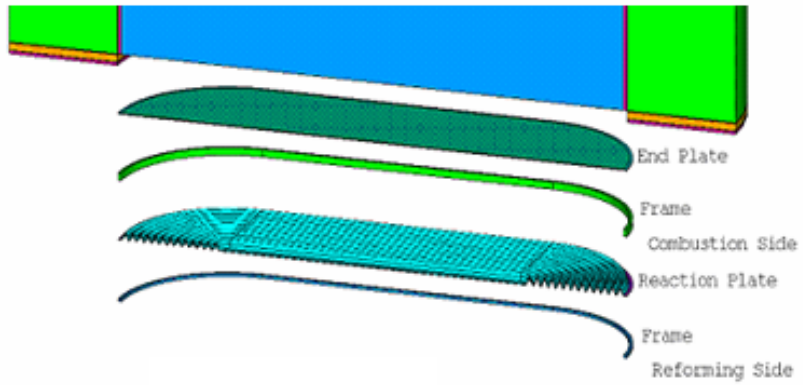

Figure 1.1.5. Modeled plate reactor design: plate of shape of a race track.

The lessons learned from the analysis completed on the four different designs revealed that the following elements contribute to a design that has adequate fatigue life:

- Minimizing the area of plate outside the reaction zone decreases the thermal gradient within the plate and therefore lowers the thermal strain.
- A frameless plate design is necessary to achieve low strain.

- Corrugations decrease strain in the direction of the corrugation. Possibly a two directional stamped pattern can relieve strain in both directions. Also, a variation of the corrugation height and pitch at the transition to flat at the edge can reduce the stress concentration.
- The race track geometry eliminates the concentrated stresses that exist in the rectangular corrugated concept.
- Greater corrugation amplitude has a significant positive effect on reducing strain.
- The frame material must closely match the plate material in thermal expansion coefficient and elastic modulus.

One key finding of the study illustrated that the large temperature gradient between the plates and the frames, especially at start up conditions generate the highest stress the plate-frame union. The plate temperature profile and the different levels of strain along the plate 20 seconds into the start-up cycle are presented in Figure 1.1.6. Note that the strain on the plates increases to unacceptable values in the corner region near the frames.

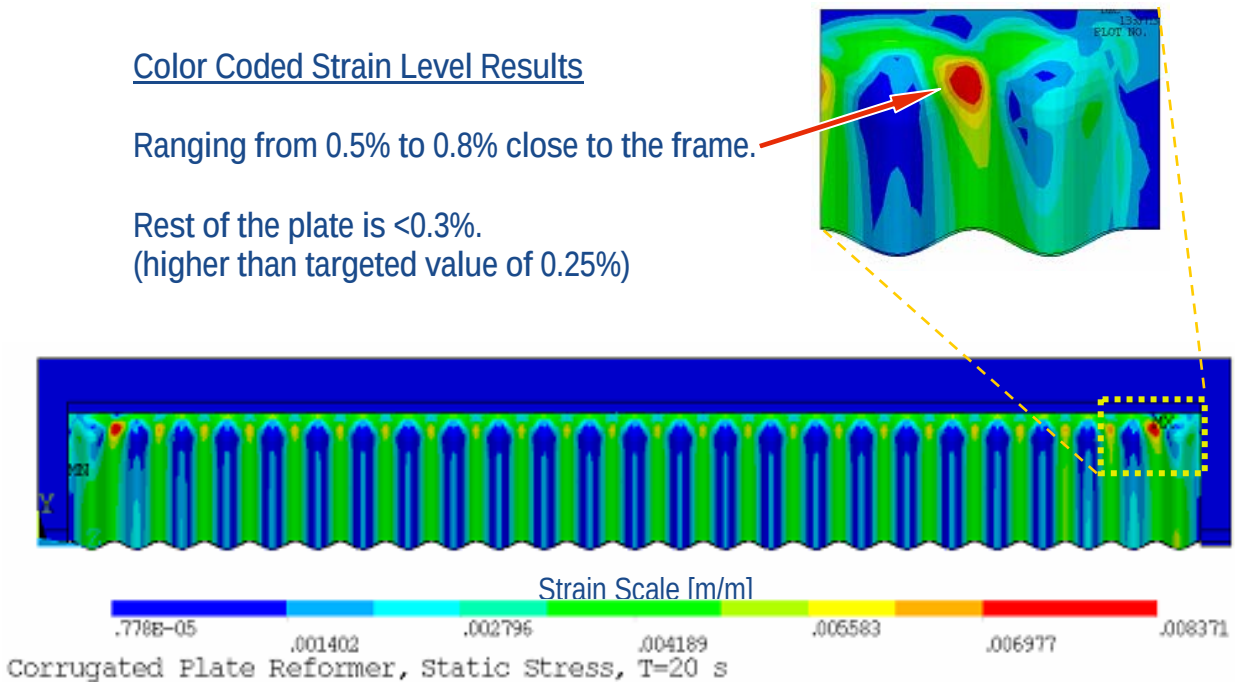

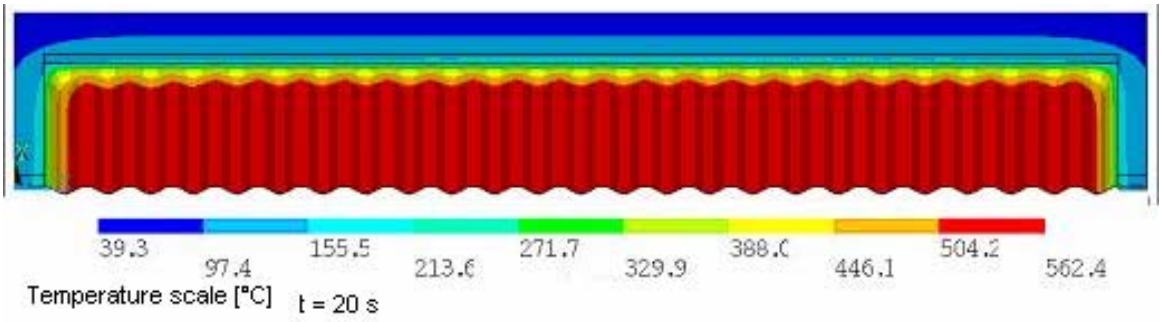

Figure 1.1.6. Plate temperature profile and static stress at t = 20 s in the start-up cycle.

The conclusions of the mechanical stress analysis revealed that in order to reduce the chances of mechanical failure, the framing used in future reactor designs needs to be removed or the frame mass minimized. Based on these findings, the team designed the first prototype, a frameless reactor called the AGT-1 reactor. The details of this design and the experimental results are discussed in section 5 of this report.

1.2 Fuel Processor System Modeling

In order to validate the usage of plate reactors for every reactor unit in the fuel processor system, it was necessary to develop a thermodynamic model that could calculate the overall system efficiency of the fuel processor. The modeled system included reactor units for the steam reforming reactor (SR), water gas shift reactor (WGS), and preferential oxidation reactor (PrOx) and also a simplified fuel cell module. Since all these reactor units have a specific optimum operating temperature, the integration of the heat management is a key factor in the optimization of the overall processor system performance. Hence, the modeling effort was focused on the optimization of the heat exchange strategy.

At the onset of the program, the first task was to decide which type of software package should be used to develop the system simulation. The software had to meet the following criteria:

1. have a pre-existing library of different reactors, heat exchangers, compressors, pumps that could be used as components to map out the system,
2. have the option to incorporate CESI's own plate reactor unit as part of the software's component library,
3. be simple enough so that the user could quickly learn how to use the software without having much previous simulation experience,
4. have the ability to solve multiple equations simultaneously,
5. have tools for optimizing temperatures and flows,
6. have a reasonable license fee.

A number of choices were reviewed, such as Hysys, Aspen, Easy5, Pro/II, Matlab, and GC Tools. Pro/II (Simsci-Esscor) was eventually selected to be the simulation software.

For the initial evaluation, a single-pass system was quickly developed that included the water and gas pumps, two of the major reactors (SR, WGS), and heat exchangers in between. Figure 1.2.a is a diagram of what the actual unit operation components looked like tied together in Pro/II.

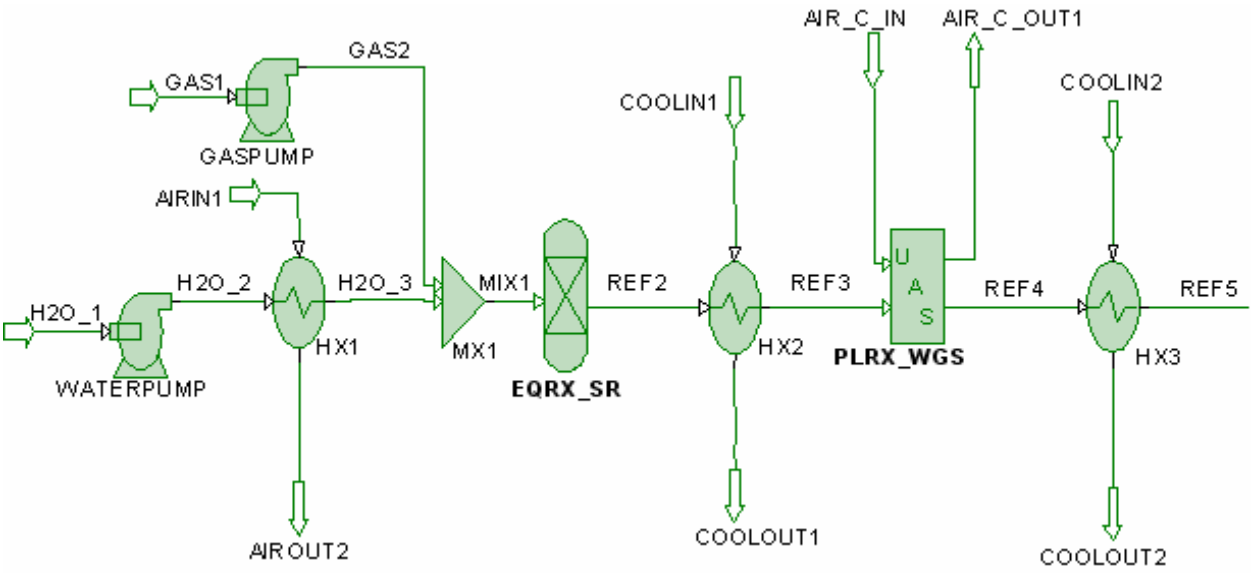

Figure 1.2.a. Single-pass system flow sheet diagram in Pro/II.

In this simulation, the SR was represented by a Gibbs' equilibrium reactor, pulled from Pro/II's library of reactors. The WGS, however, was based on CESI's internal code, written in C++; Pro/II needed the code converted to FORTRAN in order to integrate it into the component library. Once this was converted into FORTRAN, it operated as a plate reactor, taking into account the chemical reactions and heat exchange that happened between the two compartments of the reactor. Only pre-heated air was flowing on the non catalytic side of the reactor. The type of flow (co-flow or counter-flow), the reactor length, specific kinetics of the reactions, flow rates, and compositions on both sides of the reactor had to be supplied to the WGS unit operation element.

The entire system simulation became more complex over time. The steam reforming equilibrium reactor was eventually linked to a combustion reactor. An optimizer system component was used to determine the correct amount of fuel that was needed to for the combustion side to provide the heat required to complete the steam reforming reactions. More heat exchangers units were added to determine how much additional heat would be needed or was generated by the overall system. A PrOx reactor unit was added. A simplified fuel cell component was also developed and partially integrated to the fuel processor system. The fuel cell component was not integrated in the heat management, its action was simply to take the reformate stream from the PrOx and reduce the amount of hydrogen by a user-specified percentage. The hydrogen containing purge gas from the fuel cell anode compartment was then returned to the combustion side of the steam reformer reactor, thus lowering the amount of fuel that needed to be added to the combustion reactor. Figure 1.2.b is a diagram of the more

sophisticated system modeling lay-out. It illustrates the chemical unit operations necessary to process the fuel and how the system was integrated with a PEM fuel cell.

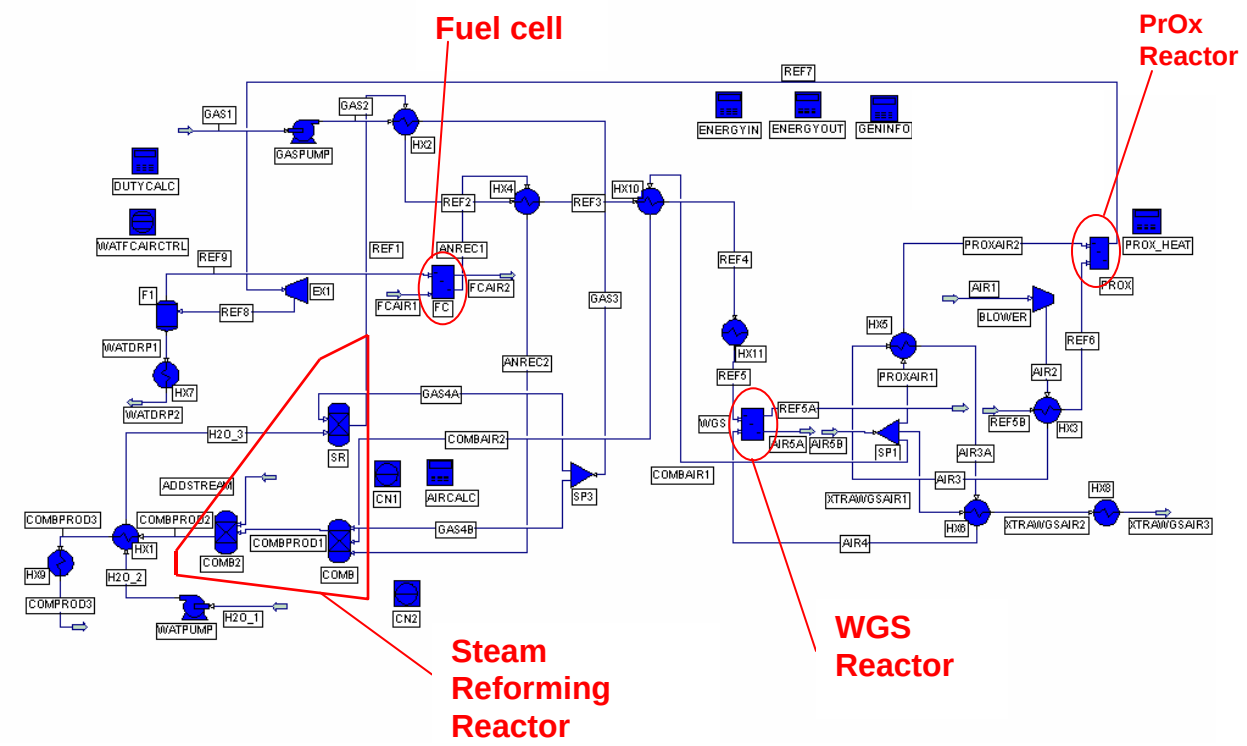

Figure 1.2.b. Pro/II diagram of fuel processor system lay-out, including fuel cell unit.

Components and streams

There are three primary stream inputs – water, air, and gasoline (in all the Pro/II simulations, gasoline is represented by pure isooctane). The water and fuel need to be vaporized, but all three inputs need to be heated to their respective operating temperatures using auxiliary heaters or system heat recycle.

Gasoline is introduced as stream ‘GAS1.’ The ‘GASPUMP’ raises the fuel pressure to 3.14 atm, while heat exchanger ‘HX2’ raises its temperature. The splitter ‘SP3’ splits the fuel for the steam reforming ‘SR’ and combustion ‘COMB’ reactors. To simulate the characteristics of a co-current plate reactor (such as both the outlet streams temperature being equal), the stream ‘ADDSTREAM’ supplies the necessary fuel and air to heat streams ‘GAS2’ and ‘COMBPROD2’ to the operating temperature of the steam reforming reactor (825°C).

'WATPUMP' pressurizes the water stream 'H2O_1' to 3.14 atm, which is then vaporized in the heat exchanger 'HX1'. The water vapor flows to the steam reforming 'SR' reactor and reacts with gasoline to generate hydrogen-rich reformate, the composition of which is determined by the thermodynamic equilibrium. Excess water vapor follows with the reformate stream from 'SR' to 'HX2', 'HX4', 'HX10', 'HX11', 'WGS', 'HX3', 'PROX', 'EX1', and 'F1'. The steam is carried out through the reformate exhaust streams and exits the system through stream 'WATDRP2'.

Air is introduced with the stream 'AIR1' through the 'BLOWER' component. Multiple adiabatic efficiency curves have been used to determine how much auxiliary power is required to run the blower at 1.14 atm. The air is heated as it flows through 'HX3', 'HX5', 'HX6', and 'WGS'. At 'SP1', the air splits into three branches:

1. 'COMBAIR1' which is used to cool down the reformate stream in 'HX10' and then flows to the 'COMB' reactor;
2. 'PROXAIR1' which is cooled down by the cold stream 'AIR3' in 'HX5' and then flows to the 'PROX' reactor;
3. 'XTRAWGSAIR1' which is cooled down by the cold stream 'AIR3A' in 'HX6' and then flows out of the integrated system through 'HX8', which is used to determine recoverable heat of stream 'XTRAWGSAIR2'.

Another air stream input is 'FCAIR1' which supplies the oxygen for the fuel cell stack 'FC.' Finally, a small amount of air is admitted through the stream 'ADDSTREAM' to the second combustor 'COMB2,' which is used to heat the stream 'COMBPROD1' to 825 °C to ensure that the steam reforming reaction simulates the correct temperature of the plate-based steam reforming reactor.

Heat management

The majority of reusable energy from the process streams is recovered through heat exchangers. The total amount of energy that is not recovered through heat exchangers can be obtained by adding up the duties of the heat exchangers 'HX8,' 'HX9,' and 'HX11.' Additional energy can be recovered from the exothermic PrOx reaction. The heat generated in the PROX is not used to increase the temperature of PROX outlet stream, but is recovered via the calculator 'DUTYCALC.' The purpose of this calculator is to balance the duties of 'SR', 'COMB', 'COMB2', 'PROX', 'HX8', 'HX9', and 'HX11'. In 'DUTYCALC', the heat available from 'PROX', 'HX8', 'HX9', and 'HX11' is used to supplement the heat that is generated by 'COMB' and transferred to 'SR'.

Heat exchangers

The constraints on the heat exchangers varied, depending on the flows and temperatures and what was thermodynamically possible for each of the individual heat exchangers. For example, certain heat exchangers were limited by the difference in temperature between the 'hot in' and 'cold out' streams, while the constraint for other heat exchangers was the difference between 'hot out' and 'cold in' temperatures.

Parametric study

One of the reasons for developing this system simulation was to study the impact of various parameters on the overall system efficiency. Since there are numerous

interactions and recycle loops within the system, it would be difficult to predict how one characteristic would affect efficiency without a fully integrated system model. The different parameters that were investigated in this case study were combustion equivalence ratio (phi), CO abatement in the WGS reactor ("WGS duty"), and steam to carbon ratio (S:C) in the steam reforming reactor. Five different cases were run: one base case, three cases where each of these parameters was varied from the base case, and one last case where all three parameters were varied at the same time. For the base case, S:C was 3.8, WGS duty was 80%, and phi was 0.5.

The parameters evaluated in the five cases (CASE I to CASE V) are graphically illustrated in Figure 1.2.c, where *SC* is steam to carbon ratio, *WGS duty* is the percentage of CO converted in the water gas shift reactor, and ϕ is the equivalence ratio in the combustion side of the steam reforming reactor.

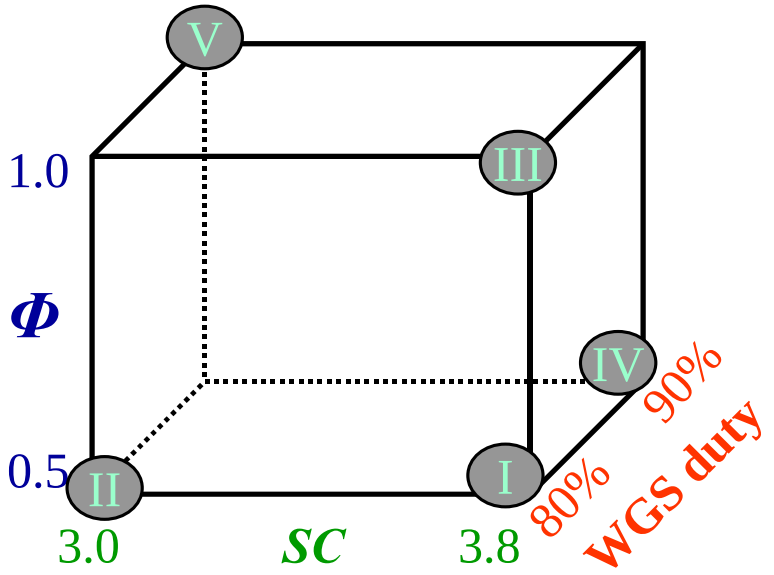

Figure 1.2.c. Normal calculation points of the 5 case studies.

These three parameters (*S:C, WGS duty,*ϕ) were investigated to quantify the influence of each parameter on the efficiency of the fuel processor. The efficiency is defined as followed:

$$Efficiency = \frac{LHV_{H2(\mathrm{Pr}Oxoutlet)} - LHV_{H2(anodepurge)}}{LHV_{gasoline\,COMB} + LHV_{gasolineSR}}$$

where LHV is the lower heating value of the subscripted gas stream. In this definition of the efficiency, the parasitic power (pumps and compressors) is not taken into account.

The resulting efficiencies for the five case studies are summarized on Table 1.2.a.

Table 1.2.a. Resulting system efficiency for the five case studies.

	Phi	WGS Duty	S:C	Efficiency
Baseline Case I	**0.5**	**80%**	**3.8**	**79.6 %**
Case II	**0.5**	**80%**	**3.0**	**79.9 %**
Case III	**1.0**	**80%**	**3.8**	**79.8 %**
Case IV	**0.5**	**90%**	**3.8**	**82.7 %**
Case V	**1.0**	**90%**	**3.0**	**83.6 %**

The comparison between CASE I and CASE II shows that reducing the steam to carbon ratio from 3.8 to 3.0 increases the efficiency by 0.4 percentage point. A similar comparison between CASE I and CASE III indicates that increasing the equivalence ratio in the combustion from 0.5 to 1.0 enhances efficiency by 0.3 percentage point. The comparison between CASE I and CASE IV illustrates that increasing the conversion of CO from 80 to 90% in the water gas shift reactor increases the efficiency by 3.2 percentage points. The combined improvement of the three parameters in CASE V yields to the highest efficiency among the five case studies and is consistent with the results of the other cases.

Assumptions

Some assumptions for the process simulation have already been described under the Heat management section. Additional key assumptions include:

- 85% fuel utilization in the fuel cell. 15% of the fuel processor hydrogen output is redirected from fuel cell anode compartment to the combustion side of the steam reforming reactor.
- No heat losses from heat exchangers or from streams to ambient.
- The combined available duty of ‘HX8’, ‘HX9’ and ‘HX11’ is completely recycled in the system through the ‘DUTYCALC’ unit.
- The heat generated in the preferential oxidation reactor is recovered through the ‘DUTYCALC’ unit.
- 100% oxidation of fuel in combustors ‘COMB’ and ‘COMB2’.
- The gasoline reforming reactor ‘SR’ is simulated by a Gibbs reactor; its outlet stream composition is obtained by solving the heat and mass balances and minimizing the total free energy of the components.

Conclusions

It was a challenge to build an interface between Pro/II and the user-added subroutine, especially when trying to integrate both the steam reforming code and water gas shift code into Pro/II. The user-added subroutines needed to be completely packaged in the Fortran/C++ codes for exporting to Pro/II.

Pro/II was not able to solve the simulation when we tried to recover the heat from 'HX8', 'HX9' and 'HX11' directly through flowing cooling air in the heat exchanger instead of through the less realistic 'DUTYCALC' calculator. The most likely reason for this problem was the improper sequencing of when the unit operations were solved. The order in which the different equations were solved was critical for the simulation to converge. Even though the user was able to individually select components and place them in different sequencing schemes, it was very difficult to determine the best sequence. The majority of the attempted sequencing was based on trial and error. Even when the user implemented the software option to automatically select the sequence, it was clear that its auto-selected sequence were often mistaken. For example, solving for the temperature of a heat exchanger's hot gas outlet before knowing its hot gas inlet was a clear example of the program's inability to consistently establish a logical sequencing scheme. This was the software's greatest weakness.

Nevertheless, the detailed case study that the software was able to solve resulted in a more efficient catalyst development and reactor design process by establishing priorities to in the development efforts. As an example, the case studies showed that it was more important to develop an active WGS catalyst able to achieve a significant CO abatement instead of developing a steam reforming reactor design that could withstand a high combustion equivalence ratio.

1.3 Mathematical Description of the Reformer Model

A schematic of a small section of the plated-based steam reformer is presented in Fig. 1.3.1. The unit modeled consists of five parts in the 'x' direction: reforming channel, reforming catalyst layer, support-foil wall, combustion catalyst layer, and combustion channel. The foil is coated on both sides along the '*z*' direction.

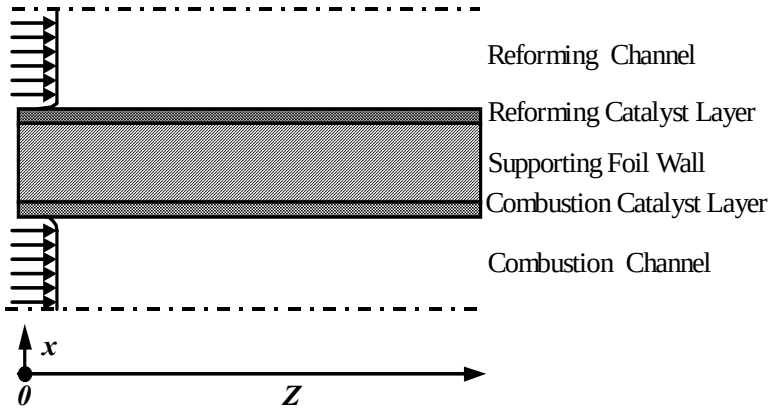

Figure 1.3.1. Schematic of Gasoline Fuel Reforming Modeling Unit

The governing equations of the model were developed from the conservation of mass, energy, and chemical species. Key assumptions for the model include:

- Quasi two-dimensional transient model.
- Ideal gas.
- Uniform mixture on the inlets of both combustion and reforming channels.
- Full combustion in the first combustion catalyst coating element.
- The heat of combustion is transferred to the reactor wall from combustion gas stream by convection
- No radiation inside the reactor.
- Heat conduction along the *z* axis.
- Reforming reactions occurs on the reforming catalyst.
- Reformed mixture comes out of the reforming catalyst and mixes instantaneously with the bulk stream.
- There is no mass transfer limitation resulting from desorption.
- Reforming gas stream is heated by the reforming catalyst layer through convection.
- Radiation and natural convection heat losses from the reactor stack are calculated based on the experimentally measured reactor surface temperatures and distributed equally to each channel.
- No temperature gradient along the height of the stack in the *x*-direction.

The following phenomena were explicitly included in the model:

- convective heat and mass transfer between flowing streams and catalyst surfaces;
- heterogeneous chemical reactions taking place on the catalyst surface; and
- the catalyst capacity of storing species and releasing it under varying conditions.

Any possible non-uniform flow distribution along the x-axis was neglected to simplify the model for computational expediency. The simplification results in a transient quasi two-dimensional model which can be separated into three equations (1.3.1, 1.3.2, and 1.3.3).

The gas phase energy balance equation in the reforming channel:

$$\rho_r C_{p,r} \frac{\partial T_r}{\partial t} + \rho_r C_{p,r} V_r \frac{\partial T_r}{\partial z} = h_r \left(T_{rs} - T_r\right) G_r \qquad (1.3.1)$$

The energy balance equation for the wall of supporting foil, combustion catalyst and reforming catalyst:

$$\begin{aligned}\rho_w C_{p,w}\frac{\partial T_w}{\partial t} &= +h_r\left(T_r - T_w\right)G_w \\ &\quad +h_c\left(T_c - T_w\right)G_w \\ &\quad +\partial\dot{Q}_{react,rs}\cdot G_{rs} \\ &\quad +\partial\dot{Q}_{react,cs}\cdot G_{cs} \\ &\quad +k_w\frac{\partial^2 T_w}{\partial z^2}\end{aligned} \qquad (1.3.2)$$

The gas phase energy balance equation in combustion channel:

$$\rho_c C_{p,c}\frac{\partial T_c}{\partial t} + \rho_c C_{p,c} V_c \frac{\partial T_c}{\partial z} = h_c\left(T_{cs} - T_c\right)G_c + \partial\dot{Q}_{react,c}\cdot G_c \qquad (1.3.3)$$

Where:

C_p : heat capacity at constant pressure, (J/mol·K)

g : mass transfer coefficient, (m/s)

G : geometric surface area, (m^2/m^3)

k : thermal conductivity, (W/m·K)

$\dot{Q}$: heat flux, (W)

t : time, (s)

T : temperature, (K)

V : velocity, (m/s)

Wall density, wall heat capacity, and wall thermal conductivity are assumed constant in the model.

The heat transfer coefficients in the above equations are calculated from heat transfer correlations. The diffusion coefficients, heat capacity, thermal conductivity, and viscosity of the bulk reacting mixture are calculated based on local compositions and temperatures. For instance, in order to obtain the heat transfer coefficient, it is necessary to determine the Reynolds number, decide if the flow is laminar or turbulent, and then calculate the Nusselt number in order to obtain the heat transfer coefficient.

The bulk velocity variations in both reforming and combustion channels take into account the influence of temperature and composition changes so that the global mass balance is satisfied. The kinetics incorporated into the code to calculate the temperature and species concentrations along the reactor are the kinetics determined experimentally that are

described in sections 2.3 and 2.6 of this report. The effectiveness factor is calculated to account for the diffusion resistance causing a concentration profile to exist in the catalyst coatings because the reactants cannot diffuse in from the bulk sufficiently rapidly. A small diffusion resistance yields a relatively flat curve of species concentration whereas a steep concentration profile is obtained for a large diffusion resistance.

The energy and species conservation equations have successfully been solved in the computer simulation. The equations have been discretized into small finite elements in the calculation domain and then the time-step forward Crank-Nicholson approach has been used to solve the governing equations.

1.3.1 Reformer modeling results

The parameters included in the model are listed below:

1. reactor or plate length (m)
2. catalyst loading length (m)
3. reactor or plate width (m)
4. channel height (m)
5. channel corrugation period (m)
6. foil thickness (m)
7. number of channels
8. reforming wetted perimeter (m)
9. reforming wetted perimeter (m)
10. hydraulic diameter of reforming channel (m)
11. hydraulic diameter of combustion channel (m)
12. reforming catalyst density (kg/m^3)
13. support foil density (kg/m^3)
14. combustion catalyst density (kg/m^3)
15. reforming catalyst loading (kg/m^2)
16. combustion catalyst loading (kg/m^2)
17. total reforming flow molar rate (mol/s)
18. total combustion flow molar rate (mol/s)
19. steam-carbon ratio of reforming inlet (mol/mol)

Several aspects of the reforming reactor performance have been modeled, such as the gas phase and wall temperature profiles along the plates, the start-up time, the effects of local lack of reforming catalyst coating, or the species axial distribution. For example, Figure 1.3.2 shows the temperature profile of the plates along the axis of flows, with a comparison with experimental point. This dynamic model validated CESI plate reactor concept.

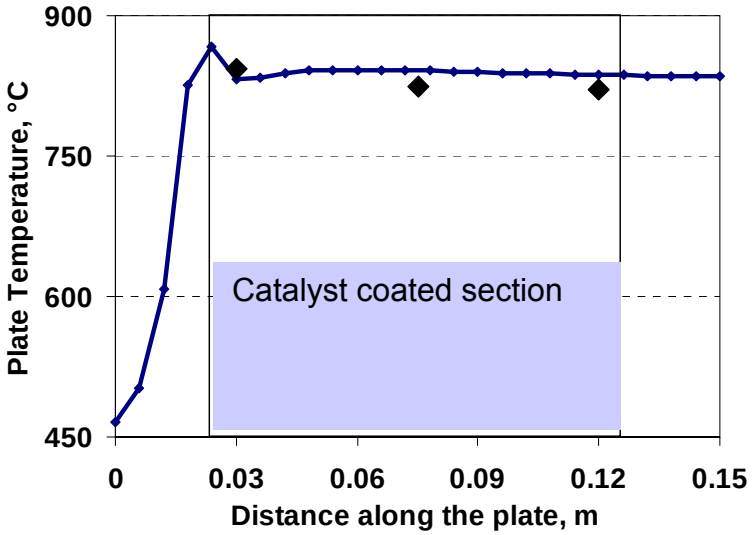

Figure 1.3.2. Steady state plate temperature profile, model (line) and experimental result (♦) in AGT-2 reactor.

2. Steam reforming catalyst development

The catalytic steam reforming of heavy hydrocarbons has been a topic widely covered in the literature in the past years due to the growing interest in on-board and stationary hydrogen generation for fuel cells technology. The traditional industrial catalytic systems based on nickel catalysts supported on refractory materials typically present a low specific activity, are prone to deactivation and coking and are not sulfur tolerant. The challenges of the new generation of reforming catalysts required for fuel cells applications reside in the need for these catalytic systems to have high activity and tolerance to sulfur (for the compactness and simplicity of the hydrogen generator device), tolerance to numerous start up and transient operation, durability, and low cost. All these aspects were integrated in the development program of a steam reforming catalyst for fuel cell application.

2.1 Catalyst for gasoline steam reforming: operating window

CESI prior experience in heavy fuel reforming included Navy F-76 Diesel fuel and gasoline reforming in an auto-thermal mode. The ATR (ATR-10) catalyst developped in that program was a noble metal based catalyst that showed an excellent stability for reforming sulfur-containing gasoline in an auto-thermal mode at an operating temperature between 700°C and 900°C, with a steam-to-carbon ratio between 1.1 and 3.3, and an oxygen equivalence ratio of 3.5 to 4.8. The good performance of this catalyst in *auto-thermal reforming* of gasoline was the reason for using it in the initial steam reforming of gasoline experiments.

In the experimental setup (Figure 2.1), syringe pumps were used to feed the liquid fuel and liquid water, which were combined in the vaporizer. The reactor (Figures 2.2 and 2.3) itself was composed of a 50.8 cm long titanium tube (0.5" O.D., 10.6 mm I.D.) situated inside an electrically heated 25.4 cm long copper block. The catalyst was

deposited as a washcoat on the inside wall of the titanium tube. A quartz rod (9.0 mm O.D.) was insterted into the titanium tube to form an annular flow path. A backpressure regulator was controlling the pressure at the outlet of the reactor. The reactor effluent was monitored continuously by an ifrared gas analyzer for methane, carbon monoxide and carbon dioxide. Gas chromatography was also used to monitor the composition of the reactor effluent.

A preliminary and simplified heat transfer study showed that in such a reactor configuration, the catalyst layer is essentially at the temperature of the heating block, even in presence of a very active catalyst for a strongly endothermic reaction such as steam reforming. The gradient between the heating block and the catalyst surface never exceeds 5°C. The precise control of the catalyst temperature had several advantages:

- better representation of the operating conditions of the plate reactor where the temperature of the reforming catalyst is maintained within a narrow range,
- maintain the catalyst at a temperature that was within its window of durable operation, and
- ideal for extract kinetics parameters.

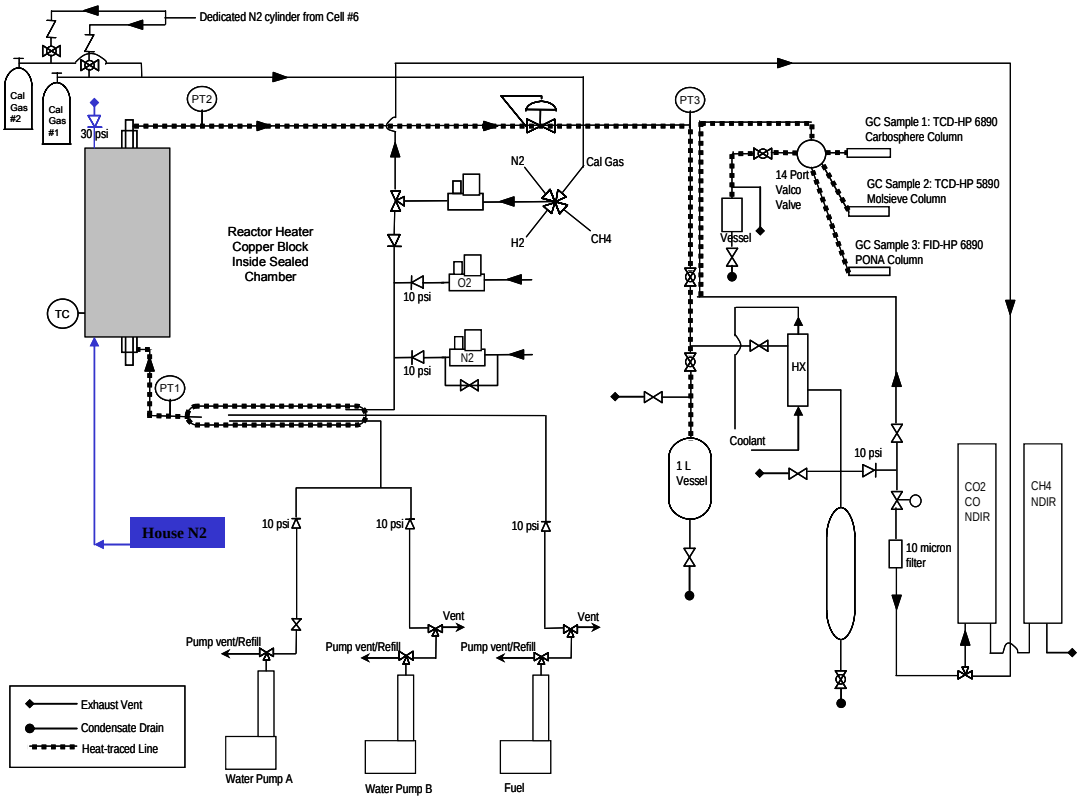

Figure 2.1. Steam reforming annular reactor experimental setup and flow sheet.

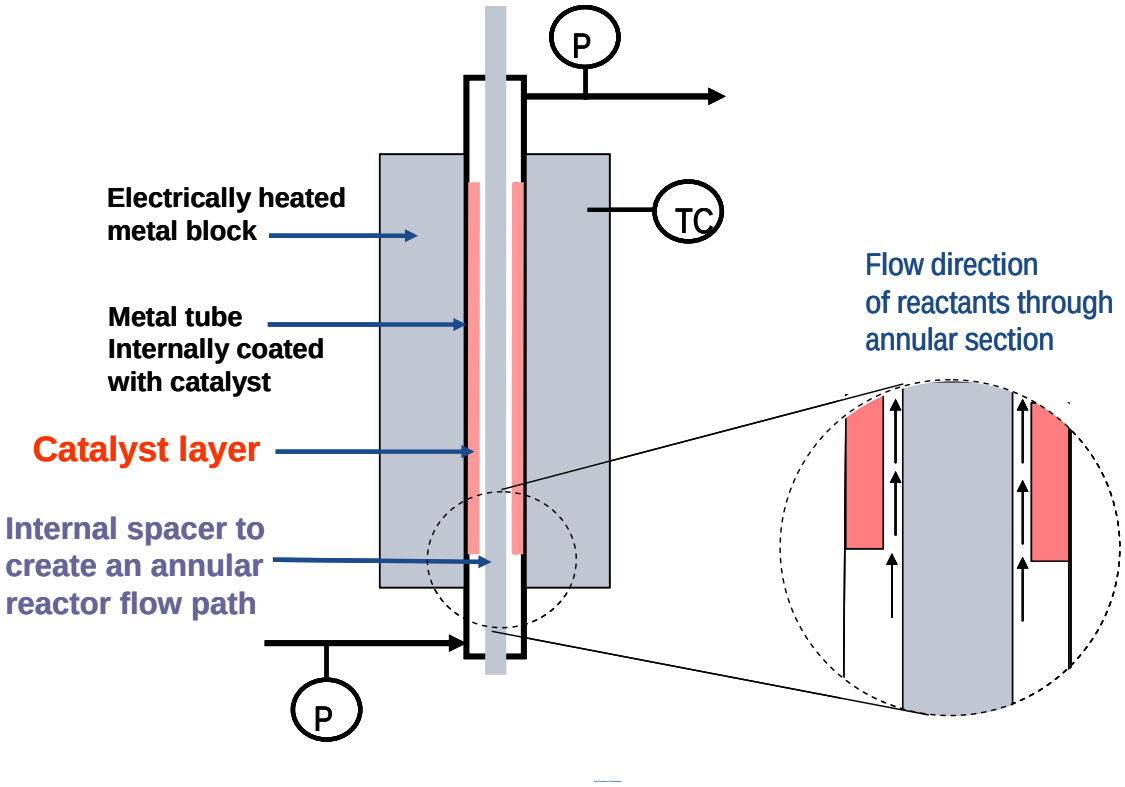

Figure 2.2. Lab scale steam reforming annular reactor schematic.

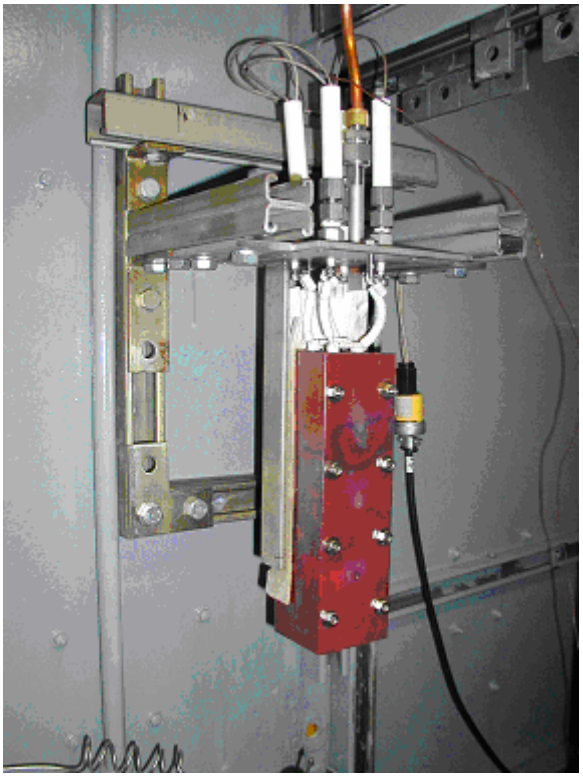

Figure 2.2. View of the lab scale steam reforming annular reactor heating copper block.

Several parameters were studied to define the appropriate window of operation of the ATR10 catalyst, where the activity and stability would be sufficient for a plate-based reformer prototype application. Initial experiments were conducted using isooctane as a surrogate for gasoline, isooctane having approximately the molecular mass of the average of the hydrocarbons present in gasoline. The average hydrocarbon chain length is certainly an important factor in the performance of a steam reforming catalyst, but the level of aromatics, alcenes and cyclic hydrocarbons determines the reforming catalyst activity and plays a major role in the catalyst propensity to coke formation. As shown in Table 2.1, the initial activity of the catalyst depends strongly on the fuel composition: the pump grade gasoline is well represented by a simple blend of 4 C_5 to C_8 hydrocarbons (composition is in Table 2.2), developed by the Argonne National Laboratory. The level of sulfur in the hydrocarbon impacts the catalyst activity as well, as shown on Figure 2.3 where the presence of sulfur in the fuel induces a significant effect on the catalyst activity.

Table 2.1 Catalyst activity *vs.* type of fuel

Fuel	**Highest WHSV (h^{-1}) sufficient to achieve full conversion to C_1's**
isooctane	223
Isooctane + 10 ppm S	90
Gasoline (retail), contains 10 ppm S	21
ANL Benchmark Fuel I +10 ppm S	23

Conditions: T = 800°C, S:C = 3.8, P = 3 atm.

Table 2.2 ANL Benchmark Fuel I composition

Compound	**% mass**	**% mol**
isooctane	74	71.87
xylenes (o-, m- and p-)	20	20.90
methylcyclohexane	5	5.65
1-pentene	1	1.58

The adsorption of sulfur on the active sites of the catalyst has an effect on the catalyst's initial activity as well as its long term stability. The formation of coke can be seen as a reaction parallel to reforming. Hence, by lowering the specific reforming catalytic activity, the sulfur enhances the risk of coking. These two competitive reactions (coking and reforming) have most likely not the same activation energy and that is the reason why it is not surprising to observe on the scale of reaction temperature a clear transition between a stable regime and a regime where the catalyst deactivation occurs. This is what Figure 2.4 illustrates: the catalyst deactivation is immediate and rapid at low reaction temperatures, while at 825°C, the ATR-10 catalyst was stable. Unfortunately, the same conclusion could not be made for the reforming of more complex hydrocarbons. Coke formed at all tested temperature ranges for pump grade gasoline and the ANL Benchmark Fuel I. Attempts to increase the reforming catalytic activity by increasing the loading of the noble metal failed to improve the stability of the ATR10

catalyst. At that point, it became evident that the formulation of the catalyst had to be modified.

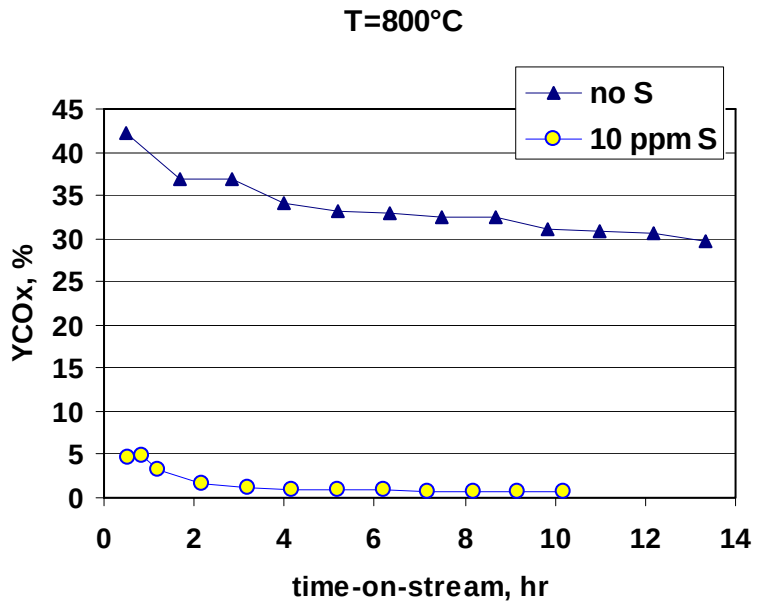

Figure 2.3. Effect of the level of sulfur in the fuel on the catalyst activity. Isooctane steam reforming, T = 800°C, S:C = 3.0.

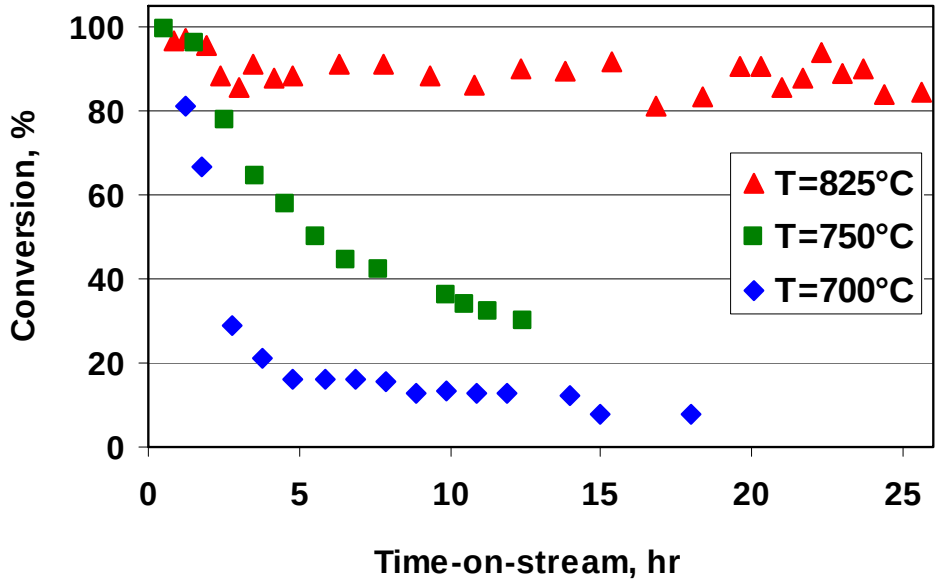

Figure 2.4. Effect of the catalyst operation temperature on the catalyst stability. Isooctane steam reforming, S:C = 6.0.

2.2 Steam reforming catalyst performance development program

The inability to find a satisfying operating window for the original steam reforming catalyst lead us to launch a catalyst development program that targeted a stable, less

expensive and widely operable catalyst. Table 2.3 lists a matrix of the different catalyst compositions that resulted from this program. The parameters that have been varied in the formulations were the support composition, the noble metal loading, the amount and nature of the promoters and various synthesis parameters, such as calcination temperature or impregnation techniques.

Table 2.3 Matrix of the steam reforming catalysts compositions.

	Support	promotors 1 and 2 ratio	Promotor 3	Noble metal loading,%
ATR-10C5	A	0.3	none	5.0
SR-1A	B	14.3	none	4.8
SR-1B	B	4.1	none	4.8
SR-2	C	5.0	none	4.8
SR-3	C	4.9	none	4.8
SR-4	D	13.9	none	4.8
SR-5	E	11.4	a	4.8
SR-6	E	12.2	b	4.8
SR-7	E	12.2	c	4.8
SR-8	E	12.2	d	4.8
SR-9	D	13.9	e	5.1
SR-10	E	11.6	d+e	5.2
SR-11	D	12.9	d+e	5.2
SR-12	D	14.0	e	0.0
SR-13	D	14.0	d	0.0
SR-14	D	14.0	d	1.1
SR-15	D	14.0	e	1.0
SR-16	E	10.0	e	1.0
SR-17	D	9.0	e	0.5
SR-18	D	4.7	e	1.0
SR-19	D	1.0	e	1.0
SR-20	D	3.0	e	1.0
SR-18-2	D	4.7	e	1.0
SR-21	D	2.4	e	1.0
SR-22	D	4.7	e	1.0
SR-23	D	4.7	e	1.0
SR-24	F	4.7	e	1.0
SR-25a	F	4.7	e	1.0
SR-25b	F	4.7	e	1.0
SR-26	G	4.7	e	1.0
SR-27	H	4.7	e	1.0
SR-28	I	4.7	e	1.0
SR-29	D	4.7	e	1.0
SR-30	D	4.7	e	1.0
SR-31	D	4.7	e	1.0
SR-32	D2	4.7	e	1.0
SR-33	D3	4.7	e	1.0
SR-34	D4	4.7	e	1.0
SR-35	D	4.7	e	1.0

The main goal of the catalyst development program was to identify a catalyst that would be stable in experimental conditions (T, P, S:C) suitable for a steam reforming plate

reactor. These conditions were determined by a mechanical stress analysis of the plate reactor that set the temperature and pressure upper limits and by an overall processor efficiency study that gave the upper limit to the S:C ratio that was still acceptable to reach a processor efficiency within the program objectives. Details of these studies are presented in sections 1.1 and 1.3 of this report, but in conclusion, a pressure of **3 atm in the reforming side, a reaction temperature of 825°C and a S:C ratio of 3.8** were selected as being acceptable on a mechanical stability and on a system efficiency point of view.

Figure 2.6 shows the results of a systematic stability test of some of the first 18 catalyst formulations. The tests were conducted under the same conditions for all the catalysts. Simple inspection of the figure shows that a significant and drastic improvement of the catalyst stability was achieved over the duration of the program. Looking in details at the performance of the different formulations that the preferred support is D rather than A or B, and the most effective promoter is "e". Based on these experimental observations, the catalyst with the highest durability was selected for subsequent kinetics tests. A second step in the optimization of the support determined the optimal ratio of two different promoters and the most favorable level of noble metal loading. Several attempts of using different supports instead of D were made with the intention of finding a support less prone to sintering. Stability tests confirmed that in D was the best support in terms of resistance to coking.

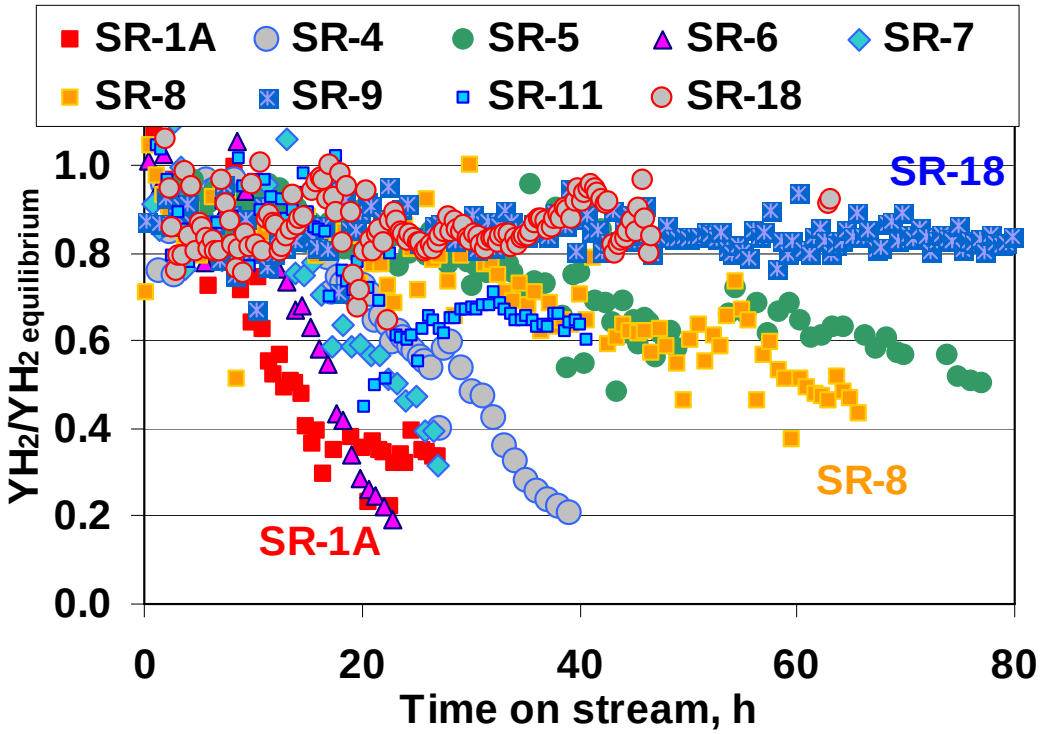

Figure 2.6. Catalyst stability tests. Operating conditions: T = 825°C, P = 3 atm, ANL Benchmark Fuel I + 10 ppm S, S:C = 3.8.

2.3 Kinetics

The primary goal of the kinetics study was to get an apparent global reaction rate expression that could then be used in the modeling of a plate-based reforming reactor. Analytical measurements of the outlet stream of the reactor showed that its composition was near equilibrium at partial and full conversion. Hence, the rate expression can be expressed as a rate of formation of C1 compounds (*i.e.* CO, CO_2 and CH_4). In addition, to maintain stability of the catalyst, all the kinetics experiments were conducted with a S:C ratio of 3.8. As a result, the large excess of steam simplified the rate expression since it was determined that the steam did not need to be included in the power-law rate expression.

The approach to measure the kinetics of the steam reforming reaction was to use an integral reactor and a differential method of analysis. Practically, the fuel conversion to C_1's was measured by GC at different space velocities (by varying flow rates or the amount of catalyst) in the annular reactor, at different temperatures within the range of catalyst stable activity (780°C to 835°C), and over a wide range of conversion (50 to 95%). Data fitting lead to the following 3-parameter power-law rate expression:

$$r = \frac{dN_{C_1}}{Wdt} = k_0 \cdot \exp\left(\frac{-E_A}{RT}\right) \cdot P^{a}_{C8H16}$$

where,

r	=	reaction rate [$mol \cdot g_{cat}^{-1} \cdot min^{-1}$]
N_{C1}	=	number of moles of C_1 species (*i.e.* CO, CO_2 and CH_4) [mol]
W	=	catalyst mass [g]
k_0	=	pre-exponential factor [$mol \cdot g_{cat}^{-1} \cdot min^{-1}$]
E_A	=	apparent activation energy [$J \cdot mol^{-1}$]
R	=	universal gas constant (8.314 $J \cdot mol^{-1} \cdot K^{-1}$)
T	=	reaction temperature [K]
P_{C8H16}	=	gasoline partial pressure [atm]

Numerical values for **E_A, k_0,** and **a** have been determined experimentally for the SR-9 catalyst using ANL Benchmark Fuel I containing 10 ppm sulfur. This rate expression and these numerical values were included in the modeling of the steam reforming plate-based reactor. Figure 2.7 illustrates that this rate expression describes the experimental measurements accurately.

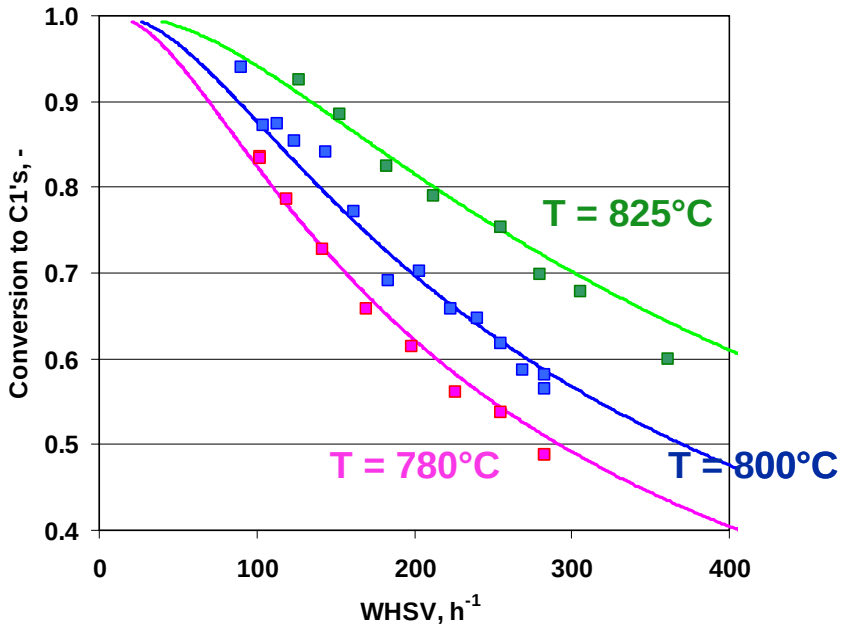

Figure 2.7. Steam reforming kinetics: tests results and model (lines). Operating conditions: P = 3 atm, fuel: ANL Benchmark Fuel I + 10 ppm S, S:C = 3.8.

2.4 Durability tests

A critical aspect of all the reforming catalyst systems is their durability in terms of their resistance to coking, particularly when heavy or complex hydrocarbons are involved. The phenomenon of coking is the main reason for reforming catalysts deactivation. The literature data shown in Figure 2.8 illustrates the process of catalyst coking is essentially auto-catalytic: an induction period is typically followed by an exponential formation of coke species. This behavior makes the durability tests essentially a determination of the induction period.

Figure 2.9 presents the results of a 1000-h durability test of the steam reforming. The reactor setup was such that the fuel flow rate was interrupted every 50 h for approximately an hour to refill the reservoirs of the pumps. During this interruption, steam was flowing. It is evident that the catalyst underwent reactivation during these short periods where fuel was not flowing. This explains the noticeable periodic increases in activity on Figure 2.9.

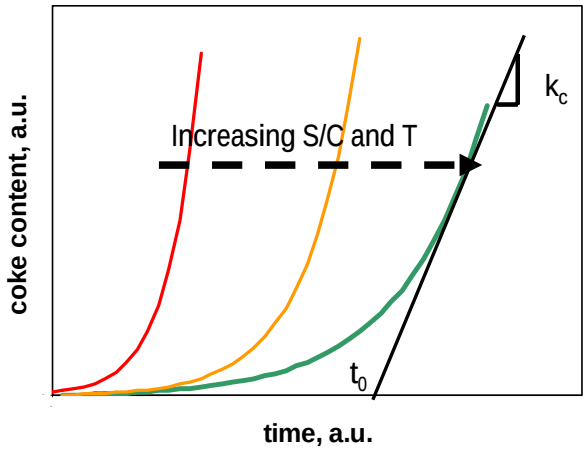

Figure 2.8. Qualitative representation of coke formation kinetics during steam reforming of heavy hydrocarbons. Induction period and the effect of S:C and temperature. [1]

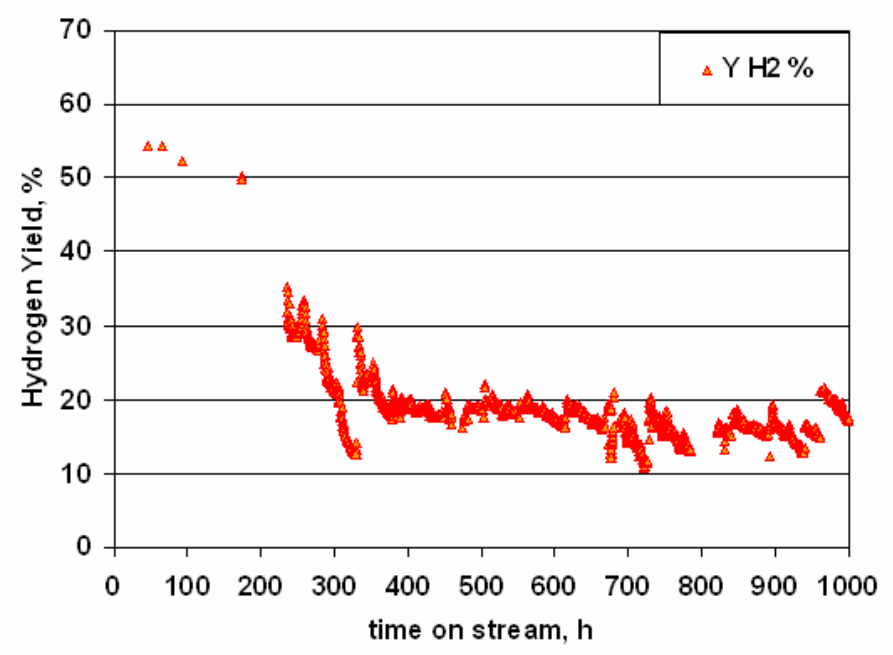

Figure 2.9. Catalyst durability tests. Operating conditions: T = 825°C, P = 3 atm, ANL Benchmark Fuel I + 10 ppm S, S:C = 3.5.

2.5 Fuel diversification

Results have been obtained in both steam reforming and dry CPOX of butane, showing excellent stability of the catalysts (SR-18 and ATR-10C). These results are shown in

[1] Reference: J.R. ROLSTRUP-NIELSEN, "Steam Reforming Catalysts", Danish Technical Press, Copenhagen, 1975.

Figure 2.10. Butane is one of the fuels available to the public on a large basis, thus a good candidate for a portable power generator based on a reformer and a SOFC.

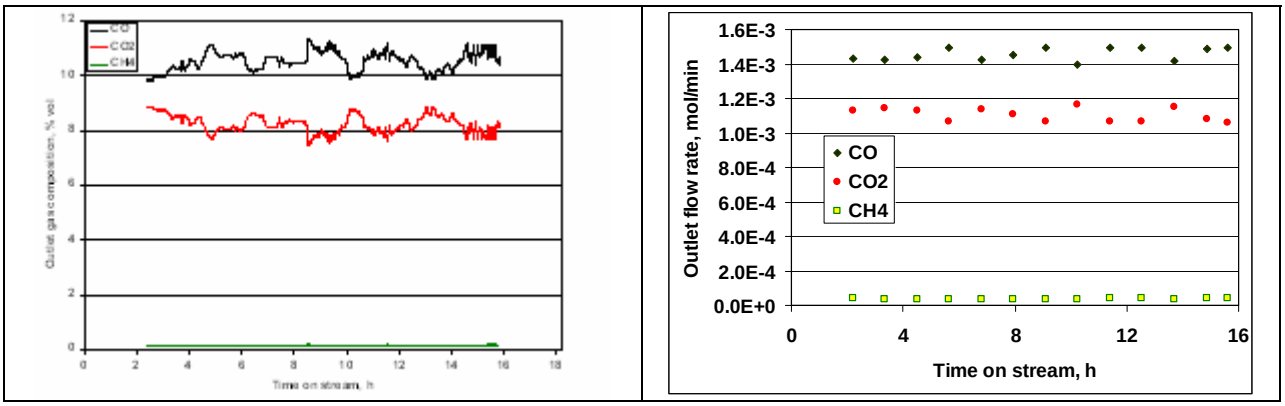

Figure 2.10. Outlet gas composition versus time-on-stream for n-butane steam reforming.

2.6 Combustion catalyst kinetics

Experiments were required to measure the kinetics of the catalytic combustion of gasoline on CESI proprietary combustion catalyst. These experiments were conducted in a wall coated tubular reactor, the metal block acting in the exothermic reaction as a temperature buffer, like in the endothermic reaction of reforming. Only a narrow range of temperature above the light-off temperature was examined since the reaction rate was too fast to be measured accurately at higher temperatures. For modeling purposes, it was assumed that the kinetic law extracted in this low range of temperature could be extrapolated to higher temperatures. Blank experiments confirmed that no gas phase reaction occurred in the range of temperature studied. It was also observed that the combustion catalyst was subject to a hysteresis between a low activity state and a high activity state, consistent with the well known oxide-to-metal transition phenomena of the catalyst active phase.

The following 5-parameter power-law reaction rate was derived from the experimental values:

$$r = \frac{dC_{C8H16}}{Wdt} = k_0 \cdot \exp\left(\frac{-E_A}{RT}\right) \cdot y^a_{C8H16} \cdot y^b_{O2} \cdot y^c_{CO2}$$

where,

r = reaction rate [mol·g_{cat}^{-1}·min^{-1}]
C_{C8H16} = number of moles of gasoline[mol]
W = catalyst mass [g]
k_0 = pre-exponential factor [mol·g_{cat}^{-1}·min^{-1}]
E_A = apparent activation energy [J·mol^{-1}]
R = universal gas constant (8.314 J·mol^{-1}·K^{-1})

T = reaction temperature [K]
y_i = mol fraction of species *i* [-]

Numerical values were determined experimentally for the following parameters: k_0, E_A, a, b and c for CESI proprietary combustion catalyst using ANL Benchmark Fuel I containing 10 ppm sulfur. This rate expression and these numerical values were included in the modeling of the steam reforming plate-based reactor. Figure 2.11 shows that this rate expression describes the experimental measurements relatively accurately.

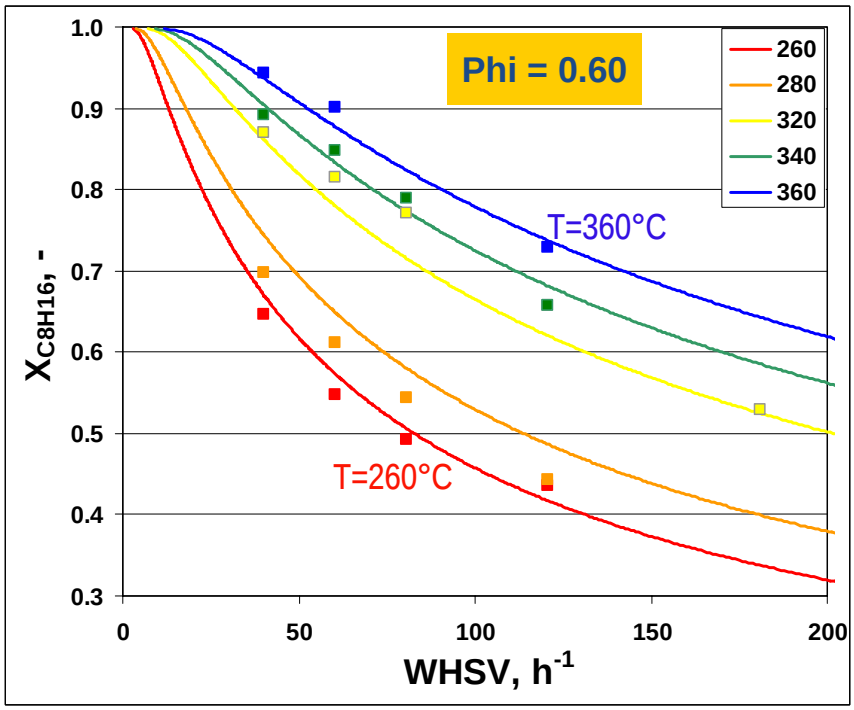

Figure 2.11. Gasoline combustion kinetics: tests results and model (lines). Operating conditions: P = 1 atm, fuel: ANL Benchmark Fuel I + 10 ppm S, Phi = 0.60.

The durability of the combustion catalyst was not tested *per se* in this program, since extensive testing of the same catalyst has been done by CESI in other projects. In these other projects, a catalyst durability of more than 8000 h has been demonstrated, exceeding the target durability of 5000 h in this program.

3 Water Gas Shift catalyst development

CESI's approach of water-gas shift (WGS) reaction was deliberately directed towards using non-noble metal based catalysts, in order to operate the reaction at a lower temperature than with noble-metal based catalysts and thus benefit from the favorable thermodynamic equilibrium. Both the kinetics and catalysts performance tests were done in a wall coated annular reactor, similar to the steam reforming reactor.

3.1 Kinetics

After a preliminary phase of catalyst development, a catalyst formulation that exhibited a reasonably stable activity was chosen to perform kinetics measurement tests. The study targeted a power-law for the expression of the reaction rate and used the differential reactor approach, varying the partial pressure of one component after the other to then extract the exponent of each of the component individually. The following model was obtained, through parameters regression using PolyMath 2.0 software. It successfully described the WGS reaction rate in the temperature range of interest ($220°C<T_{rx}<300°C$).

$$r_{wgs} = A\exp\left(\frac{-E_A}{RT}\right)\left(P_{CO}\right)^{1.03}\left(P_{H2O}\right)^{0.53}\left(P_{CO2}\right)^{-0.34}\left(P_{H2}\right)^{-0.47}\left(1-\beta\right)$$

where $\beta = \frac{1}{K_{wgs}}\frac{\left(P_{CO2}\right)\left(P_{H2}\right)}{\left(P_{CO}\right)\left(P_{H2O}\right)}$

and

r	=	reaction rate [mol CO·g_{cat}^{-1}·min^{-1}]
A	=	pre-exponential factor [mol·g_{cat}^{-1}·min^{-1}]
E_A	=	apparent activation energy [J·mol^{-1}]
R	=	universal gas constant (8.314 J·mol^{-1}·K^{-1})
T	=	reaction temperature [K]
P_i	=	partial pressure of species *i* [atm]
K_{wgs}	=	thermodynamic equilibrium constant [-]

3.2 WGS catalyst development program

The rapid deactivation of the catalysts was the primary challenge of the WGS catalyst development. Considerable progress was made on this issue as illustrated by Figure 3.1 which shows the performance of a few of the early catalyst formulations. The stability of the best performing catalysts was so high that it became necessary to develop a method to accelerate the testing of the catalysts. This is the subject of section 3.4 of this report.

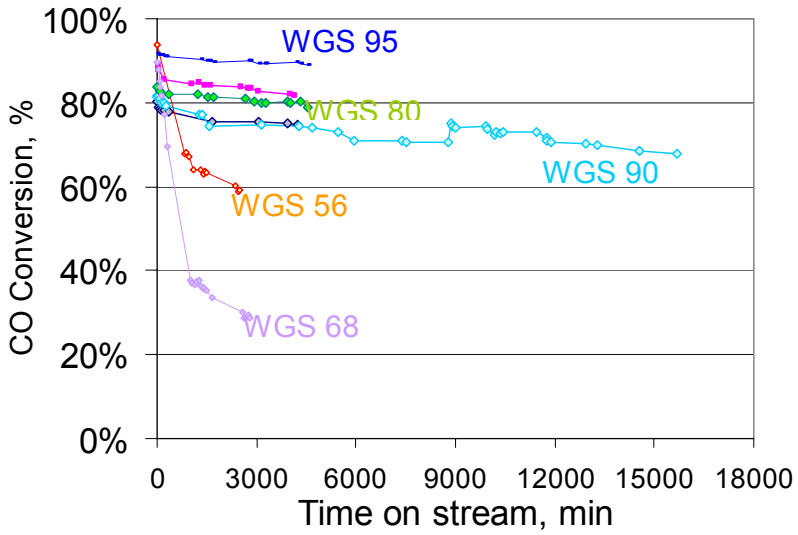

Figure 3.1. WGS catalysts durability: tests results. Operating conditions: P = 2 atm, T_{rx} = 255°C.

3.3 Reactor modeling

Among all three reactors of the fuel processor, WGS was certainly the one that required the most effort of chemical reaction engineering: the specific activity of the WGS catalyst was so low that it appeared that a single plate reactor would occupy a large part of the integrated processor volume. That is the reason why different reactor designs were considered and modeled, the objective being to reduce the size of the WGS reaction unit. A detailed study was done on a reactor design consisting of a monolithic adiabatic reactor in series with a plate reactor, as shown in Figure 3.2. Such a design allows most of the CO conversion to occur in the adiabatic stage at a higher temperature and to terminate the reaction in an isothermal plate reactor. It was found that by using such a staged reactors design, the total volume of the WGS unit can be reduced by 35%.

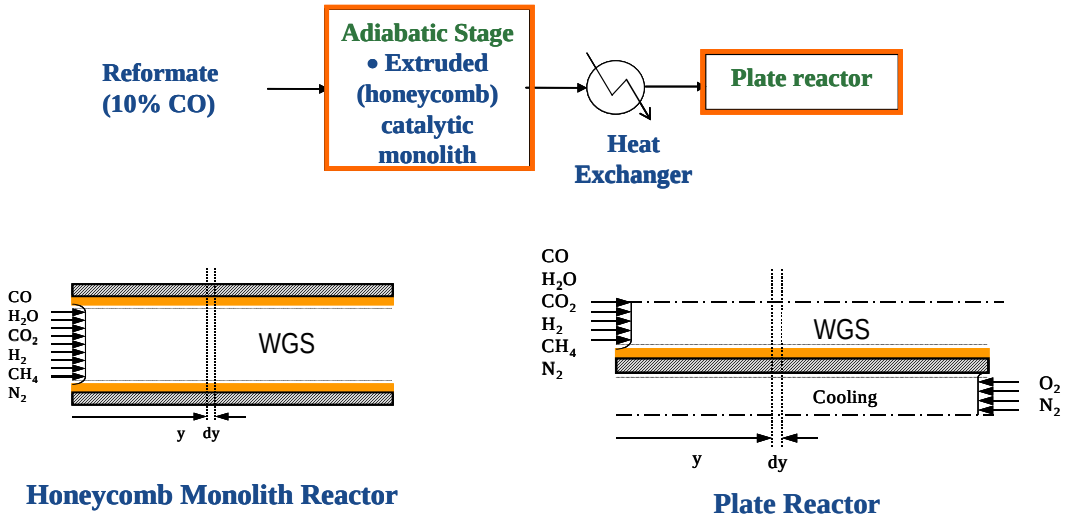

Figure 3.2. WGS reactor design: monolithic adiabatic reactor in series with a plate reactor.

3.4 Aging study

Durability data for WGS catalysts is very important due to the high sensitivity of this catalytic system to thermal degradation, reactant composition and operating conditions. For this reason, a static aging system was developed to age the catalyst materials for long times, *e.g*. up to the target durability of 5000 hours, with minimum effort and cost. The strategy is to age a large batch of the target material at conditions (temperature, gas phase composition) that simulate water gas shift reactor operation and periodically remove samples for characterization and activity testing. Unfortunately, no satisfying correlation between the catalyst activity decay in the accelerated aging reactor and the catalyst activity decay in the wall coated annular reactor was found.

3.5 Durability test

Based on the results of preliminary durability tests and static aging tests, the WGS-161 formulation was selected for a long term durability test with the objective of demonstrating at least 1000 hours of durability performance. Figure 3.3 shows the evolution of the catalyst activity (calculated using the power-law expression of section 3.1) versus time. The test included periodic catalyst regeneration, the oxidative regeneration cycle consisting of a 90-min exposure to air, at 300°C. The mechanism of the regeneration has been identified as being the removal of some carbon poisoning species from the catalyst rather than a re-dispersion of the metallic active phase. The level of activity after each regeneration is approximately constant at 1.3 to 1.5 times the initial activity for the first 4 regeneration cycles. Unfortunately, the rate of activity decay increases with each regeneration and after 4 regeneration cycles, a catalyst could not longer be adequately regenerated.

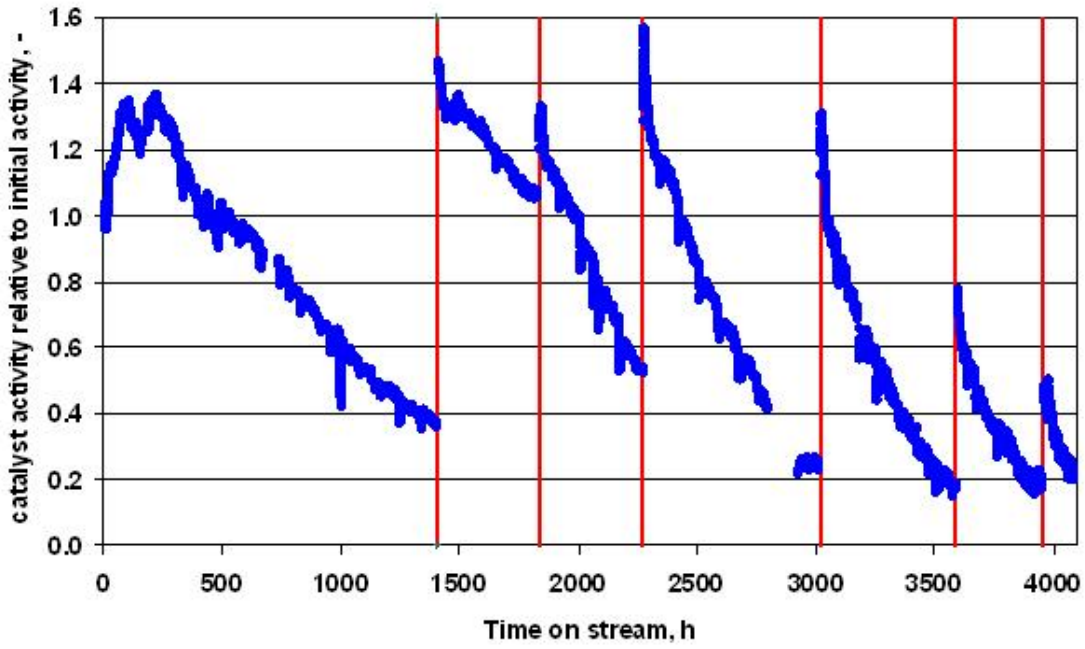

Figure 3.3. WGS catalyst long term test. Experimental conditions: T= 255°C, P = 2 atm, inlet gas: 10.3% CO, 8.5% CO_2, 35.3% H_2O, 45.9% H_2. Each vertical bar indicates a regeneration cycle.

4 PrOx catalyst development

The PrOx catalyst development followed the same approach as in the steam reforming and water-gas shift catalysts development programs: an early screening of catalysts performance, then the extraction of the reaction kinetics that were then integrated in a reactor model, then a second stage of catalyst development directed towards the findings from the reactor modeling.

4.1 Kinetics

Kinetics of the PrOx reaction were experimentally measured to model the PrOx reactor. Although a more detailed analysis of the reaction kinetics would implicate a Langmuir-Hinshelwood type of mechanism, a simplified power-law rate expression was extracted. This expression is specific to a given set of concentrations of hydrogen, water and carbon dioxide. Such a limitation is acceptable in the present situation since these concentrations are pre-determined by the steam to carbon ratio in the steam reformer and by the CO abatement in the WGS reactor, and practically these concentrations stay constant over the course of the CO preferential oxidation reaction. Hence, the CO oxidation reaction rate was represented by the following 4-parameter expression:

$$\frac{dCO}{Wdt} = k_0 \cdot \exp\left(\frac{-E_A}{RT}\right) P_{CO}^{\alpha} \cdot P_{O2}^{\beta}$$

The orders of reaction α and β, the activation energy and the pre-exponential factor were measured for the case where the inlet gas composition is the following:
O_2=1%, CO=1%, H_2=63.6%, H_2O=17.4%, CO_2= 15.1%, He= 1.9%

4.2 PrOx catalyst development program

The PrOx catalyst had to meet two performance requirements. The first requirement was given by the operation limits of the PEM fuel cells platinum electrocatalyst: the PrOx catalyst had to be able to achieve reduce the incoming CO to less than 10 ppm. The second requirement is for the PrOx catalyst to operate over a wide temperature range to facilitate the operation and control of the plate reactor under transient conditions. The PrOx catalyst development program primarily focused on achieving these two targets. The improvement of the selectivity and the durability of the catalyst come as a secondary objective.

For the inlet composition of the PrOx reactor, most of the testing has been conducted using the equilibrium steam reforming (SR) outlet concentration and a 90% CO abatement in the water-gas shift (WGS). This concentration depends on the SR catalyst temperature and on the steam to carbon ratio. Table 4.1 summarizes the range of inlet concentration that was used to test the performance of the PrOx catalysts. Typically, the inlet oxygen to carbon monoxide ratio ranged between 0.5 and 1.5. The reactor used in all the experiments was a wall coated annular reactor, similar to the one used for the WGS reactor. CO was analyzed by both IR and GC. The analysis of other products such as CO_2 and O_2 was done by GC.

Table 4.1. PrOx inlet concentration range.

	S:C = 3.0, T_{SR} = 800°C, WGS CO abatement = 90%	S:C = 3.8, T_{SR} = 800°C, WGS CO abatement = 90%
	molar fraction	molar fraction
CO	0.0116	0.0086
CO_2	0.1872	0.1633
H_2	0.5816	0.5054
H_2O	0.2174	0.3218

Figure 4.1 shows the performance of the first catalyst (PrOx-12) to achieve a CO conversion to less than 10 ppm, albeit on a narrow temperature window. PrOx-12 formulation then served as a basis for multiple subsequent catalyst developments. A matrix of the different catalyst compositions that resulted from this program is given in Table 4.2. A systematic study was conducted to quantify the effects on the catalyst performance (durability, activity, selectivity) of the following formulation parameters:

- noble metal precursor
- noble metal loading
- metal promoter
- metal promoter loading
- catalyst support pretreatment

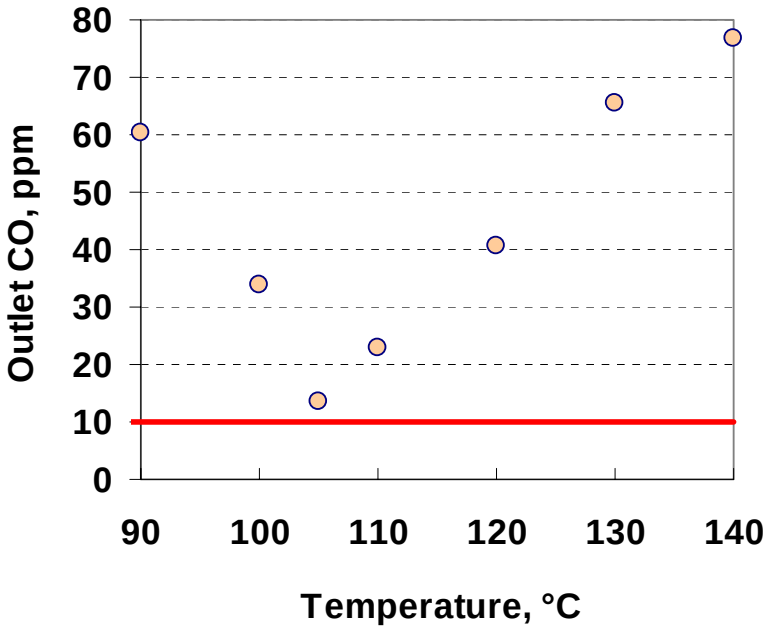

Figure 4.1. PrOx-12 catalyst performance. Operating conditions: P = 1 atm, inlet CO concentration: 1.0%, H_2 (54.3 %), CO_2 (17.4 %), O_2 (1.7 %), H_2O (25.6 %).

This study determined that none of the new formulations was significantly better performing than the PrOx-12, particularly in terms of durability. Several formulations provided a wider window of operating temperature, but deactivated rapidly. Temperature Programmed Desorption tests of fresh and used catalysts confirmed the rapid deactivation was due to loss of noble metal dispersion after catalyst exposure to steam.

After considering these results, the decision was made to explore a totally different class of catalysts which were based on a different noble metal and a different support. Very encouraging results in terms of operating temperature window were obtained with the first formulation of this new class of catalysts. This represented a breakthrough when compared to the previous class of catalysts. Figure 4.2 shows the level of CO achieved with PrOx-44: the target of a CO outlet concentration lower than 10 ppm was achieved over a temperature range of 35°C. This formulation was selected for further durability testing (described in section 4.3). Other variations of this formulation (using different noble metals or different level promoters in the support material) were also tested but did not perform as well as PrOx-44.

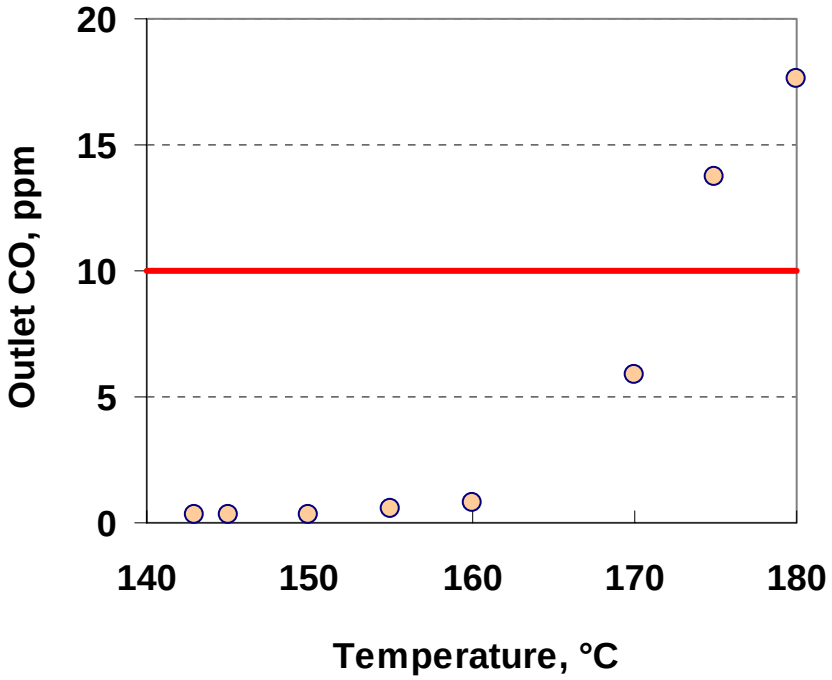

Figure 4.2. PrOx-44 catalyst performance. Operating conditions: P = 1 atm, inlet concentrations: CO (1.0%), H_2 (54.4 %), CO_2 (17.5 %), O_2 (1.5 %), H_2O (25.6 %).

Table 4.2 Matrix of the PrOx catalysts compositions.

Catalyst ID	Noble metal	Transition metals	Support
PrOx-1	A		1
PrOx-2	A		1
PrOx-3	A		1
PrOx-4	A	a	1
PrOx-5	A	b	1
PrOx-6.1	A	c	1
PrOx-7(II)	A	a	1
PrOx-7(III)	A	a	1
PrOx-7(IV)	A	a	1
PrOx-8	A	a	1
PrOx-9	A	b	1
PrOx-10	A	b	1
PrOx-11	A	b	1
PrOx-12	A	a	1
PrOx-12 (II)	A	a	1
PrOx-12(III)	A	a	1
PrOx-12(IV)	A	a	1
PrOx-12(V)	A	a	1
PrOx-12 (VI)	A	a	1
PrOx-12 (VII)	A	a	1
PrOx-12 (VIII)	A	a	1
PrOx-13	A	a+b	1
PrOx-13(II)	A	a+b	1
PrOx-14	A	b	1
PrOx-15	A	a+b	1
PrOx-16	A	a	1
PrOx-17	A	a+b	1
PrOx-18	none	c+b	1
PrOx-19	A	c+b	1
PrOx-20	A	d	1
PrOx-21	A	e	1
PrOx-22	A	e	1
PrOx-23	A	e	1
PrOx-23(II)	A	e	1
PrOx-23(III)	A	e	1
PrOx-24	A	e	2
PrOx-25	A	e	3
PrOx-26	A	e	4
PrOx-27	A	e	5
PrOx-29	A	e	6
PrOx-30	A	e	1
PrOx-31	A	f	1
PrOx-32	A	e	7
PrOx-33	A	e	8
PrOx-34	A		1
PrOx-34	A	b+e	1
PrOx-35	A	b+e	1
PrOx-36	A	e	9
PrOx-37	A	b+e	1
PrOx-38	A	a+e	1
PrOx-39	A	a	1
PrOx-40	A	a	1
PrOx-41	A	a	1
PrOx-42	A	a	1
PrOx-43	B	g	10
PrOx-44	B	g	11
PrOx-45	A	g	11
PrOx-46	C	g	11
PrOx-47	D	g	11
PrOx-48	A	g	11
PrOx-49	A	g	11

4.3 Durability tests

To follow and quantify long term PrOx catalyst deactivation, the experiments were run under conditions slightly different from the normal conditions that were used in the fuel processor. In the integrated fuel processor, the CO and O_2 conversions are essentially 100% and the reactor does not operate in a differential mode. Catalyst deactivation over time should be assessed with the reactor under differential mode. In order to maintain the reactor in a differential mode of operation, the space velocity was increased and the O_2/CO ratio lowered relative to the conditions of the performance test described in the previous section. Reaction temperature was maintained in the middle of the operating window. We also assumed that the mechanism of the deactivation of this class of PrOx catalysts would not be dependant on the O_2/CO ratio.

Results of the 1000 hour durability test presented on Figure 4.4 show a rapid deactivation followed by a stabilization of the activity. A duplicate of the first few hundred hours of the test showed a less substantial initial deactivation (Figure 4.4). To quantify the effect of time on stream on the catalyst performance, i.e. on its ability to achieve a high CO conversion, a measurement of the achievable outlet CO outlet concentration *vs.* temperature was done on a fresh catalyst and on the same catalyst after 200 hours on stream in the conditions described in the Figure 4.4 caption. The results shown in Figure 4.5 illustrate a slight narrowing and shifting of the operating temperature window.

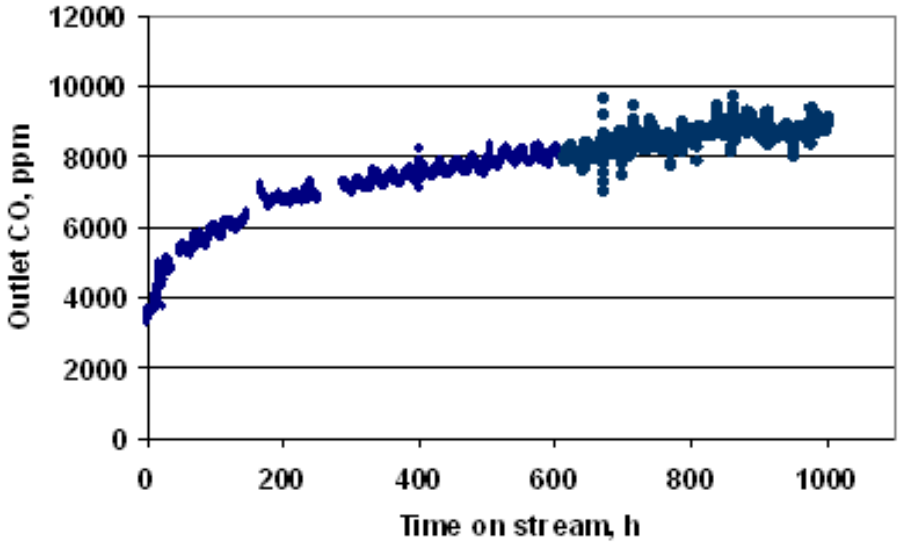

Figure 4.3. PrOx-44 catalyst long term performance. Operating conditions: P = 1 atm, inlet concentrations: CO (1.0 %), H_2 (54.6 %), CO_2 (17.6 %), O_2 (1.0 %), H_2O (25.8 %). T = 155°C.

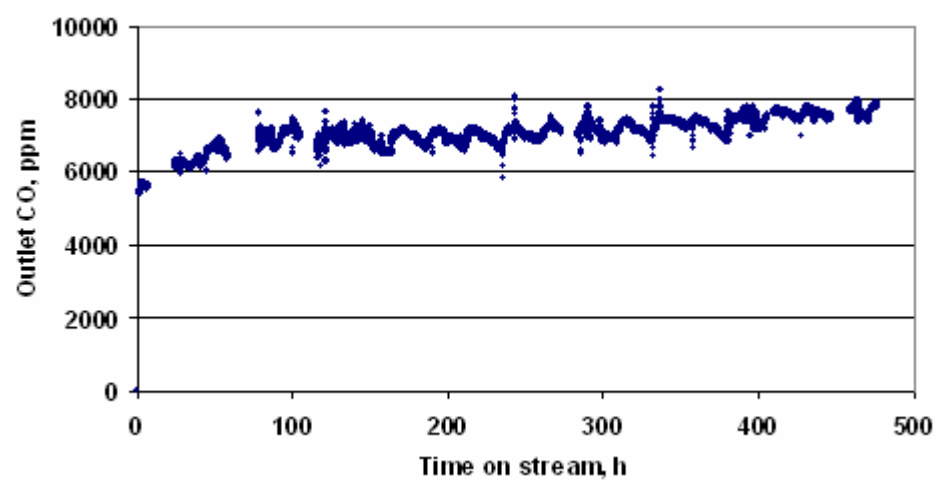

Figure 4.4. PrOx-44 catalyst. Second long term performance. Operating conditions: P = 1 atm, inlet concentrations: CO (1.0 %), H_2 (54.6 %), CO_2 (17.6 %), O_2 (1.0 %), H_2O (25.8 %). T = 155°C.

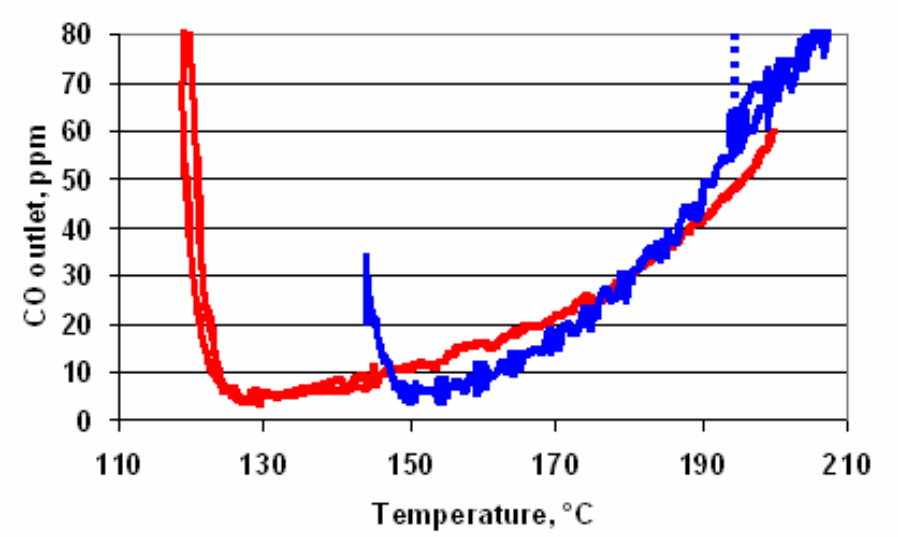

Figure 4.5. PrOx-44 operating window for a fresh (red curve) and for a used catalyst (blue curve) after 200 h on stream.

Summary of SR, WGS and PrOx catalysts performance

Table 4.3 summarizes the SR, WGS and PrOx catalysts performance in terms of specific activity, required catalyst mass per kW(e), and noble metal cost per kW(e). Numbers are based on the experimental catalysts activity after 1000 h on stream and on the average noble metals costs of November 2005.

Table 4.3. Activity, required catalyst mass, and noble metal cost of SR, WGS and PrOx catalysts

		SR-35	WGS-161	PrOx-44
specific catalytic activity	after 1000 h on stream	0.1131	0.0114	0.0074
		$g_{C8H16}/g_{cat}/min$	$g_{CO}/g_{cat}/min$	$g_{CO}/g_{cat}/min$
required catalyst mass	based on catalyst activity after 1000 h on stream	26.131	271.645	41.510
		g/kW(e)	g/kW(e)	g/kW(e)
noble metal cost	based on catalyst activity after 1000 h on stream	24.64	0.00	74.38
		$/kW(e)	$/kW(e)	$/kW(e)

5 Prototype Development

CESI's approach to designing and building a fuel processor is to base it on a plate-type heat exchanger concept. The plate-reactor design maximizes the heat transfer rate by incorporating exothermic catalytic combustion on one side of the plate to drive the endothermic steam reforming on the other side of the heat exchanger plate. A series of these plates are assembled together forming a plate stack of alternating reforming/combustion reaction zones. The idea is elegant yet simple. However, the fabrication of this plate-reactor has proven to be especially difficult. Since CESI's catalyst coating process requires the plates to undergo several high temperature calcination cycles, an oxide layer is created that covers the entire plate, including the portions that need to be welded together. The oxides act as a physical barrier to establishing a leak-free weld. Leak-free welds are critical to this reactor since any leakage between the reforming and combustion sides could result in a catastrophic failure of the reactor.

When assembling the plate stack together, channels have to be formed to serve as flow paths for the combustion reaction on one side of the plate which runs at atmospheric pressure, and the reforming on the other side which takes place at ~30 psig. This difference in pressure would most likely cause flexing of the flat plates that could eventually lead to mechanical failure. This implies that the plates need to be textured or corrugated in a manner that they can support each other. Therefore, it was decided that the foils forming these channels needed to have a self-supported structure to make them capable of filling the gap inside of the channel to avoid deformation and physically support each other while building the stack. In the face of these challenges, CESI looked into a variety of different plate reactor approaches and the feasibility of their

fabrication. The following sections describe the different designs that were researched before fabricating a prototype.

Modification of Existing Heat Exchanger Plates

One of the first ideas was to modify heat exchange plates from a commercial gas turbine recuperator. These plates did not have an ideal geometry for a catalyst coated plate reactor but did provide a relatively quick route to build a reactor system. Figure 5.0.a shows what the original recuperator plate looked like. The shaded blue section represents the cut-out sector that would act as a representative single plate for the plate reactor. Figure 5.0.b is an exploded image of this single plate, where the pink region represents the catalyst-coated section.

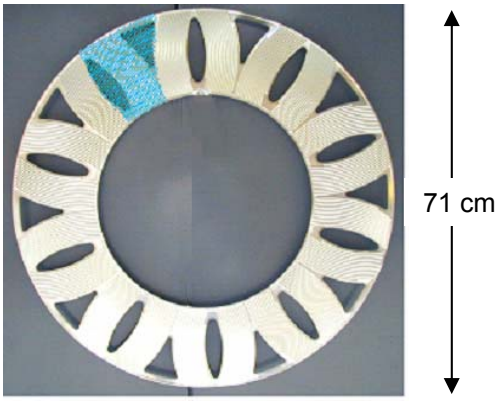

Figure 5.0.a. Recuperator plate used to make plate stack.

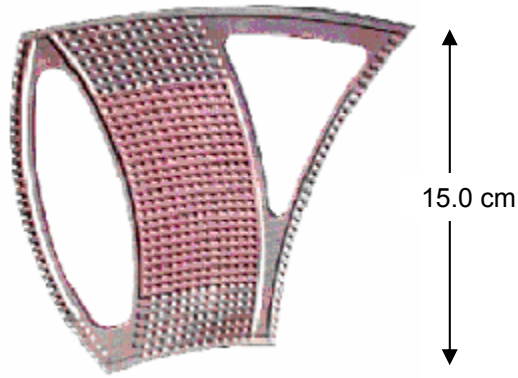

Figure 5.0.b. Individual section of recuperator.

Before deciding on if these newly cut plates could be used, two things had to be tested: 1) would the catalyst adhere to this inconel plate and 2) could the oxide layer in the welding area of calcined plates be removed so that the plates could be welded together.

To address the first issue, CESI successfully implemented a proprietary metal pre-treatment and catalyst coating process. Afterwards, the catalyst adherence was tested and showed the catalyst adherence to be adequate.

To address the second issue, it was necessary to physically remove the oxide layer in the welding area. Several samples of calcined plate were cleaned using a variety of different techniques, which included sand-blasting, solvent wash, acid wash, sand paper, and Dremel grinder wheel. Ultimately, the Dremel grinder wheel was the most effective solution for cleaning these heat exchanger plates because the laser welder was able to make a good, non-cracking weld using plates cleaned with this method. Figure 5.0.c shows an edge where the plates were successfully laser welded.

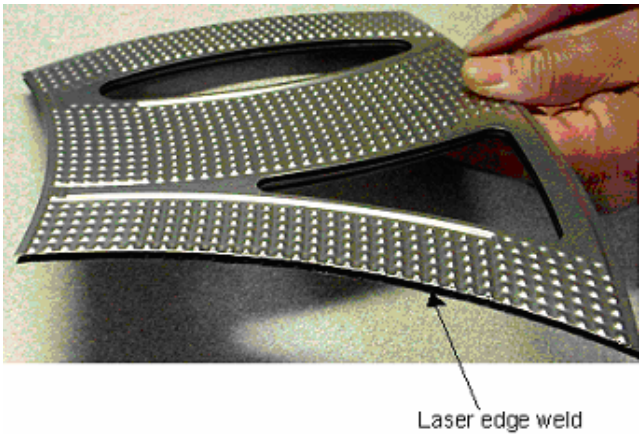

Figure 5.0.c. Laser edge weld.

Once it was determined that these calcined and cleaned plates could be successfully laser welded, it was decided that the option to modify the existing heat exchanger plates was realistic and going to be the fastest way to build a prototype. Therefore, the first prototype was indeed made from existing heat exchanger plates. This is discussed in detail in section 5.1.

Soft-tooled Custom Stamped Plates

Because there were many unknowns at the beginning of the prototype building process, it was important to explore other possible options. The second approach was to use conventional stamping technology to form flat plate stock into the required corrugated structure that would then be welded to form the desired plate reactor. This technique allowed CESI to design and choose the dimensions and material of the plate. The initial challenge was to find a vendor who would be willing to stamp plates at such low volumes and who could stamp corrugated plates without ripping through the plate material. Machining a dye to stamp plates is expensive and not worth the time investment for most vendors if fewer than 1000 plates are needed. Most vendors were not interested. The few that were interested were not able to stamp them as requested. Finally, D-Velco Manufacturing of Arizona (Phoenix, AZ) was eventually successful. Initial trials ripped through the metal at the peaks and valleys of the corrugation. Later, after modifying the corrugation dimensions, a plate was successfully stamped to dimensions similar to what was requested. Figure 5.0.d is a picture of custom-stamped foil.

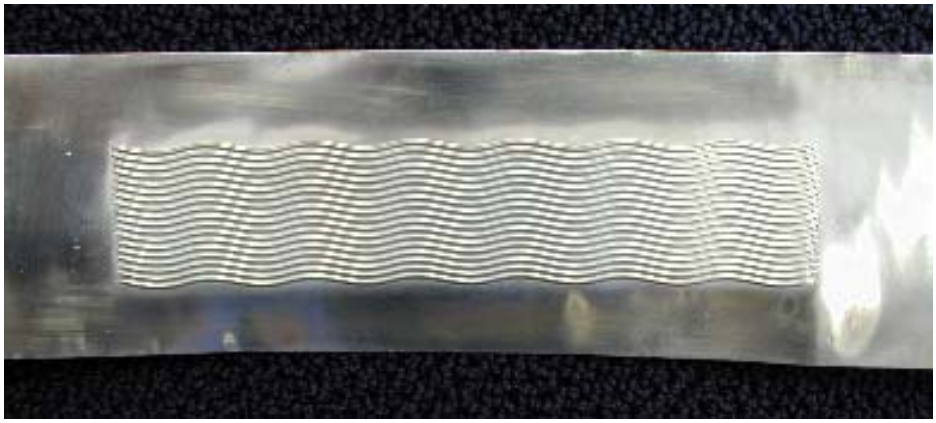

Fig 5.0.d. Custom-stamped plate.

Once custom-stamping became a realistic option, two different prototype designs were developed based on custom-stamped plates. One design required simple welds to reduce the difficulty in the fabrication process but resulted in a larger thermal mass. The other design included more complicated welds but had lower thermal mass to aid in the quick start-up time.

Eventually, weld trials that were performed on the existing heat exchanger plates were repeated on the custom stamped plates. One of the main differences, however, was that the custom stamped plate thickness was only 0.002" whereas the heat exchanger plate was 0.008". This reduction in thickness made it nearly impossible to weld, especially after being heat-treated. Many laser welders failed to make clean, leak-free weld samples. Eventually, an R&D laser welding shop named Applied Lasers, LLC (Concord, California) was able to successfully make a pressure-pocket sample that proved their welds were leak-free for the higher thermal mass design. They were selected to assemble this particular prototype. Months later, another laser shop called Southwestern Laser was found. After several attempts, they successfully fabricated a weld sample that proved their ability to make a leak-tight weld. They were selected to assemble the lower thermal mass design prototype.

Fin Folding

In parallel, a third design option to corrugate the plates using a metal folding process was being pursued. The "fin folding" process is widely used for the manufacturing of gas turbine recuperators and other heat exchangers. J.H. Benedict Co., Inc. (East Peoria, Illinois) has extensive experience with fin folding and construction of both prototype and production recuperators, so they were an obvious choice to do some test samples. Initially, trial fin folding was attempted with FeCrAlloy material, the preferred substrate material for the reactor plates. A close-up of the folded sample piece is shown in Figure 5.0.e. The FeCrAlloy has limited ductility resulting in cracking at the peaks of the folded corrugation as shown in Figure 5.0.f.

Figure 5.0.e. Pattern for test folding

Figure 5.0.f. Tears in fold pattern.

The corrugation height (0.093") for the initial attempt was taller than desired for the fuel reformer but utilized available tooling. After observing cracking with this fold pattern, straight folding with less height and no sinusoidal in-plane pattern was attempted. No fracturing could be seen in the material under 50x magnification. Therefore, new less extreme corrugation dimensions were specified and tested with success. Figure 5.0.g shows a successful repeated folding pattern with no tears.

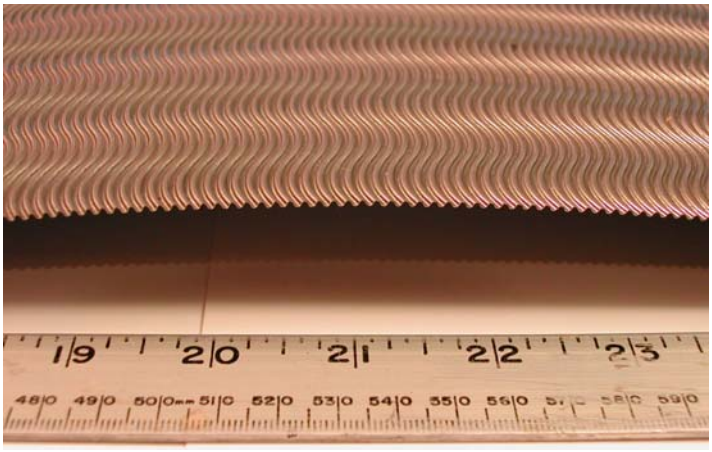

Figure 5.0.g. Repeated folding pattern with no tears.

The next issue to address was preparing the edges for welding by flattening the edges of corrugated plate. This meant that the edges needed to be crushed and flattened after the fin-folding process. This crushing, however, resulted in tiny cracks, as can be seen in Figure 5.0.h.

Figure 5.0.h. Cross-sectional view of crushed foil.

J.H. Benedict continued working on trying to resolve the cracking problem, but it was difficult to measure progress. Magnified views only provided qualitative results. Therefore, they made a pressure test sample using the edge crushing and welding process. Figure 5.0.i pictures several of the pressure samples that were welded together to test for leak-tightness.

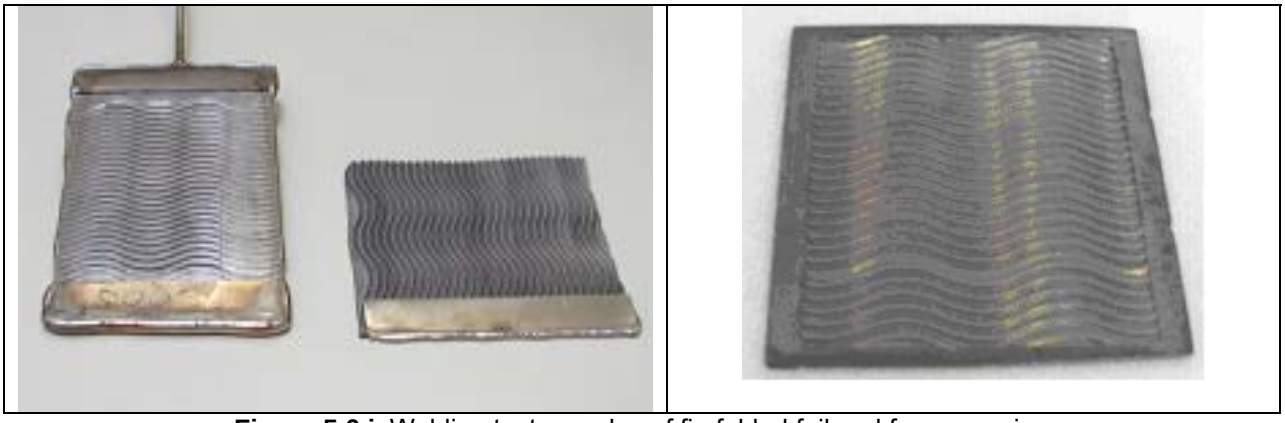

Figure 5.0.i. Welding test samples of fin folded foil and frames, using TIG (left picture) and Laser (right picture) welding techniques

Unfortunately, these welds were not leak-free. There were leaks created either during the crushing process or when the plates were welded to the frames. Even though the section was crushed, there were still air gaps that the welding could not overcome and fill. Repeated trials continued to result in leaks. This proved to be an unresolvable problem. Eventually, the design method of fin folding the metal was abandoned due to the inability to make leak-free welds.

5.1 Generation 1 prototype (AGT)

5.1.1 Build of AGT-1 prototype

As previously mentioned, the first generation prototype was made by modifying existing heat exchanger plates. The part number of the recuperator that the plates were originally designed for was AGT-1500, so AGT-1 was used as the name for the prototypes made from these plates. Once it was proven that the plates could successfully be welded together, the next step was to make a blank plate stack without any catalyst to fully develop the process that would be used with plates catalyst coated plates. Figures 5.1.a and 5.1.b illustrate the blank plate stack and its steam reforming (SR) inlet and outlet manifold flanges.

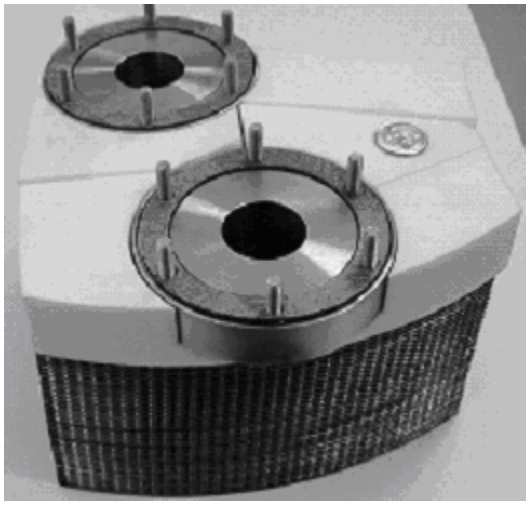

Figure 5.1.a. Blank plate stack with Macor insulation on top.

Figure 5.1.b. Blank plate stack with Fiberfrax insulation.

The white layer surrounding the manifold flanges is a rigid insulation called Macor. It was important that this insulation was rigid in order to press the plates firmly against one another. This was necessary because part of the SR channels had pressure seals as inherent design features of the corrugation. Without something rigid that the plates

could push against, these uncompressed seals would have resulted in feed gas bypassing the SR catalyst coating.

The other white insulation along the sides of the plate stack is flexible Fiberfrax. This insulation was stuffed into as much open space within the reactor housing box as possible in order to prevent the combustion gases from flowing around the stack. By filling up the open space, this forced the combustion gases to flow through the plate stack.

While a blank plate stack was being fabricated, so were the reactor housing box and top box cover. Figure 5.1.c is a picture of AGT-1 housing.

Figure 5.1.c. Reactor housing box and top box cover.

To make the coated plate stack for AGT-1, it was necessary to actually coat the appropriate sides of the plates with the appropriate catalyst with heat treatments after each coating application. CESI's coating rig was used to apply the combustion and steam reforming catalysts to the appropriate thickness and to the appropriate sides of each plate. After calcination, the plates were sent to the laser welder at D-Velco to begin the process of assembling coated plate stack. The welding of this plate stack proved to be much more difficult than the blank plate stack due to oxidization layer that built up from the calcination cycles. After the plate stack was completely welded together, it had to be pressure-leak tested. A device was fabricated that would pressurize the SR side. After pressurizing the plate reactor, a valve was then closed to isolate the pressurized side. If the pressure dropped, then there was a leak. Refer to Figure 5.1.d for a picture of the pressure-leak test device.

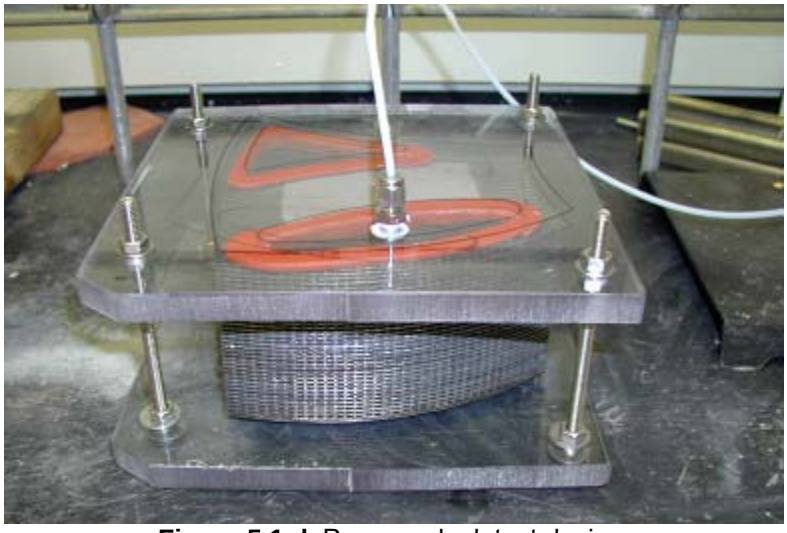

Figure 5.1.d. Pressure-leak test device.

Ultimately, this first attempt to fabricate a leak-tight plate stack proved to be unsuccessful. There were micro-holes that would allow the higher pressure steam reforming mixture to flow into the lower pressure combustion side. Given that there is hydrogen in the steam reforming mixture, this posed a potentially hazardous situation. However, it was decided to assemble the entire reactor to run preliminary combustion tests without running any reactions on the steam reforming side and to verify that all the controls, instrumentation, and software worked properly.

Supporting Laboratory Set-Up

During this prototype fabrication, it was necessary to develop the system that would handle the data acquisition, I/O, and controls. National Instruments hardware was purchased that would handle all the I/O signals. A technical work document was written that included what type of signals needed to be recorded (temperature, pressure, flowrates) and what type of outputs had to be sent to controlling equipment (mass flow controllers, valves, and fuel injectors). Eventually a software programmer was contracted to write a program in LabVIEW.

The assembly of the prototype system required that all of the supporting equipment was in place in the laboratory set-up. It was necessary to install the balance of plant equipment, such as pressure transducers, thermocouples, valves, mass flow controllers and sensors, pumps, injectors, heaters, burst disc, etc. Figures 5.1.e and 5.1.f provides some perspective of the experiment set-up.

Figure 5.1.e. Lab set-up with heat exchangers, back pressure regulators, reactor, etc.

Figure 5.1.f. Lab set-up with reactor, thermocouples, injectors, and heaters.

Figure 5.1.g shows the piping and instrumentation diagram (P&ID) that describes the system. This, however, evolved as changes were continually being made to improve the system.

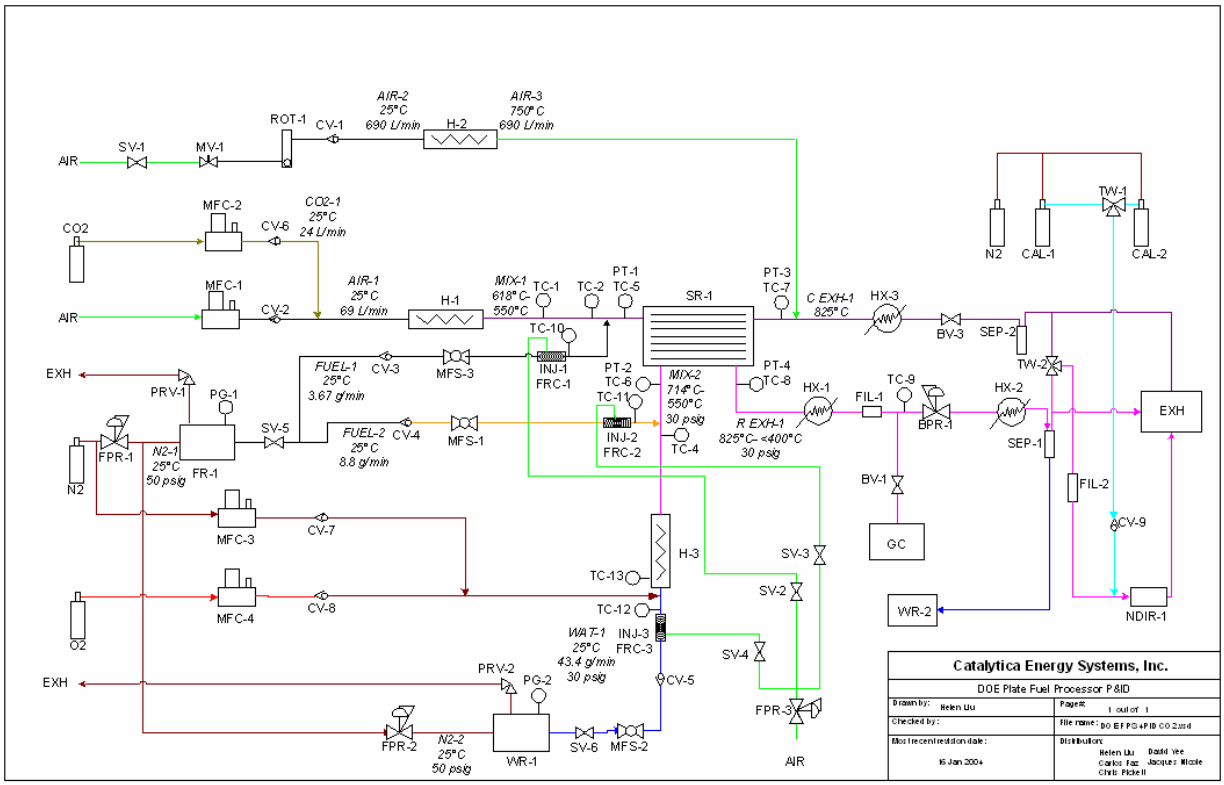

Figure 5.1.g. Piping and Instrumentation Diagram.

A systematic check of the balance of plant equipment was necessary to make sure that all the equipment was functioning properly. The fuel delivery system was an extremely important factor. Too much fuel flow on the combustion side might increase the temperature to the melting point of the metal plates. Too little fuel might decrease the temperature to the point where coking occurs on the steam reforming side. Inaccurate flows into the steam reforming side would affect the steam to carbon ratio, which could also result in an acceleration of the coking, or in incomplete conversion.

Initially, pulse-width modulated (PWM) fuel injectors were selected to control and dispense the different liquid flows. The required flow rates for gasoline and water were on the low end of the flow spectrum for the fuel injector that was selected. This was the lowest-flow injector that was found that did not have to be specially designed and fabricated for the flows corresponding to a 3 kW(e) fuel processor. Software was developed that controlled the percent duty that the fuel injector would open and the frequency at which the injector would pulse. The fuel injectors were calibrated so that different settings of these two parameters resulted in known flow rates. Further issues related to liquid delivery devices will be discussed later.

The pressure of the steam reforming side was controlled by a back pressure regulator that was installed downstream of the steam reformer. The major issue surrounding this piece of equipment was the PID loop that was going to control the upstream pressure when different flowrates of reformate flowed through it. The different parameters for P

(proportional or gain), I (integral), and D (derivative) were determined using the Ziegler-Nichols closed loop tuning method.

The heater to control the inlet combustion gas temperature also required a PID loop. These PID parameters were determined using the Cohen-Coon open loop tuning method. For start-up purposes, there was also a very large heater that was a new product with untested maximum limits. This heater, however, did not have a control feedback loop. Because it was only going to be used for a short period of time to initially heat up the stack, it was controlled by the operator who simply turned on and off the heater, depending on stack temperature. During start-up heat tests, it was determined that operating the heater at 100% power was not safe, even at the maximum flow rate of air (700 SLPM). Because this was a new product for the manufacturer, its maximum operating temperature at different air flow rates had not previously been tested and confirmed. Operating it at 100% power overheated the heater and melted major internal components. Eventually, back-up/replacement heaters were purchased and tested. It was determined that operating the heater at 80% of its maximum power at an air flow rate of 700 SLPM was safe. Heater start-up tests were performed in order to determine how quickly the plate reactor could be heated up to the required temperature for the initiation of the steam reforming reaction.

Another major challenge was generating superheated steam at the temperatures (350°C) and flow rates needed (4.5 to 45 g/min). The original idea to generate steam was to use a fuel injector to spray water onto a 5 kW, 208 V spiral heater. This idea was tested but eventually failed. The failure was most likely due to an uneven distribution of water on the heater. Without enough water falling evenly over the entire length of the heater; hot spots most likely developed and melted part of the heater. A second attempt was made using a different type of water delivery system. A number of stainless steel filters were welded together to form one long filter with an outer diameter of less than an inch. The new long filter was then filled with stainless steel beads and then inserted into a working 3 kW Watlow Starflow spiral heater. Water was pumped through the filter and vaporized more evenly along the length of the spiral heater. This idea seemed to work well at most water flow rates. However, at the desired flow rate of 45 g/min, it was just barely vaporizing all the water. After letting the heater cool and removing the filter for inspection, the filter broke in half. The high temperatures of the heater clearly compromised the integrity of the filter, making it so weak that it could not be handled. Eventually, a fixed bed steam generator was installed in the system that had a tremendously slow start-up time due to its thermal mass but could deliver the flowrate and temperature of steam required to complete the initial steam reforming tests.

The analysis equipment that was used consisted of two non-dispersive infrared analyzers (NDIR), one to measure the CH_4, CO, and CO_2 content of the reformate stream and one to measure the CO and CO_2 content combustion exhaust stream, and a gas chromatography (GC) analyzer to measure the H_2 content in the reformate stream. The NDIR analysis is continuous, whereas the GC takes a sample once every 18 minutes.

5.1.2 Preliminary tests on AGT-1

As previously mentioned, despite valiant attempts, the first coated plate stack was assembled but not without leaks. It was decided to use it to test the combustion side as well as the supporting laboratory set-up. The first test was an auto-ignition test. Because the design of the combustion side of the plate reactor required flowing a pre-heated air-fuel mixture, it was necessary to determine if auto-ignition would occur *prior* to the reactor itself. Mixtures of various oxygen equivalence ratios (phi) at different inlet temperatures were tested for spikes in the outlet temperature. If a spike in temperature should occur, this would suggest that auto-ignition of the reactive mixture was occurring.

The phi's tested for auto-ignition ranged from 0.25 to 0.95 at inlet temperatures of the plate stack of up to 450°C. Auto-ignition did occur when phi was greater than 0.4, but the belief was that reducing the inlet temperature would reduce the likelihood that auto-ignition would occur. Additional combustion tests were performed to see if reactor temperatures were close to the adiabatic temperature, depending on phi and flow rates. For these tests, more thermocouples were placed within the plate stack. Six additional thermocouples were installed within the plates of the reactor. They were placed at different heights as well as at different lengths along the plate in the direction of the flow. This temperature profile indicated that the temperatures were actually reaching temperatures much higher than the exit gas thermocouple had indicated. The adiabatic gas temperature was already being achieved close to the inlet of the plate stack. Gas phase combustion was indeed occurring a much lower phi's than 0.4. Because the temperature profile decreased along the length of the coated catalyst section, the reaction was not only occurring catalytically on the coated plates but in the gaseous phase. The graph in Figure 5.1.h illustrates the temperature profile in the reactor.

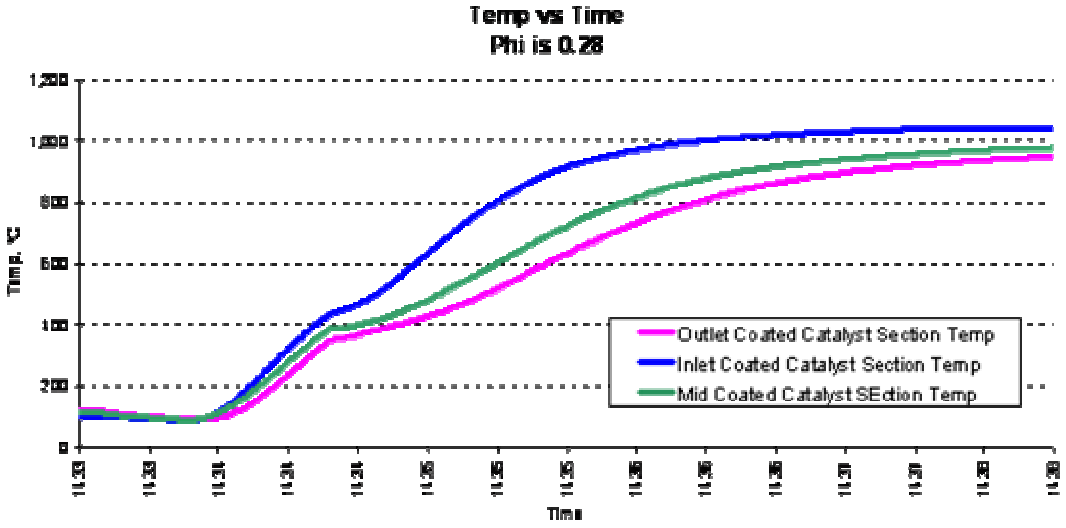

Figure 5.1.h. Temperature profile along the length of the coated section of reactor when phi = 0.28, during start-up.

The temperature of the outlet of the coated catalyst section was colder than the mid-point or inlet of the catalyst section. The inlet T was the highest temperature when phi was greater than 0.2. At phi's lower than 0.05 and inlet combustion gas temperature

less than 250°C, there was an increase in temperature as the combustion gas proceeded down the length of the reactor. But otherwise, the inlet temperature was always the highest. This was disappointing since it was preferred to have the combustion take place catalytically on the plate where heat transfer would be through conduction across the plate whereas combustion in the gas-phase would require both convective and conductive heat transfer to reach the reforming catalyst.

In order to fully understand this problem, the influence of two parameters was investigated: inlet air temperature and phi. An inlet air temperature parameter test was performed where a constant phi was maintained but inlet air temperature was increased to see how the reactor temperatures would react. Figure 5.1.i illustrates the results of a test where phi was kept relatively constant at 0.12 but the inlet temperature was varied.

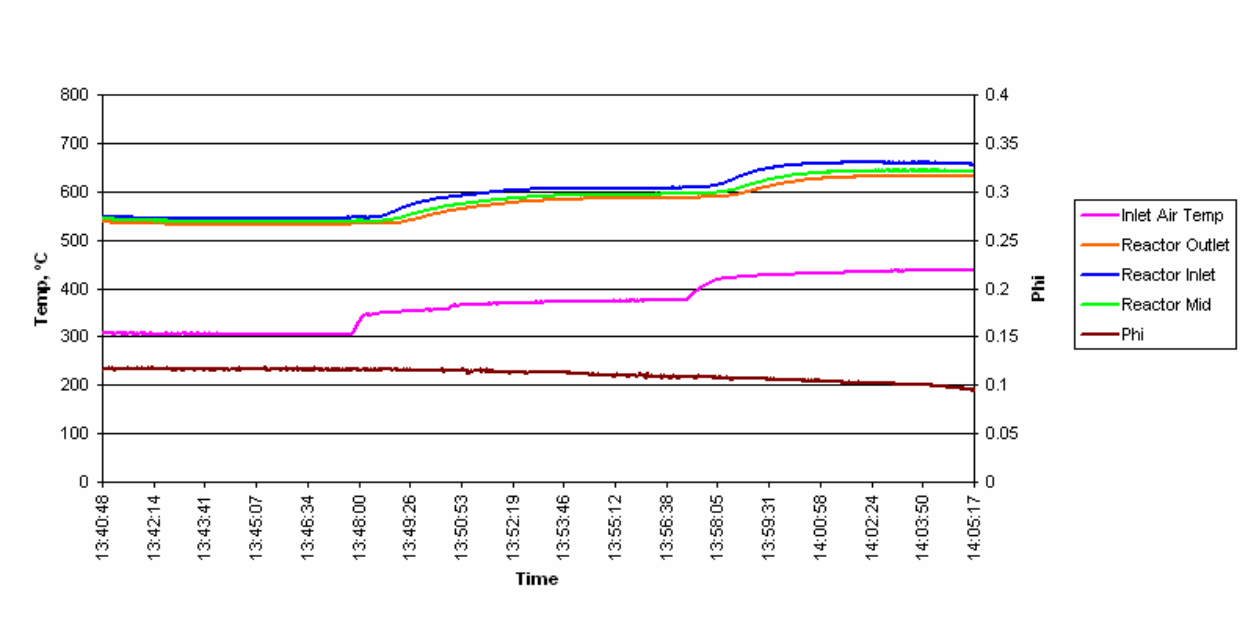

Figure 5.1.i. Temperature versus time when phi = 0.12 and inlet air temperature is varied.

The results from this graph indicated that there was complete combustion was occurring at the plate reactor inlet for each of the air inlet temperature since the reactor inlet temperature was higher than the reactor outlet temperature. The same test was performed using a different phi. See Figure 5.1.j for temperature profiles where phi was roughly 0.05.

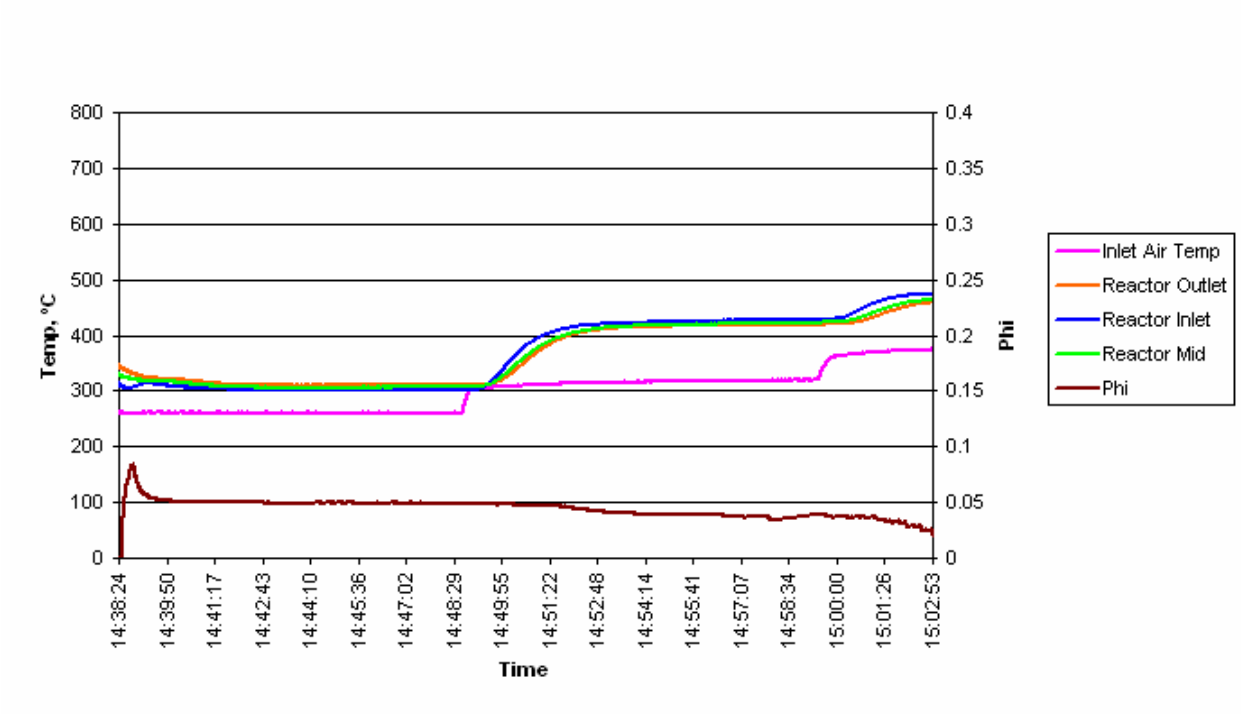

Figure 5.1.j. Temperature versus time when phi = 0.05 and inlet air temperature is varied.

The first half of the graph suggests that there was no combustion occurring since the inlet reactor temperature did not exceed the mid or outlet temperatures. This was when the inlet air temperature was close to 260°C. However, when the inlet air temperature was increased to 320°C, the reactor inlet temperature was once again the highest, which suggests that significant combustion was occurring at the plate inlet under these conditions in the reactor. Also, it was useful to know how phi affects the reactor temperature without changing the inlet air temperature. Table 1.1.a lists three different phi's and the resulting mid reactor temperature.

Table 1.1.a. Steady-state temperature of the reactor (mid-point) as a function of phi.

Phi	Air Inlet Temp, °C	Reactor Middle Temp, °C
0.06	380	500
0.1	380	575
0.2	380	750

One of the major DOE milestones was quick start-up time for the gasoline fuel processing system. The intention was to use electric heaters to pre-heat the reactor to light-off temperature and then turn on combustion gas to finish heating the system. A heating scheme was developed that used 2 heating air streams – one stream was close to 700 SLPM of air (heated by a 12 kW, 480 V 3-phase heater), and the other combustion air stream was close to 70 SLPM (heated by a 5 kW, 208 V heater). The automated heating scheme was programmed to turn off the large airflow and the larger heater once the reactor

outlet temperature indicated that the reactor was at an appropriate temperature to start catalytic combustion. The smaller 70 SLPM airflow and its corresponding heater were kept on, and the heater's temperature set point was adjusted to an optimal condition. Gasoline flow commenced at this point and was vaporized by the heated air. This hot mixture of gas and air then passed through the combustion section of the plate stack, reacting, and heating up the metal foil plates. Figure 5.1.k is an example of the temperature profile of the reactor during a rapid start-up test:

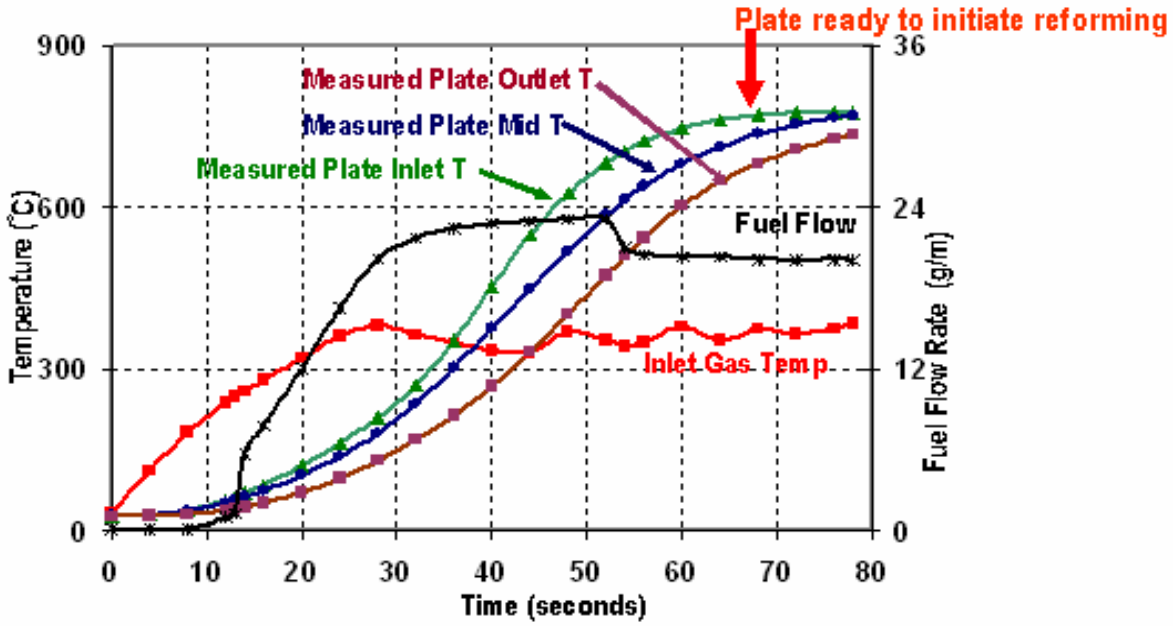

Figure 5.1.k. Rapid start-up temperature profile within reactor during April 2004 test.

This test demonstrates that it was possible to reach the SR light-off temperatures (at least 750°C) within 70 s of turning on the reactor from room temperature.

5.1.3 Build of AGT-2 prototype

Because it was known that there was a leak between the combustion side and steam reformer side of AGT-1, a second AGT plate reactor, called AGT-2 was fabricated. Some minor modifications were made to address a few of the issues that were discovered with AGT-1. During its assembly, the most important issue was to make sure that every plate pair that was welded together was leak-free. This meant that the integrity of the inlet/outlet SR manifolds that were located within the interior of the plate pairs had to be tested. A special device was built to test these manifold weld regions, and each pair was tested. Upon completion of testing of these individual pairs, the welding of the plate stack commenced. After each plate pair was welded onto the plate stack, another pressure leak testing device was used to verify that the there was no crossover between the two sides. This testing happened after each new plate pair was welded onto the plate stack.

After completing the weld assembly, the plate stack was fully instrumented to monitor temperature a various loctions. Figure 5.1.l is a picture of the instrumented plate stack with the top box cover, SR manifolds, and SR thermocouples. Figure 5.1.m shows where the thermocouples were placed within the reactor and just upstream and downstream of the reactor.

Figure 5.1.l. Plate stack with top box cover, SR inlet/outlet manifolds, and thermocouples instrumented on the SR side.

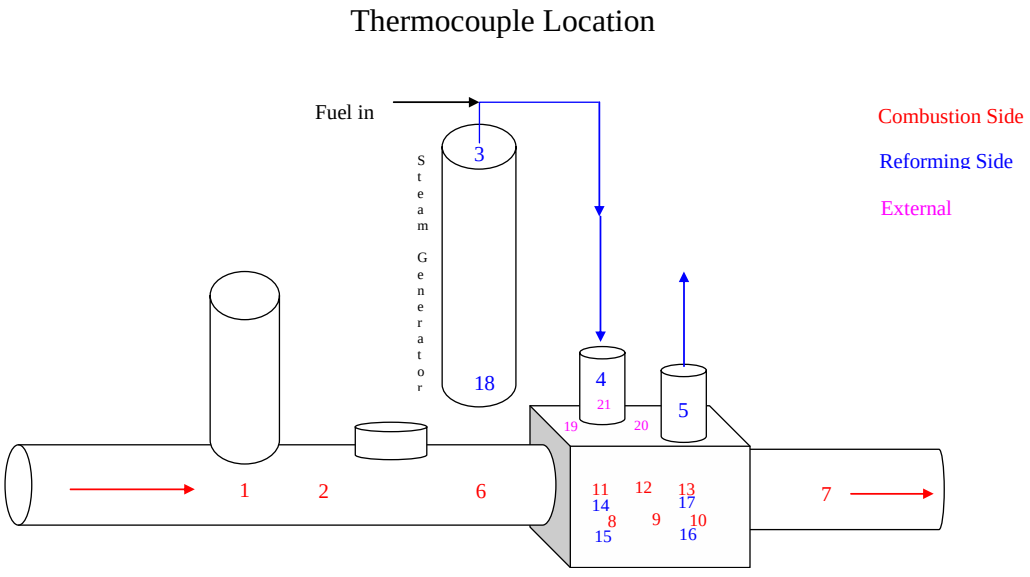

Figure 5.1.m. Thermocouple location within system tubing and reactor.

Figure 5.1.n is a birdseye view of what the reactor box looked like before the plate stack was placed in the container. The holes were drilled out of the Macor in figure 5.1.n so

that pockets of air could serve as better insulation against conductive heat losses to the outer metal box. Holes were not drilled out of the top sections because the top sections were a little more delicate and intricately-shaped in order to conform with the manifold areas.

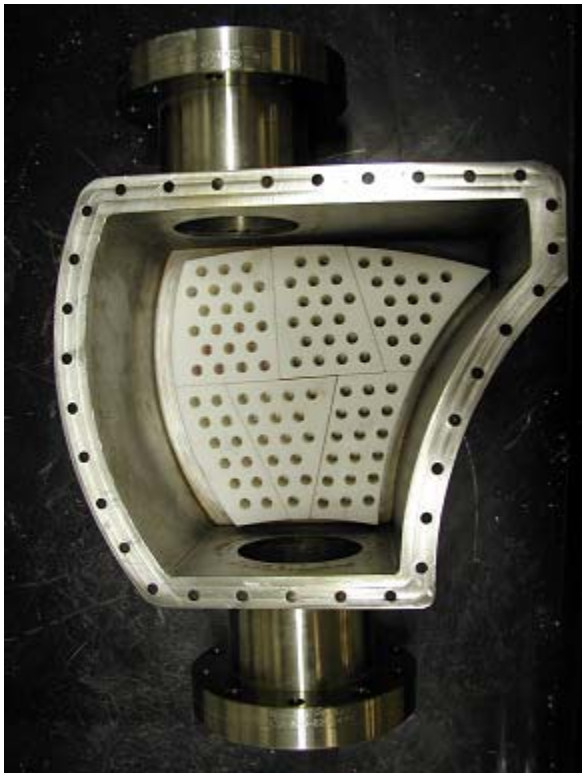

Figure 5.1.n. Bottom section of reactor box with drilled-through Macor insulation.

Another issue concerning AGT-1 was that it was very difficult to seal the top plate cover to the reactor box and to the SR manifold. Leaks were found around the gasket that connected the top plate cover to the reactor box. Originally, silver-plated copper gaskets were used, and there was a raised lip on the edge of the box that was intended to maintain a certain stress between all the plate pairs. However, this raised lip kept the top plate from bolting down enough to hold pressure. After trying numerous gasket layering schemes, the raised lip was eventually cut off. The gasket material was changed to grafoil. A simple single 1/8” grafoil gasket was cut out to fit the odd-shaped box. Without the lip, the top box cover was pressed down as much as required onto the grafoil to form an air-tight seal.

It was determined that the bolts and the threaded studs within the SR flange/manifold areas could not provide the compressive load required to deform the silver-plated copper gaskets. Simply changing the gasket material to grafoil was not an adequate solution. Three different sealing paths were investigated to prevent leakage at this manifold. One idea was to use metal C-ring gaskets which do not require as much compressive loading to properly seal. Another idea was to use custom-made O-rings

made from thin silver wire. The last idea was to change the flange/manifold on top of the plate stack by installing new type of sealing flanges. The same knife-edge sealing design of the flanges which were used to seal the tubing in other areas of the system were employed. Double knife-edge seals and silver-plated copper gaskets were designed and custom made. The new flanges were welded onto the plate stack, making this approach the most successful in addressing the leaking problems. Figure 5.1.o shows how each manifold had a double knife-edge seal.

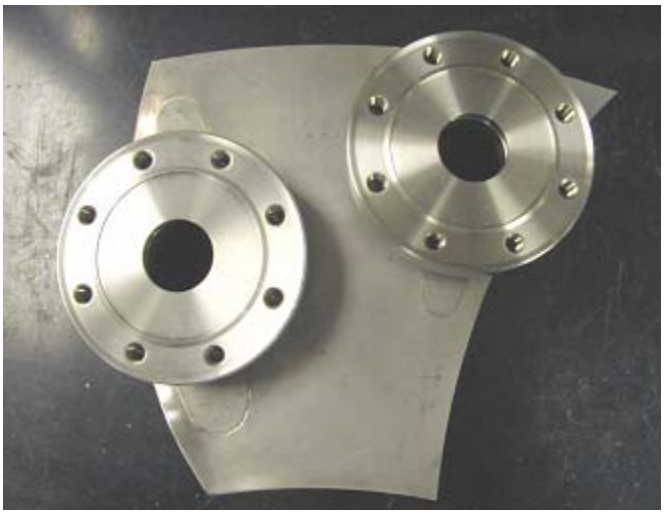

Figure 5.1.o. New SR inlet/outlet manifold seals.

5.1.4 AGT-2 testing, part 1

The goal of the initial testing was to show 5% load steady state operation, followed by a ramp up to 100% load, then continuous operation at 100% load steady state, followed by a ramp down to 10% load. A general test plan on Table 5.1.b lists the flows required to reach these levels of operation.

Table 5.1.b. Flowrates needed to reach 5%, 10%, and 100% load.

Parameter		5% load	100% load	10% load
Combustion fuel flowrate	g/min	2.5	5.5	2.5
Combustion air flowrate Used for fine tuning Temp.	L/min	127-135	157-163	110-123
Reforming water flowrate	g/min	2.2	43.4	4.4
Reforming fuel flowrate	g/min	0.44	8.8	0.88
(TC-2) Air T prior to INJ-1	°C	350	350	350
Φ	_	0.22	0.40	0.24
Reformable T prior to reactor	°C	350	350	350
Nitrogen SR tracer flow rate	L/min	1	7	1.5

Prior to testing, the steam generator was heated for over an hour, to allow it to reach a temperature of over 900°C. The testing began by starting the combustion side air flow and heating the reactor with the electric heater to about 350°C, high enough to light off the combustion catalyst. Upon reaching 350°C the combustion fuel was started and ramped up to 2-2.5 g/min to heat the plates in the reactor up to 825-850°C. The water was then started at the level of the first load condition, and within a few minutes the reforming fuel was turned on to the same load condition. The combustion side air was manually adjusted to fine tune the temperature of the plates. To decrease the temperature slightly, the air flow was increased. In general, the combustion fuel and reforming fuel were both ramped up during a load change, and combustion air flow was set to target a particular phi and then fine tuned for control. GC samples were taken at all major load intervals, and continuous NDIR data was acquired.

Testing started with 5% load conditions. The system was run at this load for one hour before beginning to ramp up to 100% load. The ramp up to 10, 20, 30 and 40% load was successful. The water flowrate, however, could not be raised above the 40% load level. The problem was that the packed-bed steam generator created a pressure drop greater than the pressure supplied by the feed pump through. Table 5.1.c below summarizes the key milestones achieved from the initial testing of AGT-2. Figures 5.1.p and 5.1.q plots the different flow rates and important temperatures.

Table 5.1.c. Milestones of testing for May 26, 2004, the reported flow rates were not recorded in LabView.

Timeline of AGT2 Testing on May 26th, 2004					
Date	**Time**	**Ref Water**	**Ref Fuel**	**% Load**	**Comment**
		mL/min	mL/min		
5/26/2004	10:34	0	0	0	Working on leak in steam generator until next noted change
5/26/2004	11:12	2	0	0	
5/26/2004	11:31	2	0	0	Combustion started
5/26/2004	11:52	8	0	0	Water increased to 8 g/min with no change in pump setpoint
5/26/2004	11:58	8	0	0	Combustion increased to 0% load level, air used to balance plates to correct temperature
5/26/2004	12:01	3.7	0	0	Achieved water flow close to desired setpoint
5/26/2004	12:28	3.7	0.61	5	Started Reforming
5/26/2004	13:23	3.85	0.61	5	Pressure spikes caused by GC injections
5/26/2004	13:33	5.5	0.61	5	Water target = 4.4 g/min, 10% load
5/26/2004	13:36	5.5	1.23	10	10% Load reached
5/26/2004	13:52	10	1.23	10	Starting ramp to 20% load
5/26/2004	13:58	10	2.47	20	20% Load
5/26/2004	13:59	11.2	2.47	20	Water Q measured at 11.2 g/min
5/26/2004	14:06	11.2	2.47	20	GC injection at 20% load, pressure control started oscillating
5/26/2004	14:08	14	2.47	20	Starting ramp to 30% load
5/26/2004	14:09	14	3.71	30	30% Load
5/26/2004	14:10	16	3.71	30	Water Q measured at 16.0 g/min, pressure still oscillating
5/26/2004	14:28	16	3.71	30	GC injection at 30% Load
5/26/2004	14:29	18	3.71	30	Start Ramp to 40% Load
5/26/2004	14:35	18	4.95	40	40% Load
5/26/2004	14:38	19	4.95	40	Water Q measured at 19 g/min
5/26/2004	14:43	19	4.95	40	Started new data file
5/26/2004	14:50	19	4.95	40	Emptied ref side condenser, water cloudy yellow color saved as sample
5/26/2004	14:53	19	4.95	40	GC injection at 40% load
5/26/2004	14:55	19	4.95	40	any more head pressure. Tried a few other pumps, but gave up due to inability to flow more water. Will try more to setup for tomorrow.

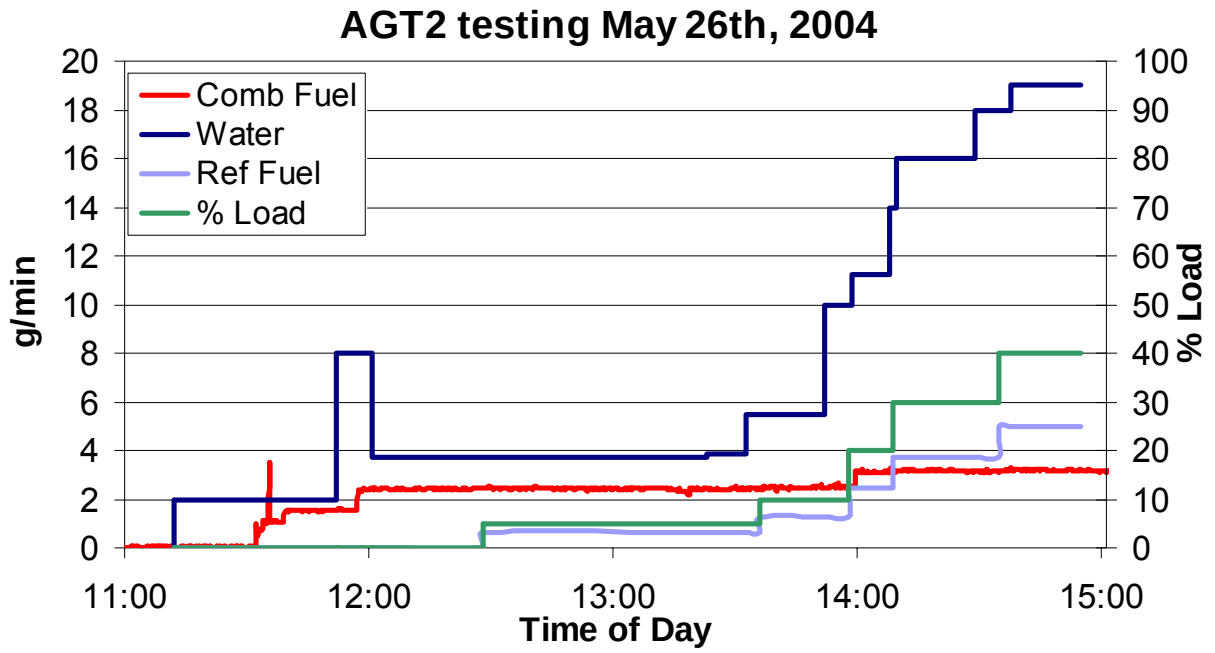

Figure 5.1.p. AGT-2 liquid flow rates and load conditions.

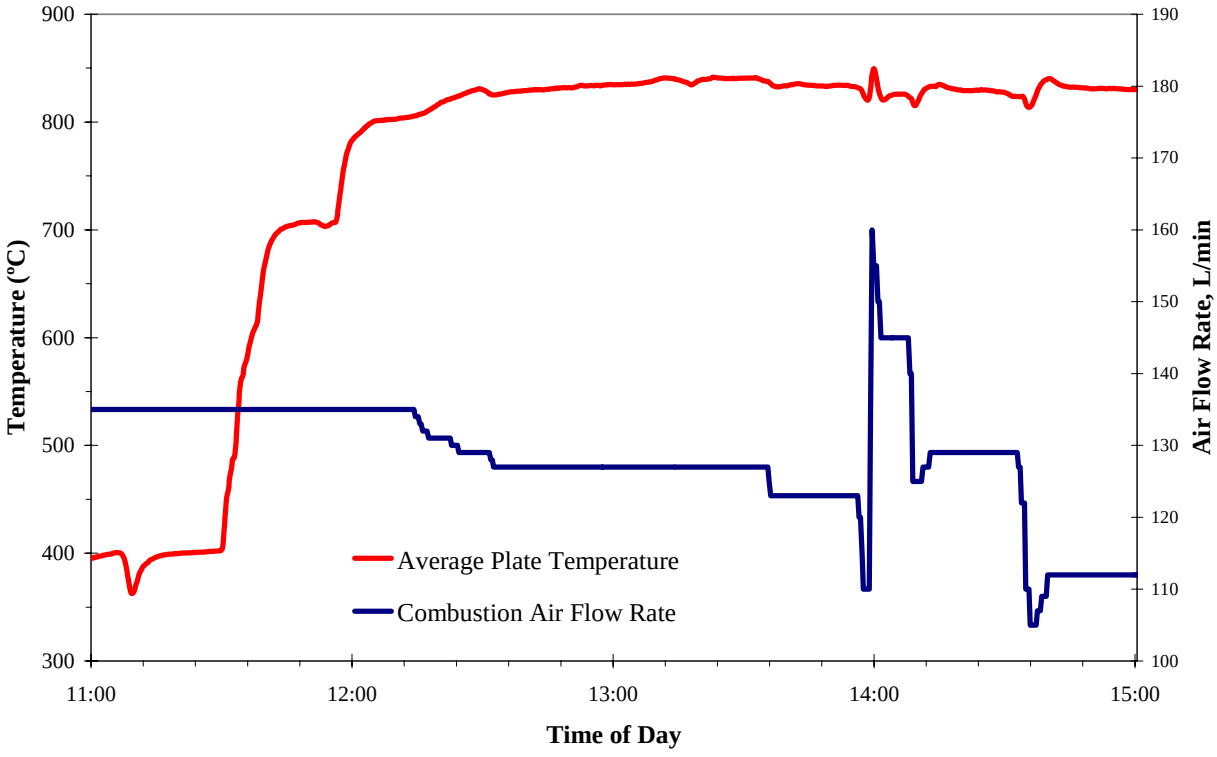

Figure 5.1.q. Air flow rate, which was used to control the plate temperature, and the resulting plate temperature, an average of TC-8, 9, 10, 11, 12, and 13.

Testing continued with an attempt to ramp up to 100% load. A higher pressure rated water pump was used to address the high pressure drop of the steam generator. This time 60% load was achieved but the new pump could not go to higher loads. The decision was made to stop reforming flows and switch to a series of two syringe pumps in a continuous flow setup. The syringe pumps were easily able to generate the pressure needed to flow the water necessary, and 100% load was achieved. 100% load was maintained for about 45 min before beginning a ramp down to 10% load. After the final GC injection at 10% load the system was shut down. Table 5.1.d contains all of the important milestones from the second day of testing AGT-2. Figures 5.1.r, 5.1.s, and 5.1.t show the flowrates, temperatures, and hydrogen production as a function of time.

Table 5.1.d. Milestones of testing for 27 May 2004.
(The reported flowrates were not recorded in LabVIEW).

Timeline of AGT2 Testing on May 27th, 2004					
Date	**Time**	**Ref Water**	**Ref Fuel**	**% Load**	**Comment**
		mL/min	mL/min		
5/27/2004	8:04	0	0	0	Start Heating with H-1
5/27/2004	8:11	0	0	0	Start combustion fuel at about 1 g/min
5/27/2004	8:18	0	0	0	Combustion fuel = 2.15 g/min
5/27/2004	8:46	5.8	0	0	Start H20
5/27/2004	8:51	5.8	1.23	10	Start Ref fuel, 10% load
5/27/2004	9:14	5+	1.23	10	10% Load GC injection
5/27/2004	9:20	9	1.23	10	Start ramping load to 20%
5/27/2004	9:26	11	2.47	20	20% Load
5/27/2004	9:40	11	2.47	20	20% Load GC Injection
5/27/2004	9:47	14	3.71	30	Ramp to 30% load
5/27/2004	10:03	14	3.71	30	30% Load GC Injection
5/27/2004	10:04	18	3.71	30	Start ramp to 40% load
5/27/2004	10:13	18	4.95	40	40% Load
5/27/2004	10:18	18	4.95	40	After the last reforming fuel change, the fuel stopped all together (only reforming side). The pressure on the syringe pump was going all the way up to 1000 psig and not flowing, indicating a clogged line. It turned out that the entrance into the furnace was coking and clogging the line. We replaced the line, and didn't insert it so far into the furnace. During that period the combustion air flow rate was raised from 120 to 160 LPM to prevent the plate temperature from going too high.
5/27/2004	10:33	0	0	0	Lower combustion fuel to 2.25 g/min (about 0% load keeping the plates at 850°C)
5/27/2004	11:07	20	0	0	Ramp combustion fuel back up to 40% load level
5/27/2004	11:15	20	1.23	10	10% Load
5/27/2004	11:20	20	4.95	40	40% Load
5/27/2004	11:31	20	4.95	40	40% Load GC Injection
5/27/2004	11:36	28	4.95	40	Start ramp to 60% load
5/27/2004	11:37	28	7.43	60	60% Load
5/27/2004	11:55	28	7.43	60	60% Load GC Injection
5/27/2004	11:56	28	7.43	60	Tried to ramp up water, single pump couldn't go any higher in flow. Even attempted two pumps in parallel, still wouldn't go higher than 28 g/min. Will switch to Syringe pumps, shutting down for change in pumps.
5/27/2004	12:20	28	4.95	40	Ramping ref fuel and comb fuel down in increments.
5/27/2004	12:20	28	2.47	20	
5/27/2004	12:20	28	0	0	
5/27/2004	14:43	0	0	0	Replaced fuel line again due to blockage, now using two syringe pumps to pump water.
5/27/2004	14:43	26.4	0	0	Started load ramp again
5/27/2004	14:48	26.4	3.71	30	30% load
5/27/2004	14:50	26.4	6.19	50	50% load
5/27/2004	14:51	26.4	7.43	60	60% load
5/27/2004	14:57	26.4	7.43	60	60% Load GC Injection
5/27/2004	14:59	35.2	7.43	60	Start ramp to 80% load
5/27/2004	15:00	35.2	9.91	80	80% load
5/27/2004	15:16	44	9.91	80	Start ramp to 100% load
5/27/2004	15:17	44	12.39	100	100% load, combustion fuel = 5.4 g/min, air =168 LPM, N2 = 7 LPM
5/27/2004	15:21	44	12.39	100	100% load GC injection
5/27/2004	15:32	44	12.39	100	Perturbation during fuel pump switch, fuel stopped for about 5 seconds
5/27/2004	15:45	44	12.39	100	100% load GC injection #2
5/27/2004	16:09	44	12.39	100	100% load GC injection #3
5/27/2004	16:34	44	12.39	100	100% load GC injection #4
5/27/2004	16:35	44	9.91	80	Start ramp down to 80% load
5/27/2004	16:37	35.2	9.91	80	80% load
5/27/2004	16:39	35.2	7.43	60	Start ramp down to 60% load
5/27/2004	16:42	26..4	7.43	60	60% load
5/27/2004	16:43	26.4	4.95	40	Start ramp down to 40% load
5/27/2004	16:45	17.6	4.95	40	40% load
5/27/2004	16:46	8.8	2.47	20	20% load
5/27/2004	16:49	8.8	1.23	10	Start ramp down to 10% load
5/27/2004	16:52	4.4	1.23	10	10% load
5/27/2004	16:54	4.4	1.23	10	10% Load GC injection
5/27/2004	17:00	4.4	0	0	0% load
5/27/2004	17:07	0	0	0	All liquid feeds off
5/27/2004	17:10	0	0	0	All heaters set to 0°C

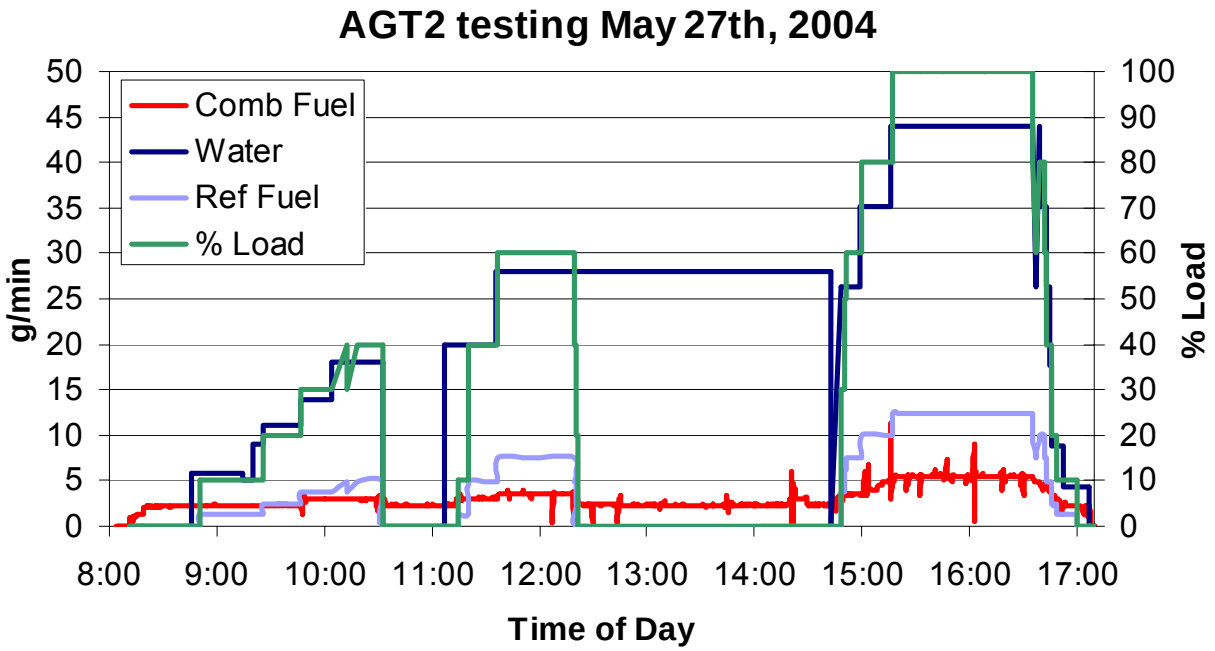

Figure 5.1.r. Liquid flow rates and the corresponding load condition.

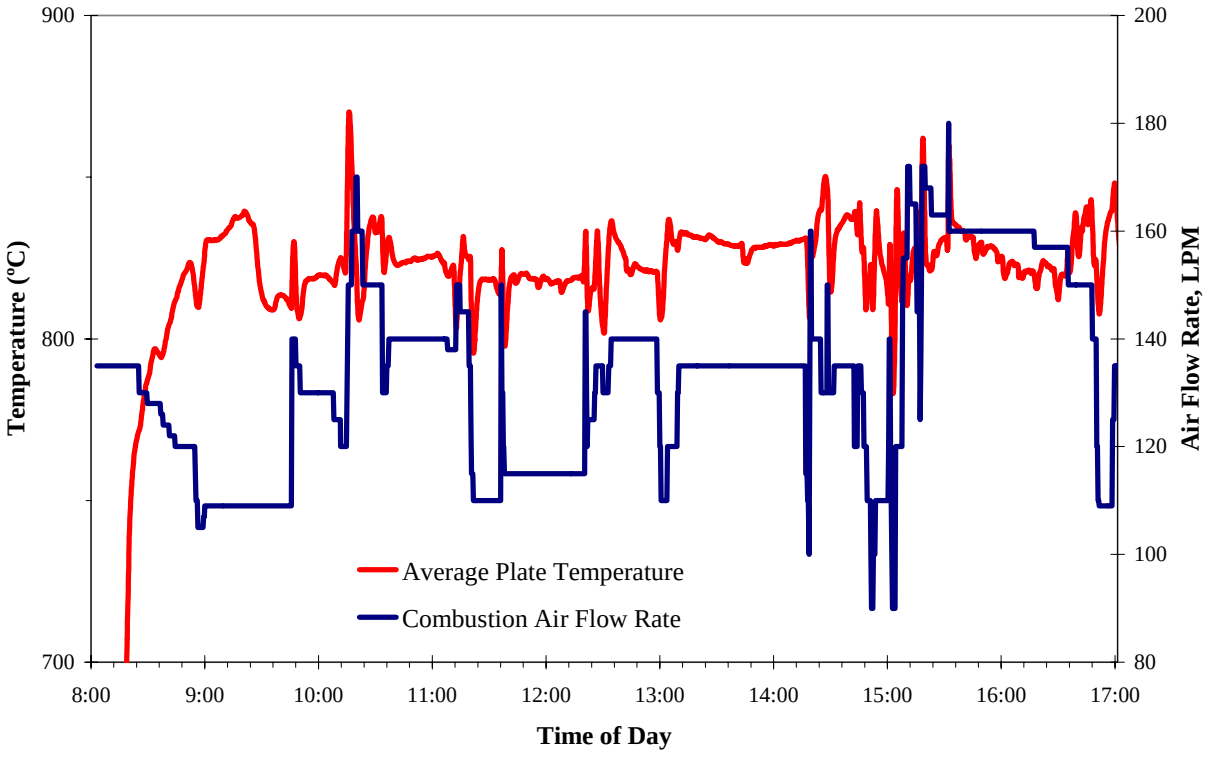

Figure 5.1.s. Combustion air flow rate, and the plate temperature throughout testing on 27 May 2004.

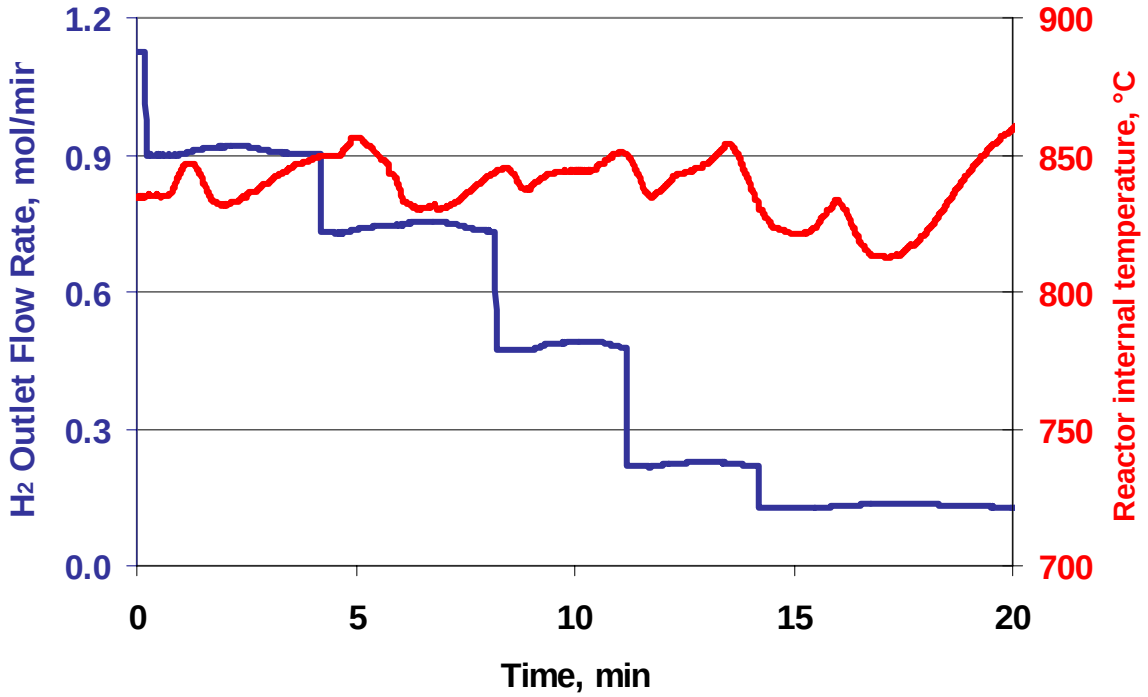

Figure 5.1.t. Hydrogen molar flow rate produced in AGT-2 during the ramp from 100 to 10% load.

The hydrogen production at 100% load conditions was not as high as expected due to incomplete fuel conversion. This was most likely due to the feed fuel bypassing the SR catalyst. Because sections of the SR channels were pressure seals, it was possible that these seals were not sufficiently compressed and allowed the feed gases to flow across the width of the SR coated section instead of through the length of the coated section. Figure 5.1.u depicts the possible flow path that the SR gases took in green, rather than the expected flow path in blue.

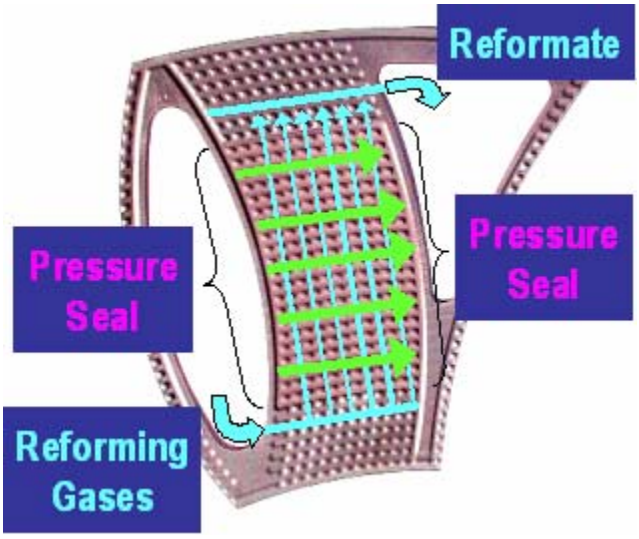

Figure 5.1.u. Explanation for incomplete conversion – SR gas bypass of coated section.

5% and 100% load steady state operation were successfully demonstrated, proving the ability of the system to meet the 20:1 turndown ratio required by the DOE. The 10% to 100% load ramps up and down were also both completed successfully. The next step was to improve this system in order to be able to achieve faster, more direct transients from 10% to 100%, as well as to have a more automated plate temperature control system.

Major Overhaul of AGT-2 Prototype System

A number of improvements were identified for AGT-2's supporting system. First, it was important to develop a new method of generating steam and feeding it into the system. Next, the control and measurement of liquid flows needed to be more reliable and repeatable. Finally, a user friendly control methodology was needed to automatically control the plate reactor temperature and to minimize the temperature fluctuations.

Because the start-up time was so critical, it was important to be able to quickly generate steam. Though using the furnace heater provided reliable steam, its start-up time was unacceptably long. Therefore, a new steam generator was designed using a combustor and a microchannel steam generator developed by Pacific Northwest National Laboratory (PNNL). This vaporizer also generated a lower pressure drop, which reduced the pressure delivery requirements of the water pump. Figure 5.1.v is a picture of the microchannel vaporizer.

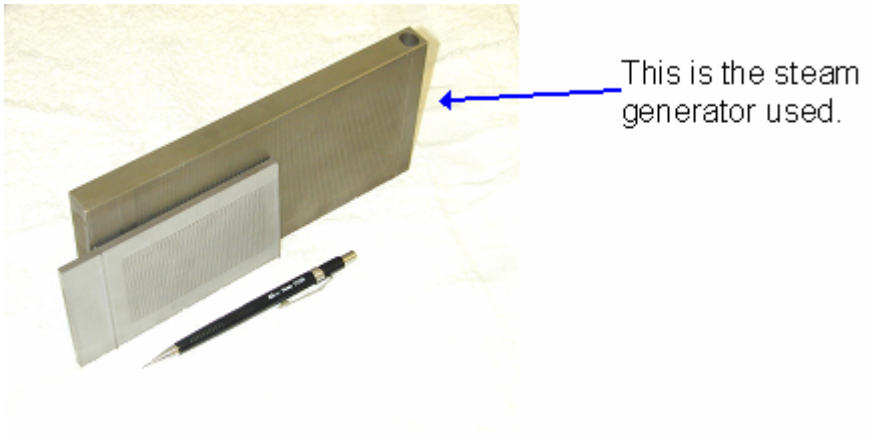

Figure 5.1.v. Microchannel vaporizer used to generate superheated steam.

The microchannel steam generator required a certain amount of energy in order to generate steam. This energy was provided by a hot air stream that passed through the vaporizer. To create this hot air, an off-the-shelf combustor with the correct power requirement was procured and modified. It was determined that at the flowrates used, combustion was incomplete. In order to fully oxidize all of the fuel entering the combustor to maximize heat output for the steam generator, a small monolith coated with CESI's combustion catalyst was placed in the exhaust tube of the combustor. This proved to generate more heat than without the catalyst-coated monolith and raise the exhaust gas temperature entering the steam generator.

As an interface between the combustor and microchannel steam generator, a metal box was designed and constructed to house an insulating box in which the steam generator was housed. This metal box was deemed to be a necessary component in case some of the combustor exhaust gas leaked out of the insulating box. Also, the basic construction of the insulating box had to be revisited and improved after initial testing demonstrated that it was not structurally stable. Figure 5.1.w shows the current combustor/steam generator box setup. The steam generator is located within the metal box and cannot be seen in this photo.

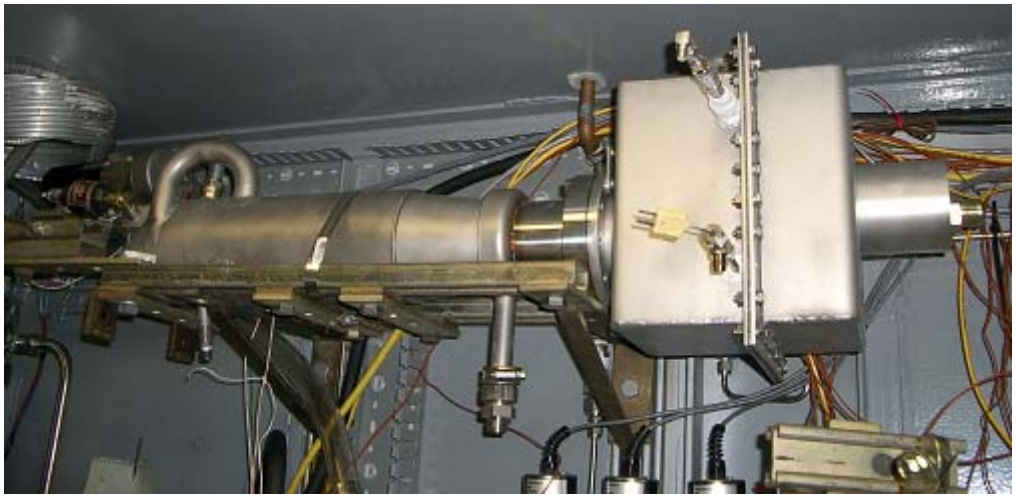

Figure 5.1.w. Combustor and metal box enclosure with steam generator.

Finally, a secondary heater was added to the system to provide enough energy to heat the superheated steam to a temperature of at least 400°C. A PID controller was incorporated to control the amount of power sent to the heater, based on the temperature feedback downstream of the heater. Figure 5.1.x illustrates the flowrates and temperature of the water/steam and the temperature of the air into steam generator. This data illustrates the controllability of the steam temperature under various conditions.

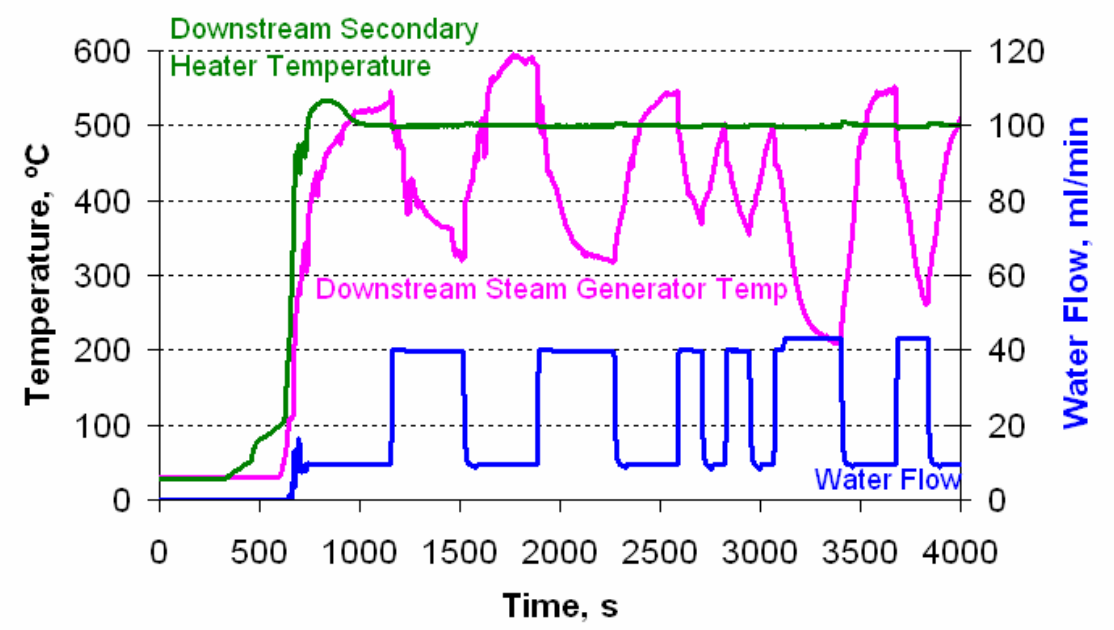

Figure 5.1.x. Temperature and flowrate of H_2O, and temperature of exhaust gas into steam generator.

The control of the fuel flow during the AGT-2, Part 1 testing proved to be extremely difficult with the PWM fuel injectors. During the testing, it was observed that the flow rate out of the injectors was inconsistent with the frequency and percent duty settings. The fuel injector calibration would drift over time after repeated exposure to high temperature. Attempts to cool the injector were unsuccessful.

Another form of fuel delivery needed to be found. Low flow atomizing spray nozzles and low flow HPLC pumps were eventually identified, tested, and used to introduce liquid fuel into the system. However, the low flow sprayers had very small orifices where fuel could accumulate and form carbon under the high temperatures of the combustion and steam reforming streams. Any carbon build-up/deposit could block the fuel flow into the system. Therefore, these sprayers were modified to incorporate a cooling jacket to minimize this possible coking scenario. Figure 5.1.y illustrates the modified sprayers.

Figure 5.1.y. Air/N_2-assist atomizing nozzles that include a separate water cooling jacket. The white jacket is added ceramic insulation.

The fuel injectors were tested using liquid gasoline to see what air-assist flowrates were necessary to achieve a good, uniform, atomized spray. The following table shows that the required air or N_2 assist flowrates were not the same for the same gasoline flowrates. This could be due to the slight fabrication variations in the orifice.

Table 5.1.d. Air/N_2-assist required in sprayers for acceptable spray.

Sprayer 1 Gasoline (ml/min)	Air (lpm)	Sprayer 2 Gasoline (mL/min)	N2 (lpm)
1	6	1	5
2	6	2	5
3	6	3	5
4	6	4	5
5	7	5	5
6	7	6	6
7	7	7	6
8	8	8	7
9	8	9	7
10	8	10	7

The air assisted spray nozzles worked well to deliver fuel in the combustion side. However, when used to deliver fuel to the reforming side, the amount of nitrogen needed to atomize the fuel significantly cooled the fuel-steam mixture before it entered the reforming side, reducing temperature down to as low as 70°C. This was not acceptable since the preferred inlet gas temperature on the steam reforming side was 450°C. To address this issue, a new fuel delivery system was designed for the reforming side. With the new delivery system, the fuel was injected into the steam flow through a perforated piece of 1/8" diameter closed-end tubing. When the fuel came into contact with the super-heated steam, the fuel immediately vaporized. The resulting fuel-steam mixture entered the prototype reactor at a temperature of roughly 250°C. Figure 5.1.z shows a view of the reforming fuel-delivery device that replaced the nitrogen-assisted nozzle.

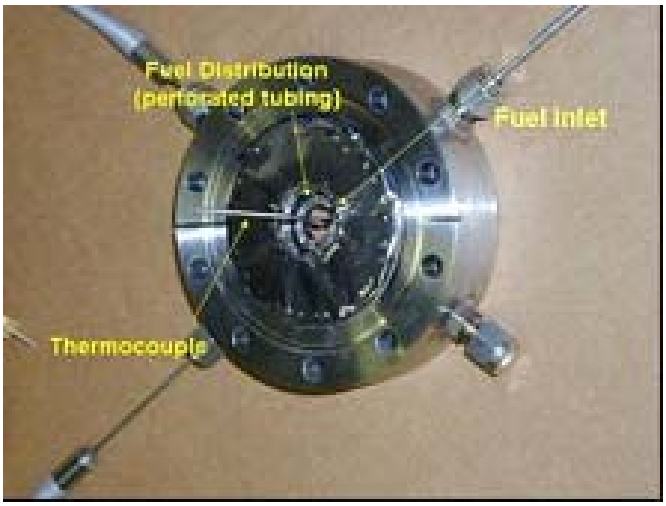

Figure 5.1.z. Reforming fuel-delivery system

The fuel processing system required the control of many different flowrates, depending on load and temperature of the plate reactor. To improve the temperature control, a new control strategy was devised that automatically set all the different flows based on these two factors. The improved control scheme allowed the user to enter the prototype % load and the average plate temperature. The reforming gasoline, reforming water, combustion gasoline, N_2 on the reforming side, and the primary combustion air were automatically set to specific flowrates based on the load requested. These specific flowrates were predetermined and mapped out in a look-up table within the control software. Then a fraction of the combustion side air was set by a PID controller that looked at the average plate temperature set-point as the control variable. If the actual average plate temperature was higher than the set point, the control air would increase, making the mixture leaner and reducing the temperature. If the actual temperature was lower than the setpoint, then the PID controller would decrease the control airflow. As in the previous set-up, the power delivered to the heater that was downstream of the steam generator was set by a PID control loop that looked at the downstream flow temperature as the control variable. All of these different controls were implemented in order to enable the user to easily control the system without having to manually input so many different flow and temperature setpoints.

Using PID controllers to control the back pressure regulator, the combustion side heater, and the combustion side control air was a critical part of the new control methodology. Tests were performed using either the Ziegler-Nichols or Cohn-Coon method to find the appropriate PID parameters for these components. The following two figure illustrates the behavior of the back pressure regulator when the flowrate on the steam reforming side was perturbed, and the setpoint for the regulator was 25 psig.

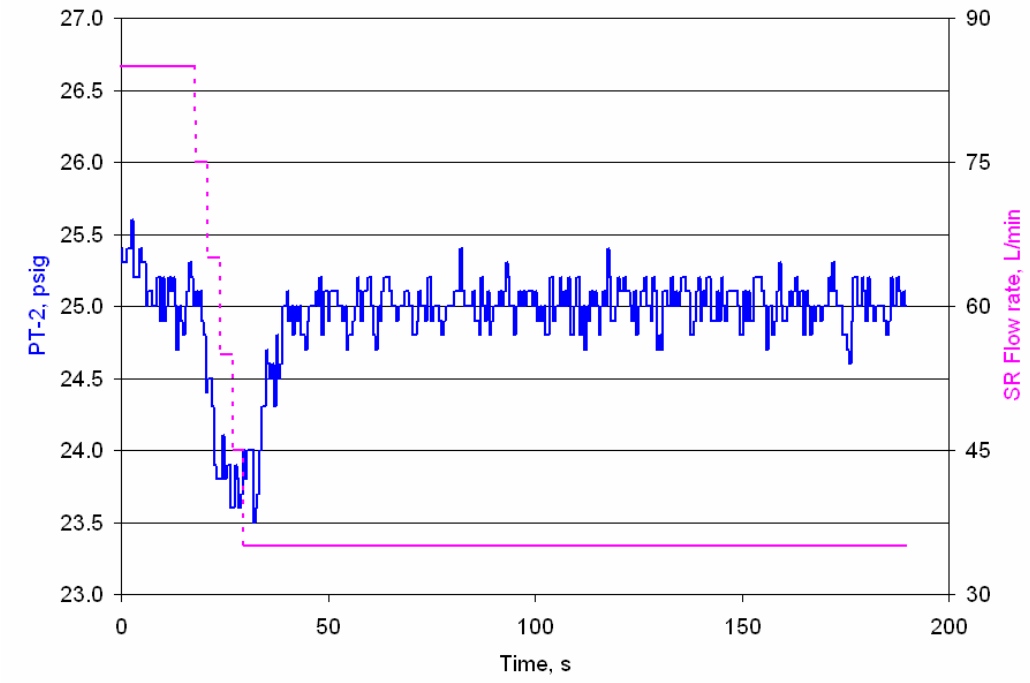

Figure 5.1.aa. Pressure fluctuation on the steam reforming side when the flowrate was changed from 85 L/min to 35 L/min in increments of 10 L/min every 2 s.

Figures illustrating how other PID parameters were found can be seen further in the report, in the AGT-2 Testing, Part 2 Section. Ultimately, the PID parameters that were selected were chosen because they provided the best compromise among small over/undershoot, quick time to reach steady state, and relatively stable pressure afterwards.

5.1.5 AGT-2 testing, part 2

A methodical and detailed test plan was used to guide the testing and validation of the system improvements on AGT-2. The following list summarizes the purpose of each of the tests:

- Test #1: Without gasoline flowing on the reforming side, verify that
  - the settings from the look-up table are implemented when requested,
  - the system can be controlled to different average plate temperatures,
  - the system can maintain the desired temperature during a step change in nitrogen flow on the steam reforming side (a simulated load change).
- Test #2: Without gasoline flowing on the reforming side, verify that
  - the system can maintain the desired average plate temperature during a step change in nitrogen and steam flows (a simulated load change).
  - the steam generation system operates as required.
- Test #3: With gasoline flowing on the steam reforming side, verify that
  - both the combustion and steam reforming sides of the plate reactor can operate at 10% load and maintain steady state conditions.
- Test #4: Perform 4 minute-, 1 minute-, 15 second-, 5 second-, and 1 second transients of 10:1 turndown.
- Test #5: Determine the shortest start-up time possible.

Test #1

The look-up table feature was newly-added, so it was necessary to ensure that the equipment responded when different loads were input at different time ramp rates. Table 5.1.f is an example of a typical look-up table.

Table 5.1.f. Example of Look-up Table.

% Load	Reforming Water PCR-1	Reforming Fuel PCR-2	Combustion Fuel PCR-3	Bulk Combustion Air MFC-1	Nitrogen assist for SR side MFC-3	Propane Combustor Propane MFC-7	Gaseous Ref Fuel MFC-8	Air assist for Comb side MFC-5
%	mL/min	mL/min	mL/min	L/min	L/min	L/min	L/min	L/min
0	0.0	0	0.00	0.0	0	0	0	0
10	4.3	1.23	2.36	20.0	5	2.8	0	6
100	43.0	12.3	20.40	20.0	8	5.7	0	6

The use of these tables was particularly convenient when the change of any of the flow rates was not exactly proportional with the change in load. The LabVIEW software linearly interpolated values in between any two specified points in the table. As an example, a load setting table that changed only MFC-1, combustion air, was tested. Figure 5.1.ab shows how MFC-1 responded to the different load inputs.

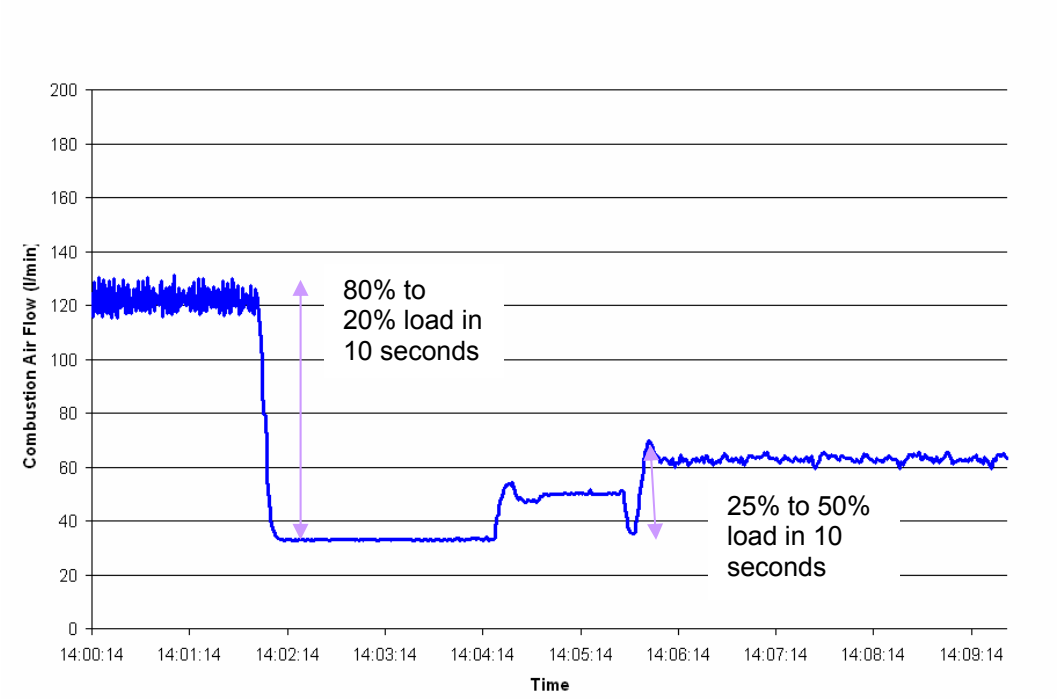

Figure 5.1.ab. MFC-1 response to different load setting inputs using the look-up table.

Test #1 also included tests using the Cohen-Coon method to find the optimum PID values for the back pressure regulator (BPR-1), Heater 1 (H-1) which heats up the combustion air, and combustion control air (MFC-1b). Table 5.1.g lists these parameters.

Table 5.1.g. PID parameters for system control.

		BPR-1	H-1	MFC-1b
Proportional gain	(Kc)	2.16	18	-4
Integral time	(Ti, min)	0.11	0.113	1.466
Derivative time	(Td, min)	0.009	0.028	0.239

Because Heater 2 (H-2) is used for rapid start-up, its control is more or less binary, which means it does not require a similar type of PID control. PID parameters for Heater 3 (H-3) which is the secondary steam heater were previously discussed.

Another test that was performed included changing the N_2 flowrate to simulate a load change on the steam reforming side. This was to verify that MFC-1b would respond in order to maintain a constant average plate temperature on the combustion side. Figure 5.1.ac shows how the average plate temperature was kept constant even while there was a step change of N_2 flow on the other side of the plates on the steam reforming side. The overall air flow rate increased when the N_2 was decreased in order to decrease phi. This lower phi resulted in a lower adiabatic gas temperature since the rate at which heat was being removed decreased with the decrease in N_2.

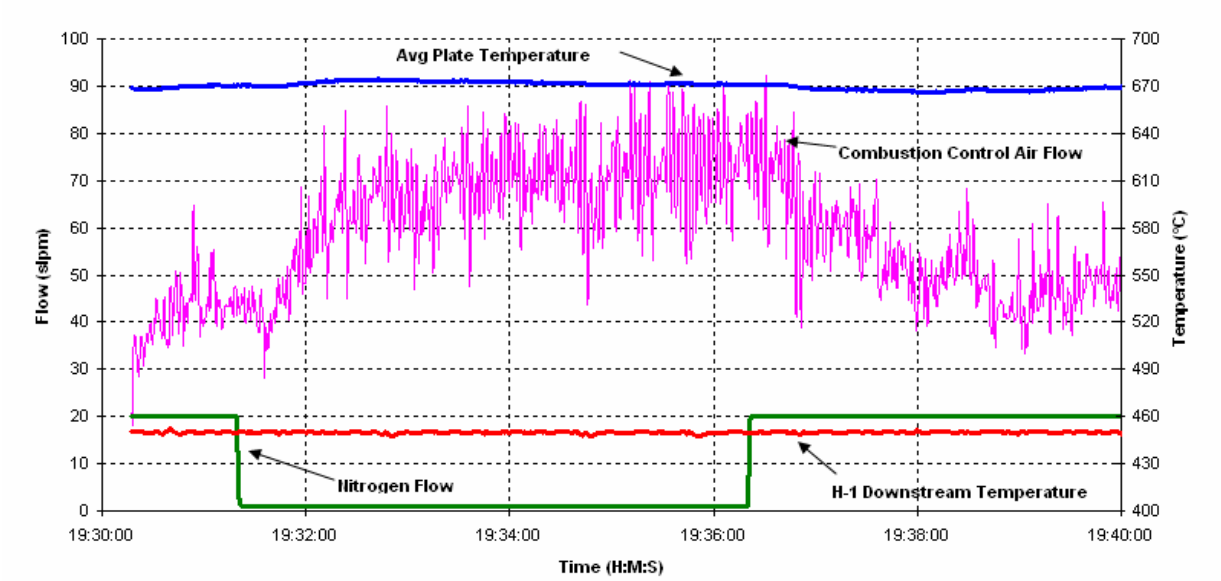

Figure 5.1.ac. MFC-1b Temperature control during N_2 perturbation on SR side.

The control air was also plotted on the graph. It fluctuated up to +/- 20% of what appeared to be the average target flow setpoint. Because the actual average plate temperature setpoint of 670°C was maintained relatively well, this was not considered a critical problem. However, this fluctuation problem was solved by increasing the tubing diameter of the outlet of the control air mass flow controller from ¼" to 3/8". It seems that with the ¼" tubing, the rapid changes in the **control** air flowrate affected the downstream pressure of the **bulk** air mass flow controller, which affected its flowrate, which in turn affected the flowrate of the **control** air mass flow controller, creating a cyclic feedback problem.

Test #2

Figure 5.1.ad illustrates the control of average plate temperature when a % load change was induced using the look-up table settings. The look-up tables called for decreased water and fuel flowrates. Even though the combustion fuel flowrate and steam flowrate were reduced, the control air MFC-1b responded accordingly in order to maintain a relatively average plate temperature of 620°C.

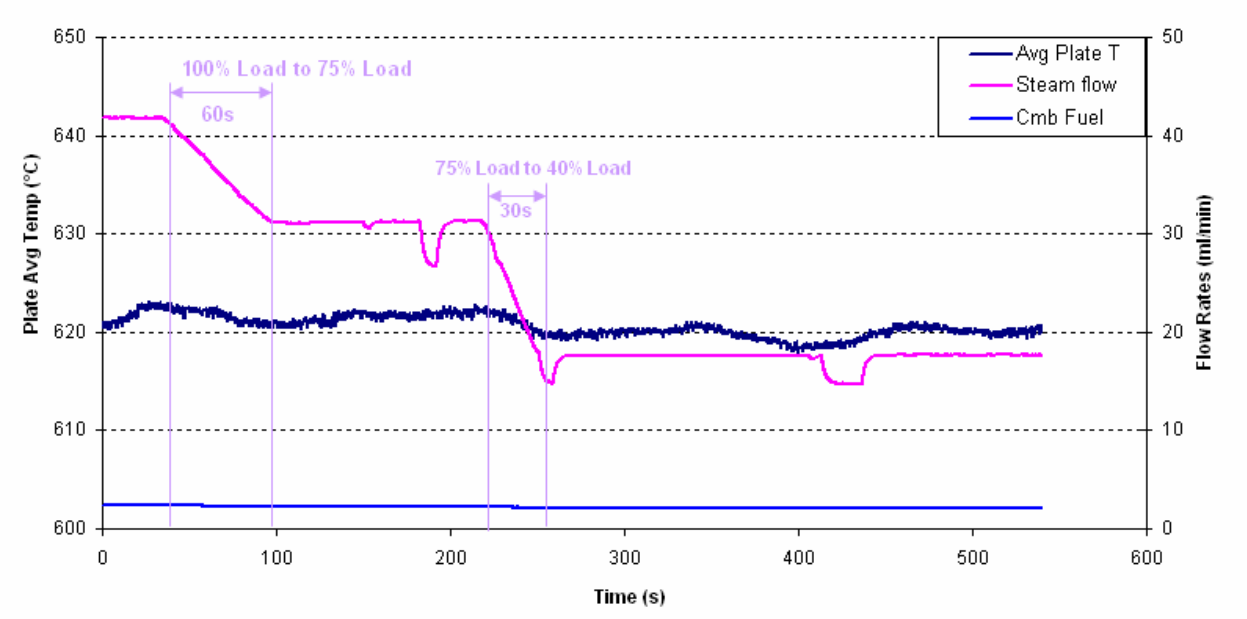

Figure 5.1.ad. Average plate temperature during transients.

Test #3

The next test was to operate the steam reforming and combustion sides simultaneously at 10% load. The following table lists all the different flow rates that were used to run this condition.

Table 5.1.h. Operating Parameters at 10% Load.

Table of Operating Parameters (gas volumes are at STP) at 10% Load	
Combustion Air (L/min)	145
Assist Air (L/min)	6
Combustion Fuel (mL/min)	5.3
Control Air (L/min)	10-25
Target Average Plate T (°C)	825
Steam Reforming Fuel (mL/min)	1.23
Water (mL/min)	4.34
Nitrogen (L/min)	6.0
Combustor Fuel, propane (L/min)	2.5
Combustor Air (L/min)	200

Test 3 was successfully performed controlling MFC-1b in its auto mode and using the look-up tables to change the flowrates to reach 10% load. Also, the performance of the new steam reforming reactor inlet design was tested to ensure that the temperature into the inlet of the steam reforming reactor was high enough. Figure 5.1.ae illustrates that

even though the temperature downstream of the secondary heater was not different than for the previous tests, the temperature of the steam reforming inlet was above 300°C. This was because there was a significant reduction in thermal mass, which reduced the heat loss between the outlet of the secondary heater and the steam reforming inlet.

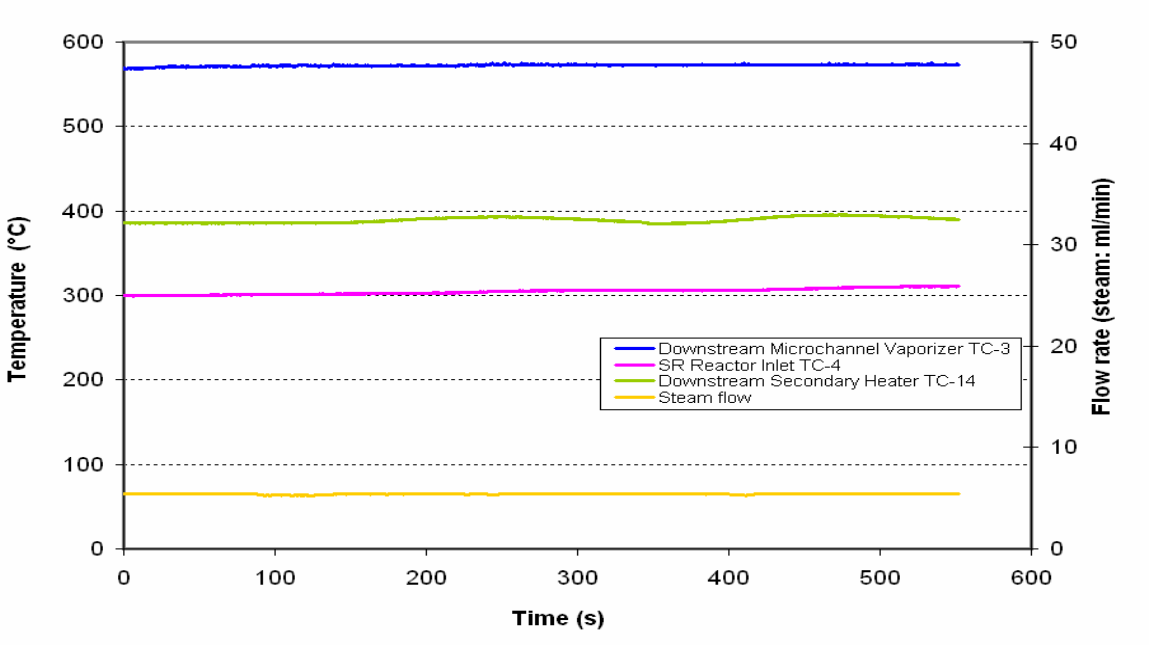

Figure 5.1.ae. Steam temperatures.

Figure 5.1.af demonstrates that even with the steam reforming fuel flowing, MFC-1b was still able to control to the target average plate temperature relatively well with some very gradual oscillations of 10°C.

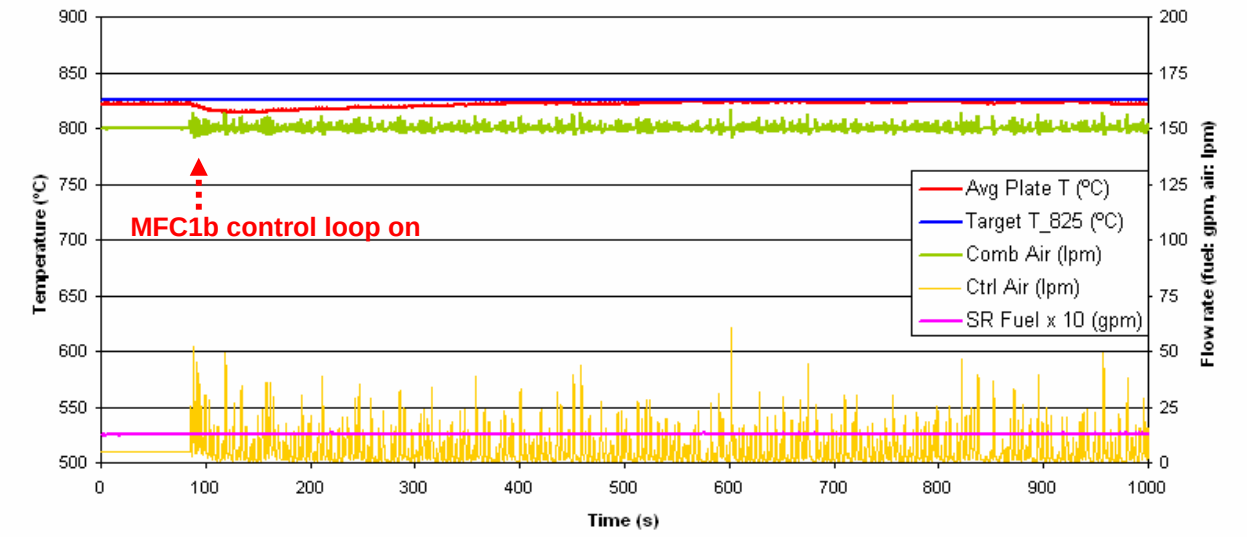

Figure 5.1.af. Average plate temperature with combustion and steam reforming fuels flowing at 10% load, flowing 145 L/min as bulk combustion air.

The flowrate of the bulk combustion air affected the stability of the average plate temperature. For example, the bulk combustion air was changed from 145 to 125 L/min. This required MFC-1b to flow roughly 20 L/min more than it had been previously. A slightly flatter line for average plate temperature can be seen in Figure 5.1.ag, where combustion air is only 125 L/min. The standard deviation of the average plate temperature decreased from 3.0 to 1.2 when the bulk combustion air was decreased from 145 to 125 L/min.

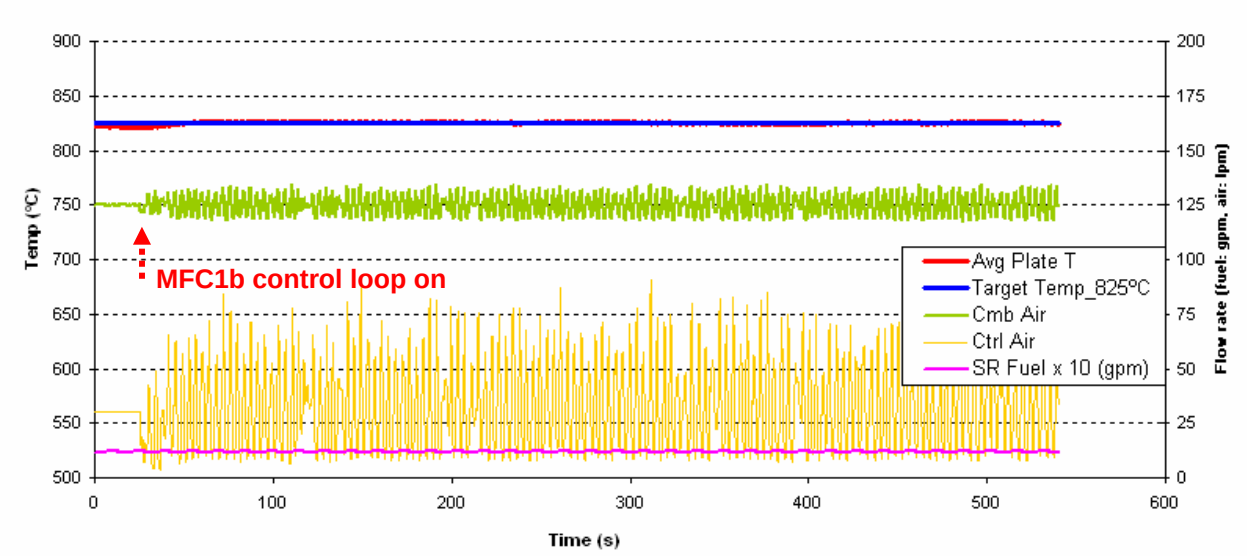

Figure 5.1.ag. Average plate temperature with combustion and steam reforming fuels flowing at 10% load, flowing 125 L/min as the bulk combustion air.

The minor fluctuations in fuel flow are due to the pulsations of the double piston pump. The specification for the pump when purchased was that it was a non-pulsating pump. It is believed that at such low flowrates, the pump has difficulty preventing oscillations. These fluctuations do not seem to have a noticeable effect on the outlet composition readings, so the pumps were not changed.

Test #4

Once the automatic control system behavior was deemed satisfactory at a constant load, the system was put to the ultimate test of controlling the complete system during the transition from low to high loads and vice versa, in periods as short as 1 s, using the Percent Load Lookup Table. The LabVIEW program controlled the corresponding setpoints based on the load map shown in Table 5.1.i.

Table 5.1.i. Look-up table for automatic flowrate settings for transients.

Load Control Table

% Load	Reforming Water PCR-1	Reforming Fuel PCR-2	Comb Fuel PCR-3	Cmb Air MFC-1	Nitrogen MFC-3	Nzl Assist Air MFC-5	Cmbst Air MFC-6	Propane MFC-7
0	2.17	0.00	4.61	134.0	7	6	230	2.40
10	4.34	1.23	4.95	135.5	7	6	230	2.55
20	8.68	2.46	5.38	137.0	7	6	230	2.59
30	13.02	3.69	5.77	138.5	7	6	230	2.63
40	17.36	4.92	6.16	140.0	7	6	230	2.67
50	21.70	6.15	6.55	141.5	7	6	230	2.71
60	26.04	7.38	6.94	143.0	7	6	230	2.75
70	30.38	8.61	7.33	144.5	7	6	230	2.79
80	34.72	9.84	7.72	146.0	7	6	230	2.83
90	39.06	11.07	8.11	147.5	7	6	230	2.87
100	43.40	12.30	8.50	149.0	7	6	230	2.90

Load Control File

C:\SR Prototype LV Files\tables_lookupTab\2005-02-07 lookup table_txt file\2005 02 07 test4b.txt

Read

Use of this table in conjunction with the automatic temperature control should have relieved the operator of the need to make any adjustments except for entering the desired load. Results proved that this strategy was successful. Data was obtained for 4 min, 1 min, 15 s, 5 s, and 1 s 10:1 turndown transients. The following graphs show the results of the most extreme transient test of 1 s.

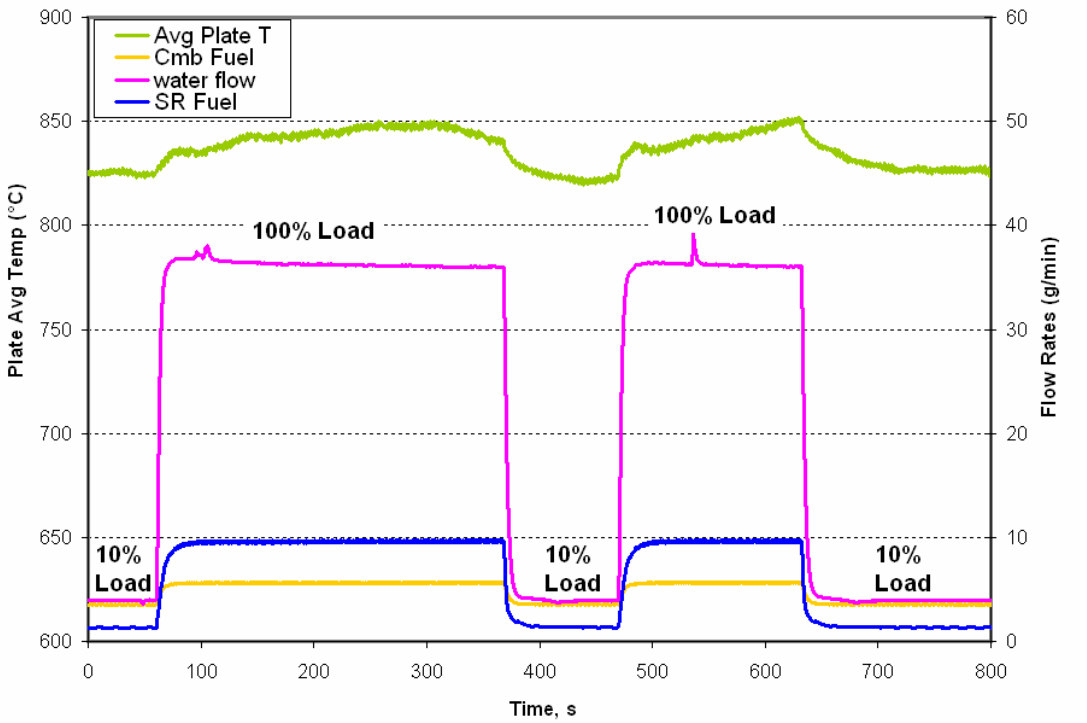

Figure 5.1.ah. 1-s transient performance using automatic temperature control and the percent load lookup table.

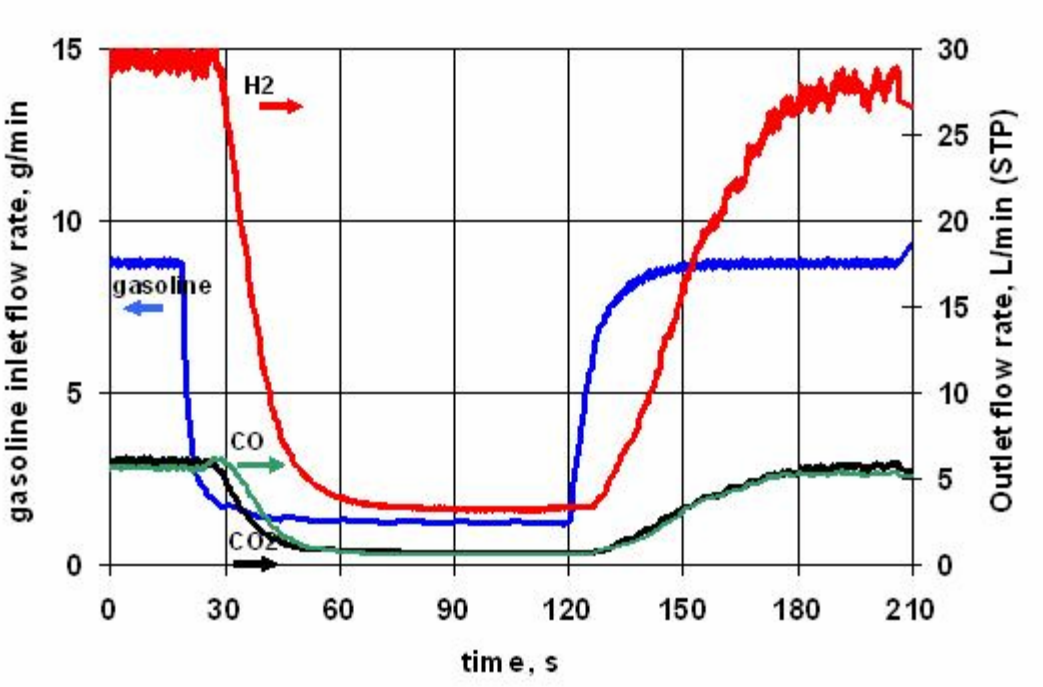

Figure 5.1.ai. Reformate outlet composition during 1-s 10:1 turn down and turn-up transient operation.

The principal achievement that Figure 5.1.ah shows is that the AGT-2 prototype and its control scheme was able to perform a fast transient in load while keeping the plate temperature relatively constant in a temperature window of 25°C. No excursion in the plate temperature was observed in the turn-down transient or during the turn-up transient. The plate temperature stayed in the safe window of operation, avoiding the risk of coking the catalyst at low temperature and the risk of catalyst sintering or plate stack structural failure at high temperature.

Figure 5.1.ai shows a detail of the outlet gas composition vs. time, as measured by the infra-red gas analyzer during a 1-s transient from 100% to 10% load operation and vice versa. The H_2 flow rate is calculated from the CO and CO_2 signals, using a mass balance and a know N_2 tracer gas flowrate. The gasoline flow rate represented on the figure is the signal coming from the mass flow sensor. Both the IR gas analyzer and the mass flow sensor have response time constants that explain why the response to the fast 1-s transient is so slow. A simple deconvolution of the transient responses on Figure 5.1.ai shows that the CO_x signal time constant for the transient up is longer than the time constant for the transient down. A detailed study of the cause of this phenomenon using a lab scale reactor and a controlled fast transient of the feed was able to demonstrate that the reason for the difference in the time constants was not due to an intrinsic inertia of the reforming catalyst but truly due to a slower response of the *analytical system* in the case of a transient up. A change of the location of the IR sampling port and especially a change of the type of back pressure regulator could have eliminated most of the apparent time constant in the response of the outlet gas composition.

Figure 5.1.ai also indirectly shows that the conversion of the gasoline was incomplete at low load, like at high load. Since the incomplete conversion occurred at low load as well, a low activity of catalyst cannot be responsible for the fact. As discussed in ***AGT-2 Testing Part 1***, the partial conversion is the consequence of part of the feed flow by-pass the catalyst-coated zone of the reactor. Future designs of the steam reforming reactor address this issue.

Attempted Rapid Startup

One of the goals of the DOE is to produce PEM fuel cell quality hydrogen within 60 s of starting the fuel processing reactor. This means a substantial amount of energy needs to be supplied to the reactor within a short period of time to quickly raise the plate temperatures to the necessary steam reforming operating temperature. In April 2004, a test was conducted where the heaters were turned on to their maximum output power, and a very large flowrate of air was introduced to the system in conjunction with enough fuel to operate at a phi of 0.38. This phi was chosen because it was believed that a phi of 0.40 was the cut-off of when auto-ignition might occur. Flowing these flowrates resulted in the temperature profile previously show in the section 5.1.2, **Preliminary Tests on AGT-1,** Figure 5.1.k.

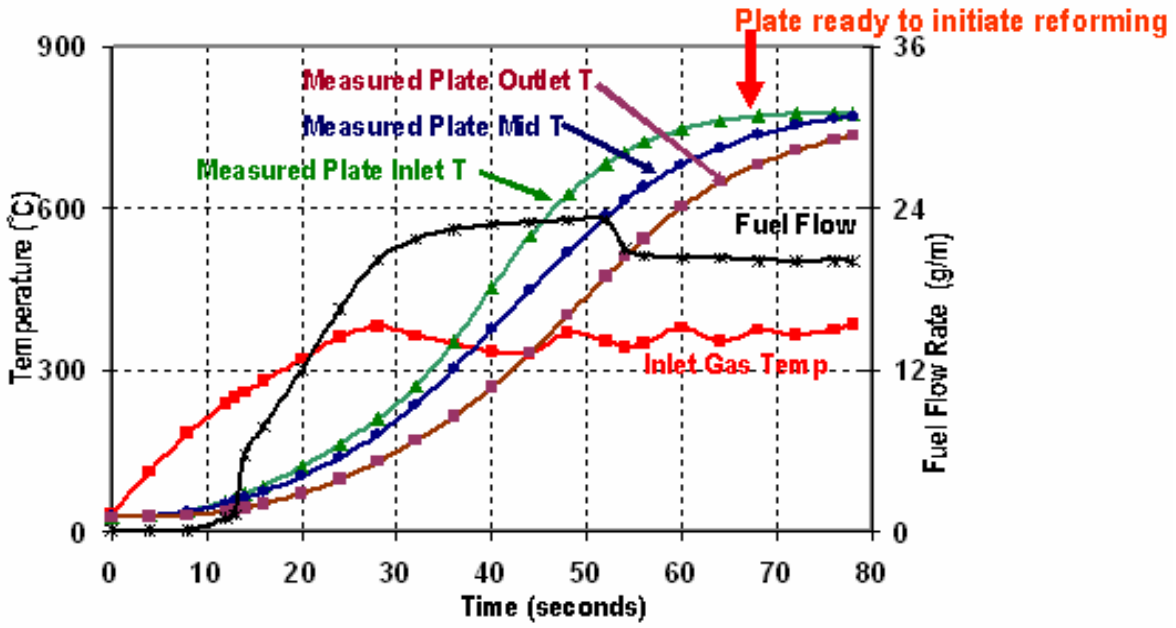

Repeated Figure 5.1.k. Temperature profile of April 2004 rapid start-up test.

Figure 5.1.k suggests that the plate temperatures were hot enough to start the reforming reaction after 70 s of operating the combustion side at high heater power and high flows. However, this test was performed on AGT-1, which already had crossover leaks and holes between the combustion and the steam reforming sides. For this particular test, 10 L/min of N_2 was flowing on the steam reforming side to try to prevent combustion exhaust gas from entering the steam reforming side, but keeping the two sides completely isolated was not feasible. It would have been difficult to tell if any additional damage had occurred to the plates since a leak already existed at this time.

When it was time to test AGT-2 for rapid start-up, a similar approach was taken. For the rapid start-up test, a phi slightly lower than before was chosen, 0.31. A higher air flow rate and a lower fuel flow rate compared to the April 2004 testing were used. It was believed that these operating conditions for AGT-2 would be safe because it was believed that the April 2004 operating conditions for AGT-1 had been safe. Table 5.1.j compares the operating conditions of the two different test runs.

Table 5.1.j. Operating conditions for rapid start-up tests in April 2004 (AGT-1) and March 2005 (AGT-2).

	AGT-1	AGT-2	Units
ΔH Combustion of ANL Benchmark Fuel I	**-4856**	**-4856**	kJ/mol fuel
Fuel flow rate	**23.00**	**22.20**	g/min
Fuel flow rate	**0.00342**	**0.00330**	mol fuel/s
Air flow rate	**690**	**830**	L/min
N_2 flow rate	**10**	**20**	L/min
CO_2 flow rate	**0**	**0**	L/min
Inlet gas T	**383**	**430**	°C
Exhaust gas T	**1338**	**1193**	°C
Phi	**0.38**	**0.31**	-

Figure 5.1.aj shows fuel flow, average plate temperature, and the inlet gas temperature for the March 2005 rapid start-up test.

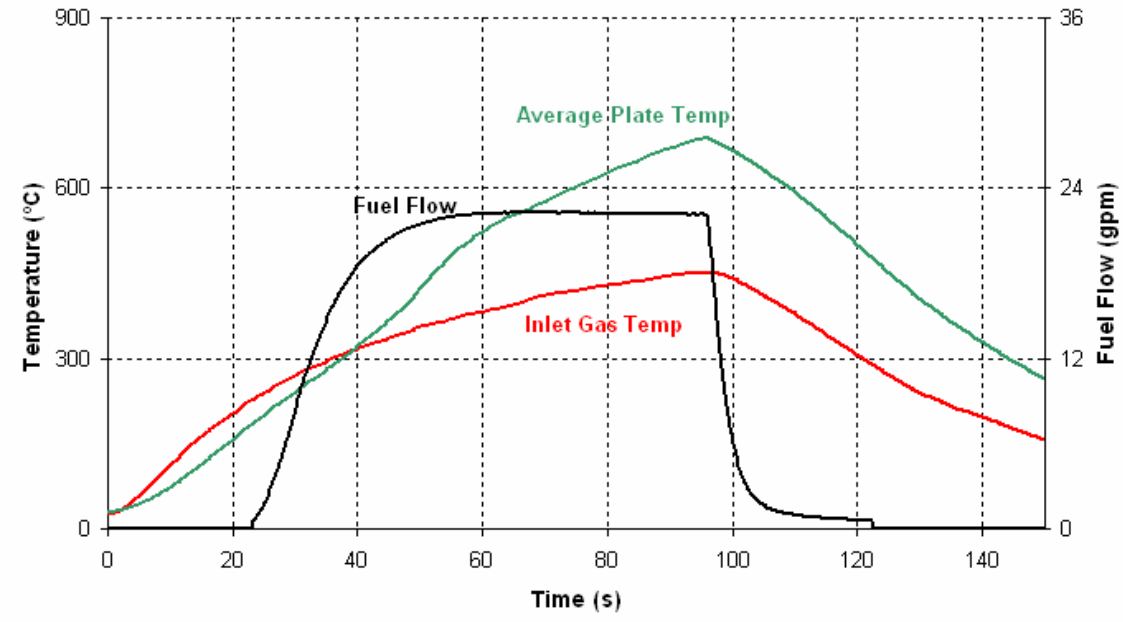

Figure 5.1.aj. Temperature profile of March 2005 rapid start-up test.

The results suggests that the time to initiate the steam reforming reaction was longer than the 70 s found in April 2004, which was to be expected since the phi was slightly lower. In fact, a high temperature alarm triggered the shutdown sequence to commence even before the average plate temperature reached 800°C. AGT-2 instrumentation included thermocouples on the steam reforming plate inlet and outlet. AGT-1, however, did not have this instrumentation. Figure 5.1.ak shows that it was the plate temperatures on the steam reforming side that actually triggered the shutdown sequence.

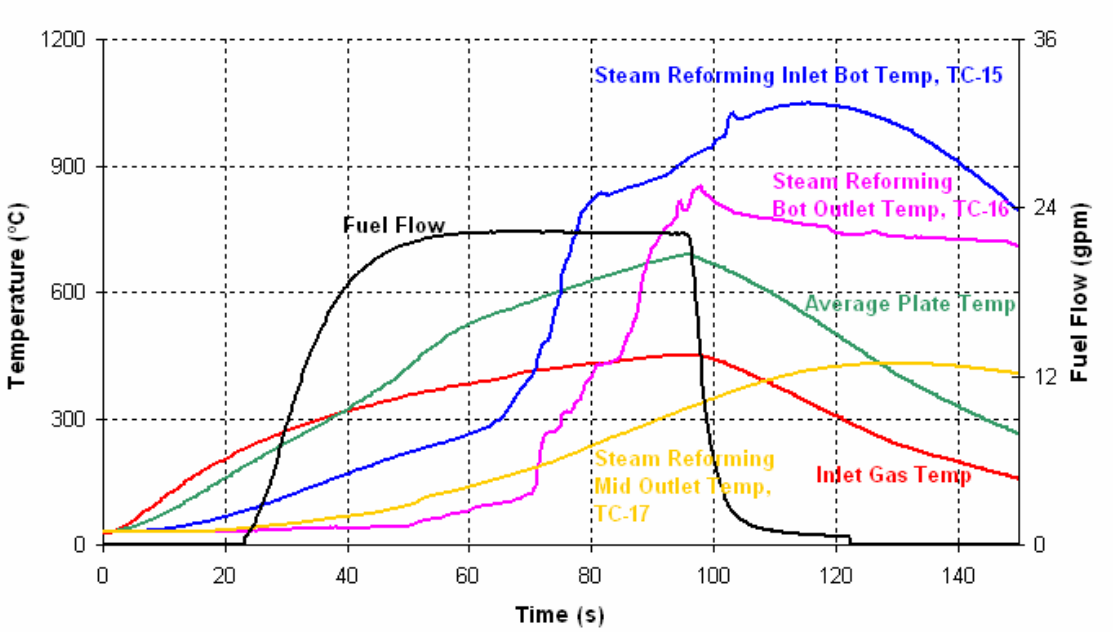

Figure 5.1.ak. Temperature profile including steam reforming inlet/outlet temperatures of March 2005 rapid start-up test.

Figure 5.1.ak shows that at roughly 70 s, TC's 15 and 16, which were both located 6 plates away from the bottom of the plate stack, climbed very steeply on the steam reforming side, even though the average plate temperature on the combustion side and the TC located in the middle vertically on the SR side did not. This might suggest that the vertical gas distribution among the plates was non-uniform. Perhaps some gas with a fuel/air mixture of a phi greater than 0.38 passed through the bottom plates and less than 0.38 passed through the middle or upper plates. This could explain why SR TC's 15 and 16 were so much higher than any of the other ones.

The cause of the uneven vertical flow distribution was investigated. One possible explanation for uneven distribution may have to do with the assist air on the combustion spray nozzle was unable to flow the desired air flowrate. The setpoint for that mass flow controller was 6 L/min. However, the datalog file shows that the mass flow controller was actually flowing only 0.9 L/min. This was may have been due to the large start-up air was flowing and generating a huge back pressure on the system, roughly 38 psig. This system back pressure translated into a high downstream pressure on the mass flow controllers. It is possible that there was insufficient pressure drop across the mass

flow controller to flow the requested air flowrate. In addition, it is also possible that there was not sufficient air coming from the compressor because the large air was being used for more than just a few seconds. The buffer was being more quickly depleted. This could have resulted in the upstream pressure on the mass flow controllers not being sufficiently high any more. Given that the spray nozzle assist air was flowing at only 15% of the requested setpoint, it is very likely that the combustion fuel spray was not well mixed which may have resulted in uneven vertical mixing. Figure 5.1.al shows the temperature profile of the TC's on the SR side during the 4-min transient testing. These conditions did not include a large air flow, so the assist air on the combustion spray nozzle actually was flowing 6 L/min the entire time.

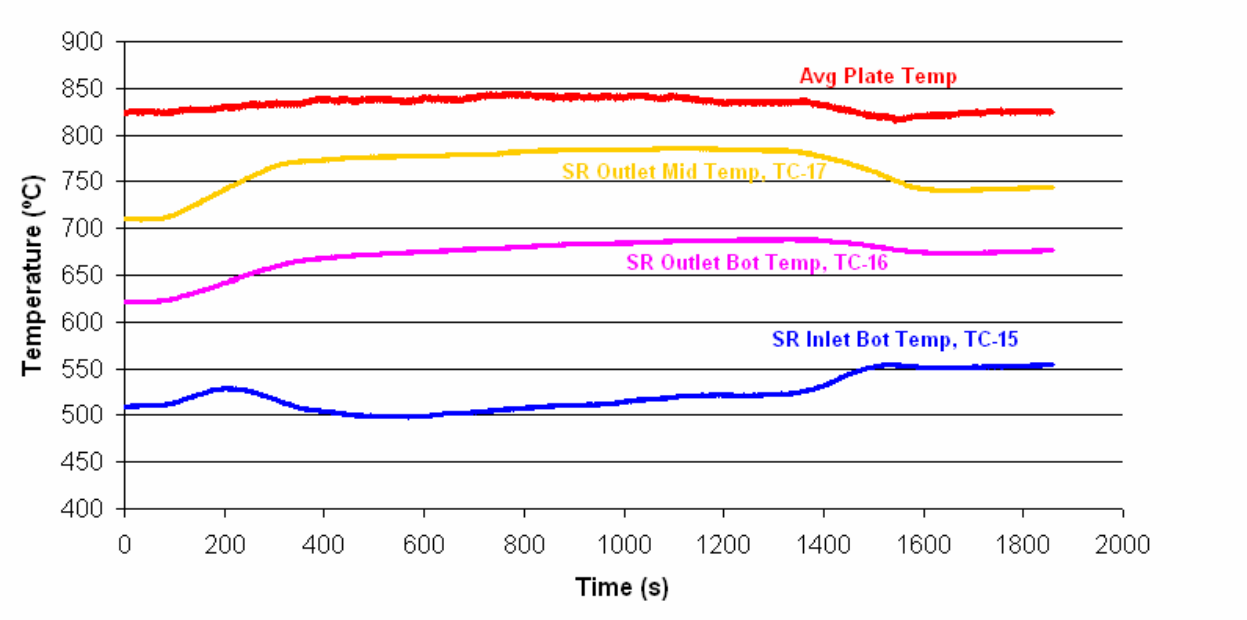

Figure 5.1.al. Temperature profile of TC's on the SR side during 4-min transients.

When Figures 5.1.ak and 5.1.al are compared, it is evident that the temperature profiles on the SR side were different between these two different tests. The inlet temperature on the bottom side is clearly the lowest temperature during the 4-min transients, as to be expected since there was no high air flow generating a high system pressure, allowing the fuel nozzle to behave normally. However, the inlet temperature on the bottom side is strangely the highest temperature during the rapid start-up test. Uneven vertical mixing due to insufficient atomizing air flowing through the spray nozzle could explain this observation.

Table 5.1.j shows that the operating conditions for AGT-1 resulted in an adiabatic gas temperature of 1338°C. Conditions for AGT-2 resulted in a gas temperature of 1193°C. Both of these temperatures are too high for the safe operation of the plate reactor. Unfortunately, the adiabatic gas temperature for the rapid start-up case of AGT-1 was not verified before the rapid start-up test on AGT-2. And since AGT-1 already had holes that allowed the nitrogen purge on the reforming side to flow into the combustion side, it was difficult to conclude from studying the combustion side plate temperatures that a phi of 0.38 was inappropriate. It was only after the combustion and reforming sides of

AGT-2 were no longer able to maintain the same differential pressure that we suspected a phi of 0.38 was inappropriate. Figure 5.1.am shows the change in pressures between the combustion and reforming sides of the plate reactor.

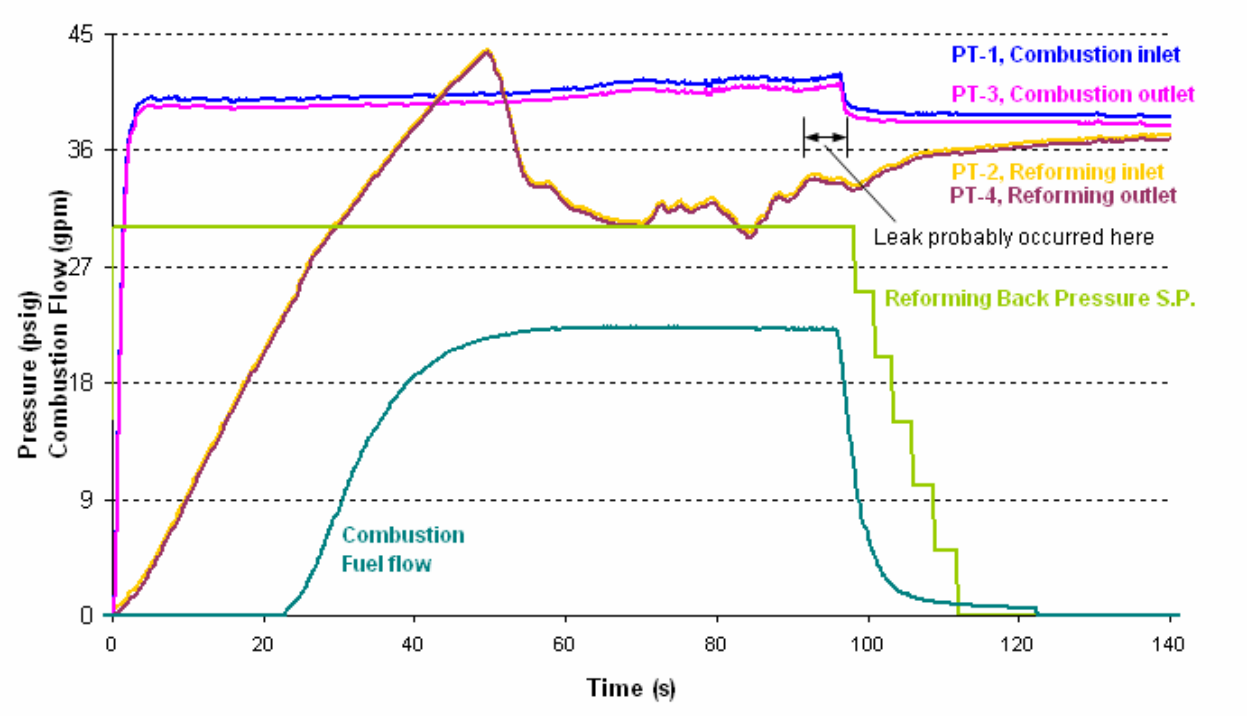

Figure 5.1.am. Pressure profile on combustion and steam reforming sides.

The inability of the reactor to hold different pressures on the combustion and steam reforming sides suggests that there was some type of damage that resulted in a leak. Figure 5.1.am illustrates a leak most likely occurred somewhere between 90 and 100 s, based on when the pressure on the reforming side started to climb to meet the pressure on the combustion side. The first overshoot in pressure at 45 s was most likely due to a slow response time of the back pressure regulator's PID control, not to a leak. The set-point of the back pressure regulator eventually dropped to 0 psig within seconds after the shutdown sequence was triggered, but the pressure data on Figure 5.1.am indicate that the pressure on the steam reforming side continued to climb towards the pressure on the combustion side. Even a slow response from the back pressure regulator would not increase pressure unless flowrate on the steam reforming side increased, which it did not. This suggests that the combustion side gases, which included the high air flow, were bleeding over into the steam reforming side.

A disappointing conclusion that can be drawn from this analysis is that the rapid start-up time that had previously been assumed to be correct, 70 s, was actually not representative of how long it takes to safely start-up up AGT-1. This time would be accurate only if it were possible to operate the plate reactor at 1337°C, which it is not. The fuel injection system was different on AGT-1 and did not require atomizing air. The air/fuel mixture was most likely well-mixed during the AGT-1 test. Assuming a well-mixed air/fuel combustion mixture, phi should not exceed 0.19 in order to maintain an

adiabatic temperature below 900°C. This results in a flow rate of 13.5 g/min of fuel, when using the maximum amount of air the system can provide, roughly 830 L/min (STP). This fuel flowrate is only 59% of the original amount tested in AGT-1. It is unclear exactly how much longer the rapid start-up time will be due to this required reduction in fuel flowrate.

5.2 Custom Stamped Plate Design

The lessons learned with the AGT prototype, made using sections of existing commercial plates, emphasized the need to produce custom stamped plates which would help optimize many of the functional characteristics of the finished unit such as optimizing dimensions to minimize heat losses and thermal mass in order to achieve rapid start-up requirements. The design team took into consideration the manufacture feasibility of the unit and the need to eliminate flow bypass of the reactants that occurred in the AGT design. The new reactors' names share the letters "SP" which stand for "Stamped Plates".

After reviewing different design ideas, two ideas were selected as the most promising. The team decided to build the two different designs in parallel; one prototype built with framed plates (SP-1) to help over-come welding challenges and the other prototype built frameless to achieve less total mass (SP-2). Some technical challenges encountered during the construction related to welding thin foil and frames instigated the need to add a modified version of SP-1, built with thicker plates and thinner frames, and it was named "SP-1b". Table 5.2.a summarizes some of the details for each of the prototypes.

Table 5.2.a. Characteristics of each of the prototypes designs.

Reactor ID	Stamped Foil Thickness	Corrugation height[2]	Frames Thickness	Key advantages
SP-1	0.002"	0.017"	0.008"	Most of the critical welding is done before calcination. Once the plates are coated and calcined, the only areas that need oxide removal before welding the plate stack together are the frames, not the foil.
SP-1b	0.005"	0.015"	0.005"	Similar reactor as SP-1; a thicker foil gives a more robust plate to work with. Thinner frame of the same material as the foil.
SP-2	0.002"	0.017"	Frameless	Thermal mass of SP-2 is 55% of SP-1 thermal mass

Dimensioning of the Plate Reactor: The dimensioning of the individual plates for the plate reactor is a critical issue. Several factors had to be considered such as flow distribution which is affected by pressure drop across the plates, sphericity of the stack

[2] Corrugation height is defined as the valley to peak vertical distance.

(or its surface to volume ratio) which affects overall heat loss, weight hourly space velocity, activity of the catalyst, number of plates, catalyst loading density, corrugation height, fabrication limitations from the plate manufacturers, and weldability. During the calculations, the assumption was made that SR-18 was the catalyst formulation to use in the next prototypes. A careful study was conducted to balance the various factors and final characteristics for both designs were adopted. Table 5.2.b summarizes these characteristics.

Table 5.2.b. Steam reforming prototypes designs: dimensions and key performances.

	unit	SP-1	SP-2
Catalyst-coated length	cm	19.3	20.0
Catalyst-coated width	cm	4.0	4.0
Corrugation height	mm	0.432	0.432
Number of plates	plates/kW(e)	10.7	13.0
Plate stack thickness	cm/kW(e)	0.45	0.57
Power density volumetric (reactor only)	mL/kW(e)	49.4	70.7
Power density massic (reactor only)	g/kW(e)	77.9	27.9

5.2.1 SP-1 and SP-1b designs

Some test trials were performed to demonstrate the technical feasibility of stamping and welding the custom made plates. After several trials and adjustments, D-Velco successfully stamped the plates and sent them to CESI for catalyst deposition tests. A picture of the stamped foil for SP-1 is shown in Figure 5.2.1.

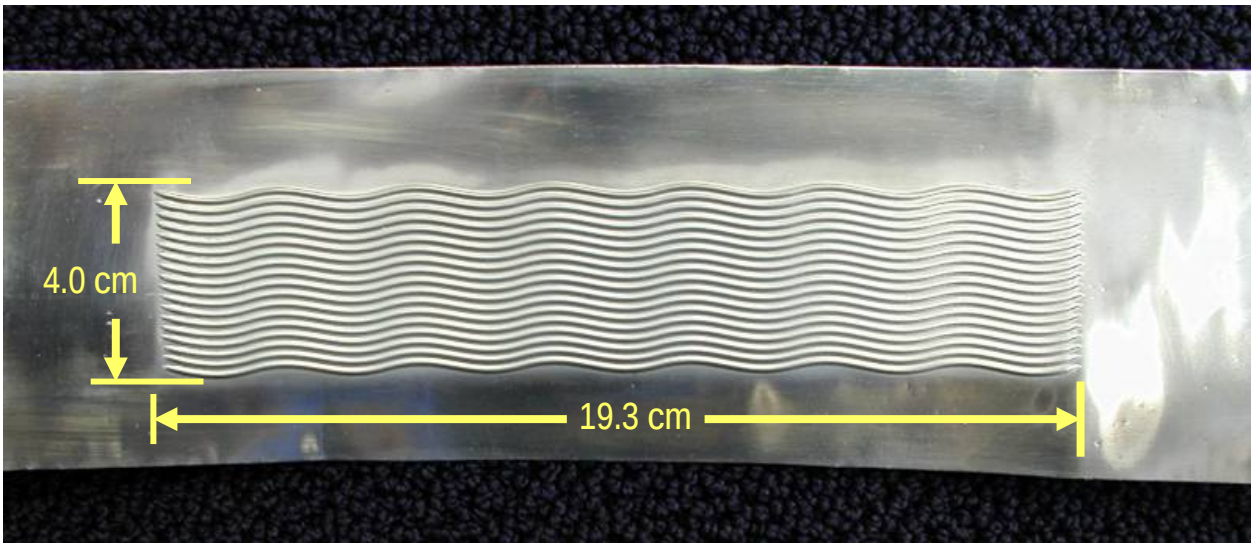

Figure 5.2.1. SP-1 stamped foil.

With the plates in house, CESI contacted Applied Lasers to perform several laser welding trials using the stamped plates and frame material. Once they fine tuned their system, they fabricated two “pillows.” Both welded assemblies past the leak test. Based on the success of these welding trials, the team decided to proceed with the TWD and

continue using Applied Lasers for the assembly of SP-1. Figure 5.2.2 shows one of the finished pillow assemblies.

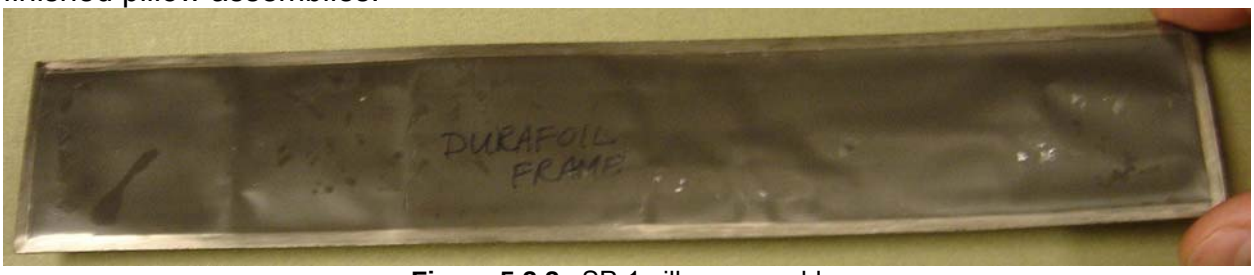

Figure 5.2.2. SP-1 pillow assembly.

The overall design of the SP-1 and SP-1b reactors was finalized, ensuring that the inlet and outlet connections of the unit would match the existing test system used on AGT. Ideally, once the fabrication of the reactor was completed, it could simply replace the exiting AGT reactor location and be ready to test.

As explained before, the experimental test unit is automatically controlled by LabVIEW, and the most critical input value to achieve good control is the temperature of the plates during the reaction. Therefore having thermocouples strategically installed at several sections in the catalytic zone of the plate stack is a key element for the successful operation of the reactor. Therefore, special thermocouple ports were designed into the plate reactor housing to allow the plate reactor to be properly instrumented. A solid-model view of the components of the SP-1 and SP-1b reactors, dimensions and the direction of the flows are shown in Figure 5.2.3.

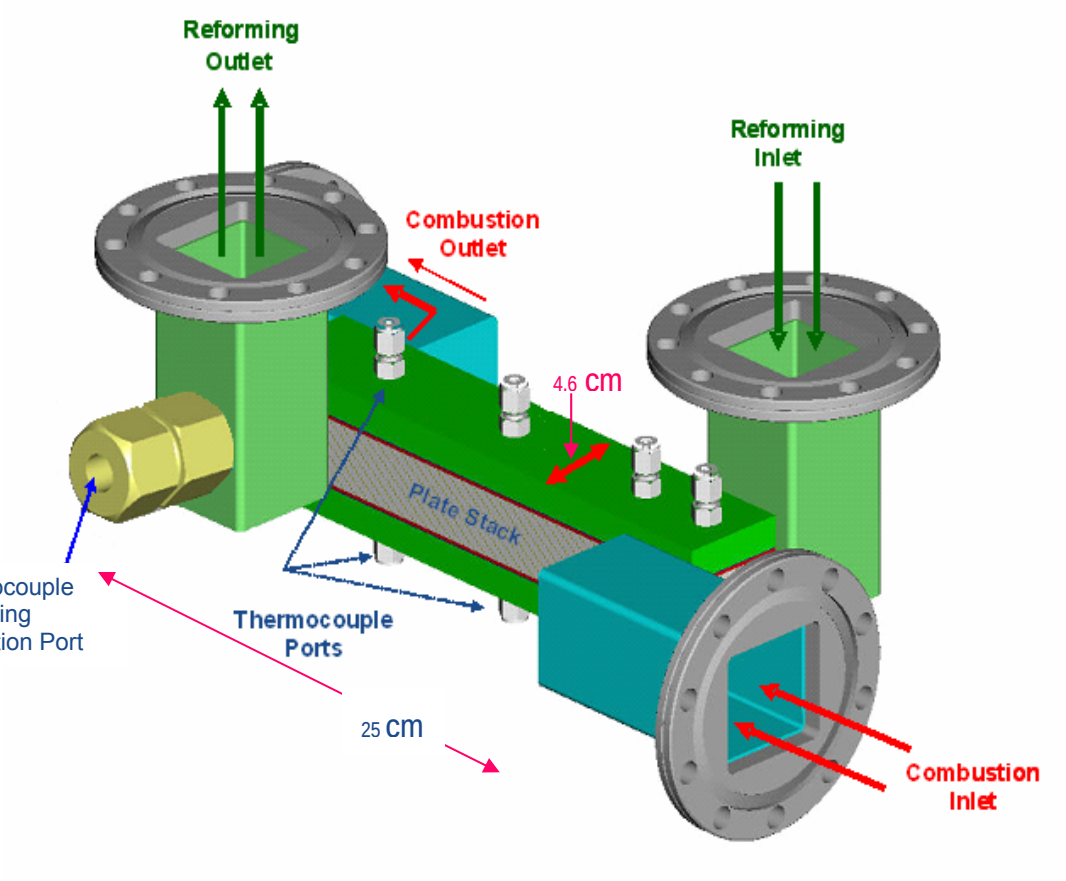

Figure 5.2.3. SP-1 reactor design.

Square channels rather than regular round tubing were selected for the inlet and outlet manifolds to facilitate the welding of flat to flat rather than round to flat surfaces. Flow path of the reactants as they enter into the openings created when assembling the plate stack together are represented in Figure 5.2.4.

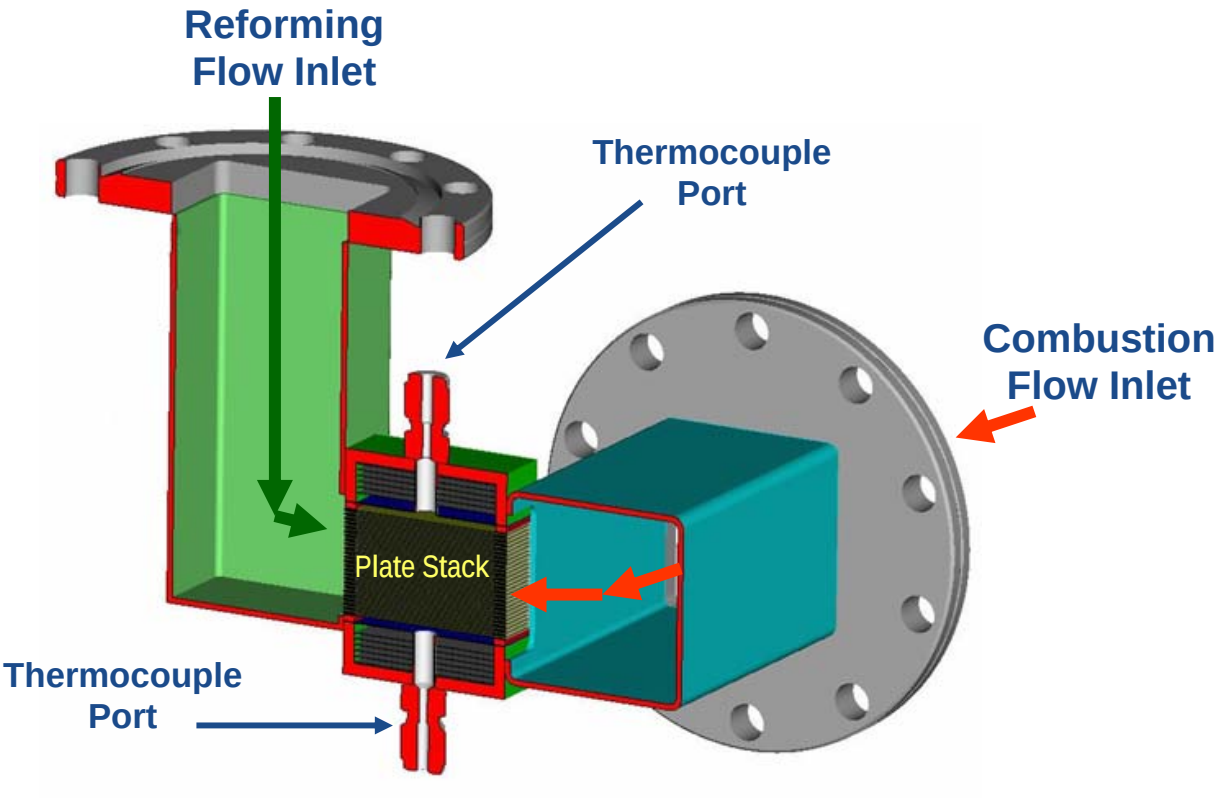

Figure 5.2.4. SP-1 reactor inlet manifold.

Once the design was finalized, Applied Lasers proceeded to laser cut the stamped corrugated foil to the final dimensions of the plate. They also started welding the frames onto the plates to form two different plate genders (A & B). The two genders ensure that when the plates are stuck-up together, the corrugation pattern does not mesh. Figure 5.2.5 shows the location of the frames on the plates.

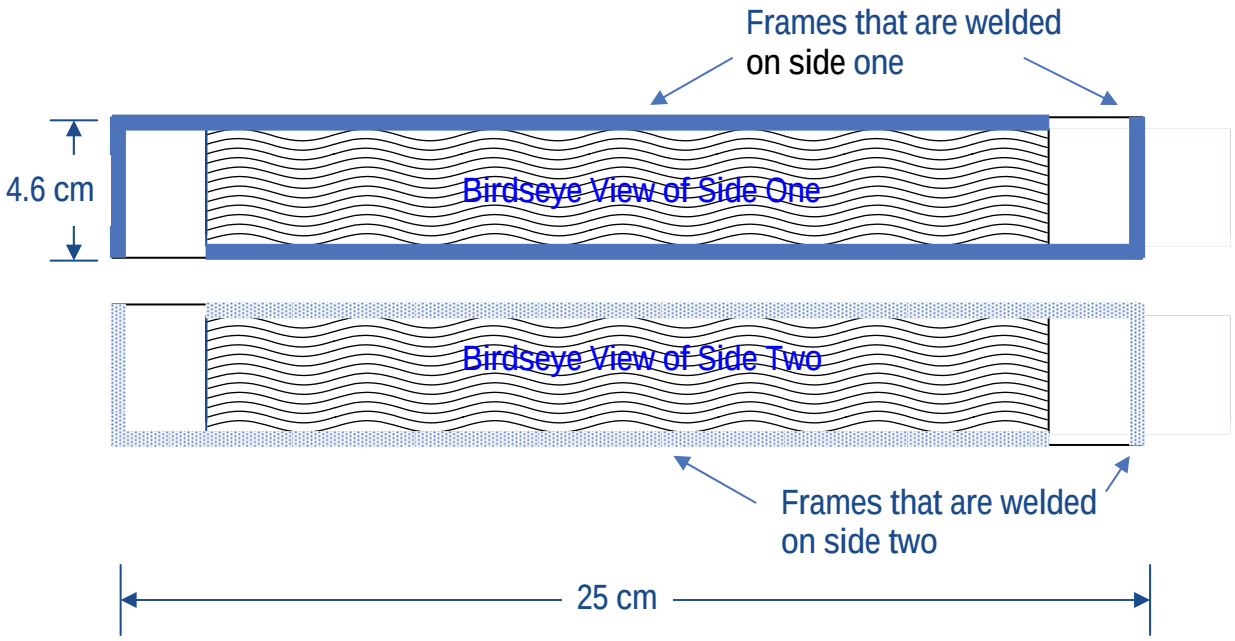

Figure 5.2.5. SP-1 plate: location of the frames.

Once the SP-1 plates and frames were welded together, they were sent to CESI to start catalyst application. This procedure includes several high temperature calcinations which cause the formation of an oxide layer on all areas of the framed plates. As discussed earlier, the oxide layer must be complete removed completely from the frame edges in order for the welding process to be successful. A picture of a completed framed stamped plate including catalyst coatings is shown in Figure 5.2.6.

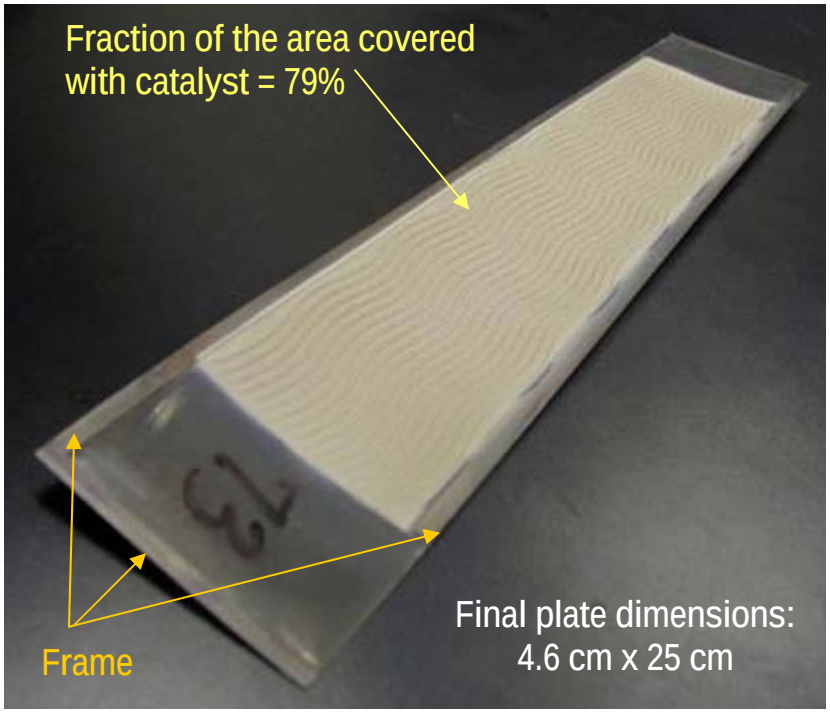

Figure 5.2.6. SP-1 plate coated with reforming catalyst.

A series of oxide removal techniques were tested, some of them abrasive, such as sandpaper, diamond dust hand lap, sand blasting and fiber pads; others include the use of chemicals like acid solutions, solvents and several polishing agents. The most successful cleaning technique was a combined usage of sandpaper, diamond pad and fiber pad.

The cleaned plates were sent to Applied Lasers to start the assembly. They started by successfully assembling a 6 plate stack and a 4 plate stack. The problems started when they tried to weld the two stacks together to form a 10 plate unit. The welders reported that the welding process created some rigidity on the plate stacks that prevented them to securing the two stacks together.

Applied Laser investigated the issues with the welding process. Applied Lasers cut plates and frames out of calcined and uncalcined material and proceeded to test their welding technique. The two samples tried are shown on Figure 5.2.7; one was put together with uncalcined foils and uncalcined frames, to test if the poor results obtained were caused by the nature of the setup or the material. The other stack was built with calcined foils and uncalcined frames. The welding of the uncalcined sample resulted in a clean weld whereas the calcined foil and uncalcined frames resulted in several gaps and pin holes along the welds.

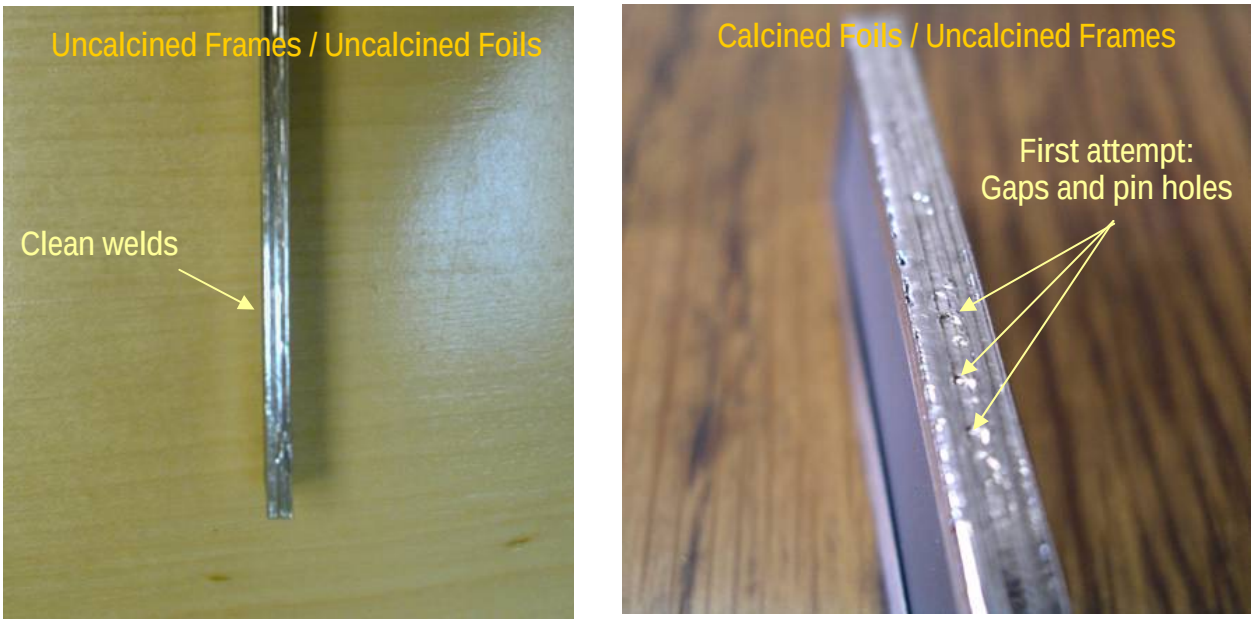

Figure 5.2.7. SP-1 plate welding process tests.

Additional trials determined that the best procedure to use for building the plate stack, is to spot weld uncalcined frames to the calcined catalytic plates, form the plate stack by lining up genders A & B and clamp them all together. Once all the plates and frames are in place, the edges of the stack are milled in order to remove oxide and create a smooth surface. The new surface is then welded using a wide laser beam, capable of welding 4 sets of plates together in one pass. This technique solved the previously encountered problem of rigidity, and also eliminated a significant number of gaps and pin holes. The 25 plate assembly shown in Figure 5.2.8 was built to prove the new successful procedure. Unfortunately, the welds were not 100% pin-hole free.

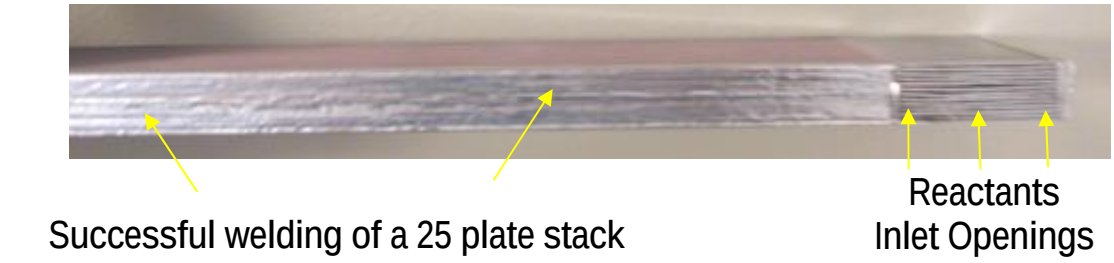

Figure 5.2.8. SP-1 25 plate assembly.

This last welding technique developed proved that even though the assembly of the SP-1 plate stack is challenging, it is feasible. The development of unconventional techniques involves a certain amount of trials, time and expanse. The key to developing this technique is finding the right services provider, in this case a welding company that is willing to work on R&D projects.

5.2.2 SP-2 design

The need of developing a plate reactor prototype capable of rapid startup directed the team to consider into new designs and new methods of fabrication. The SP-2 reactor has a frameless plate stack. This characteristic makes it the ideal reactor configuration because based on the structural analysis completed at the beginning of the program, the absence of frames makes it less susceptible to localized stress. The overall design of the SP-2 gasoline reformer reactor is shown on Figure 5.2.9.

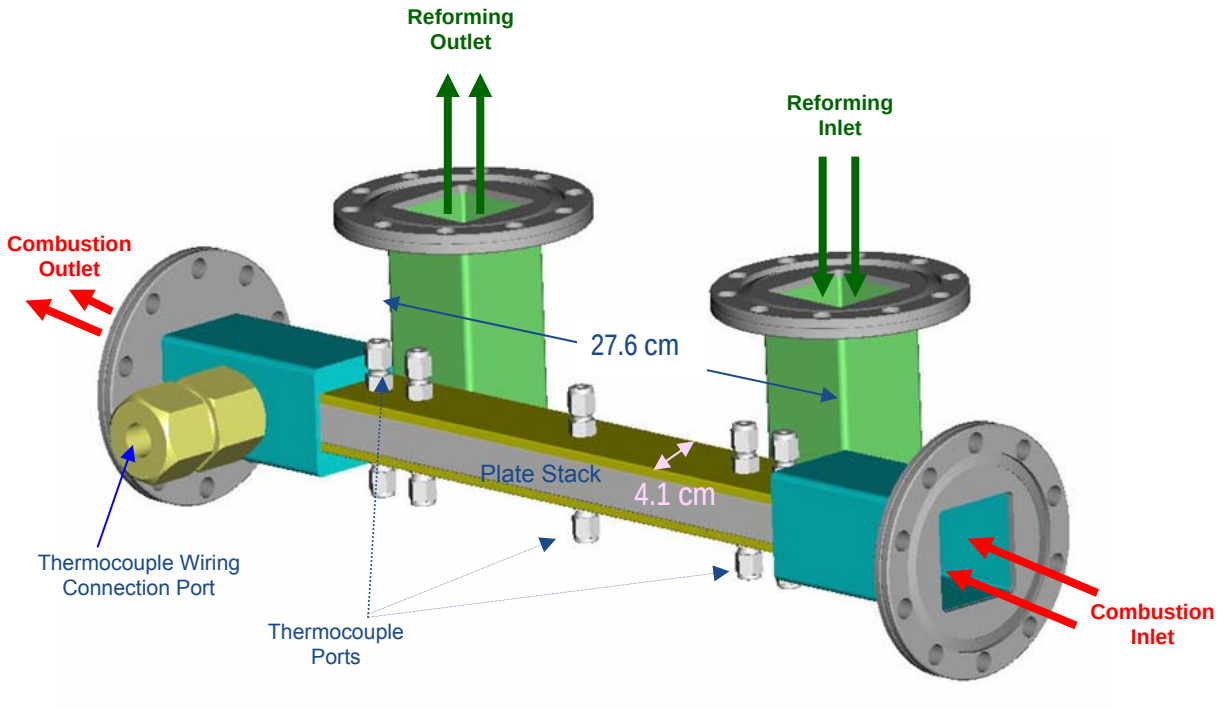

Figure 5.2.9. SP-2 reactor design.

A custom made stamped plate was designed and manufactured. The shape of the plate is designed in such a manner that when the plates are stacked together, they form a flow path for the reactants to enter the reforming and combustion reaction zones. A drawing of a SP-2 plate is shown on Figure 5.2.10.

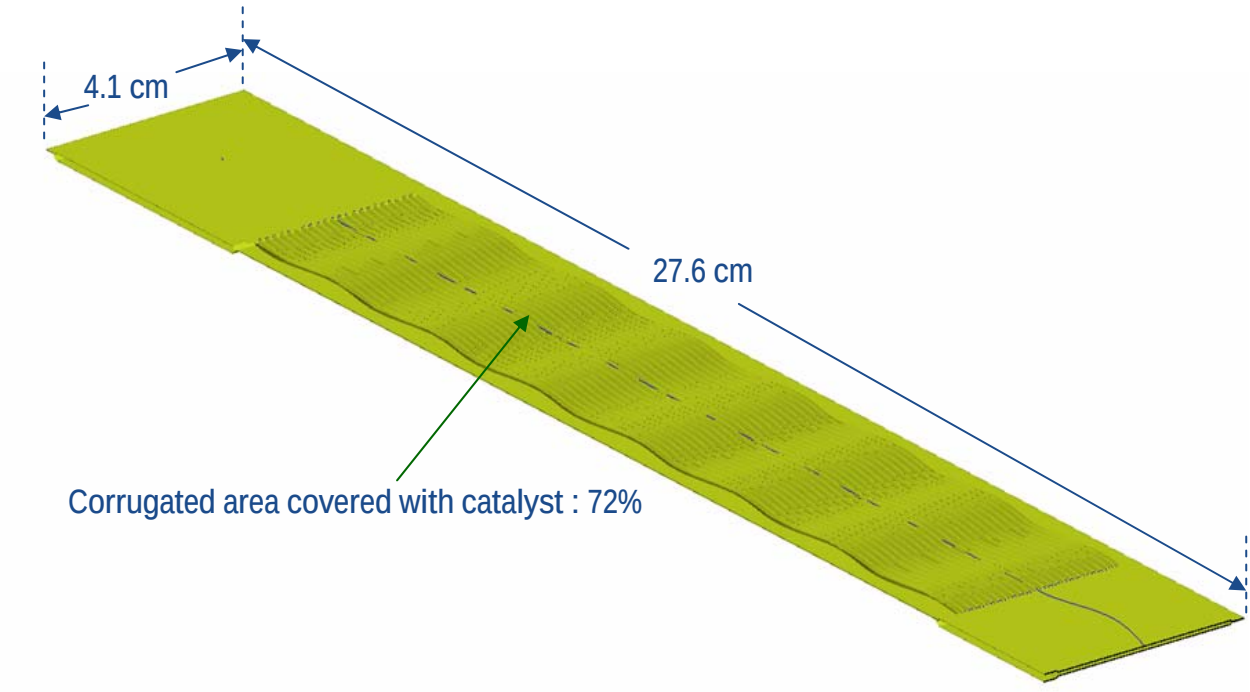

Figure 5.2.10. SP-2 plate.

The close-up view of the plate stack for SP-2 presented in Figure 5.2.11 shows the cavities formed after the custom stamped plates are assembled together, that are used to manifold the inlets and outlets to the reactor:

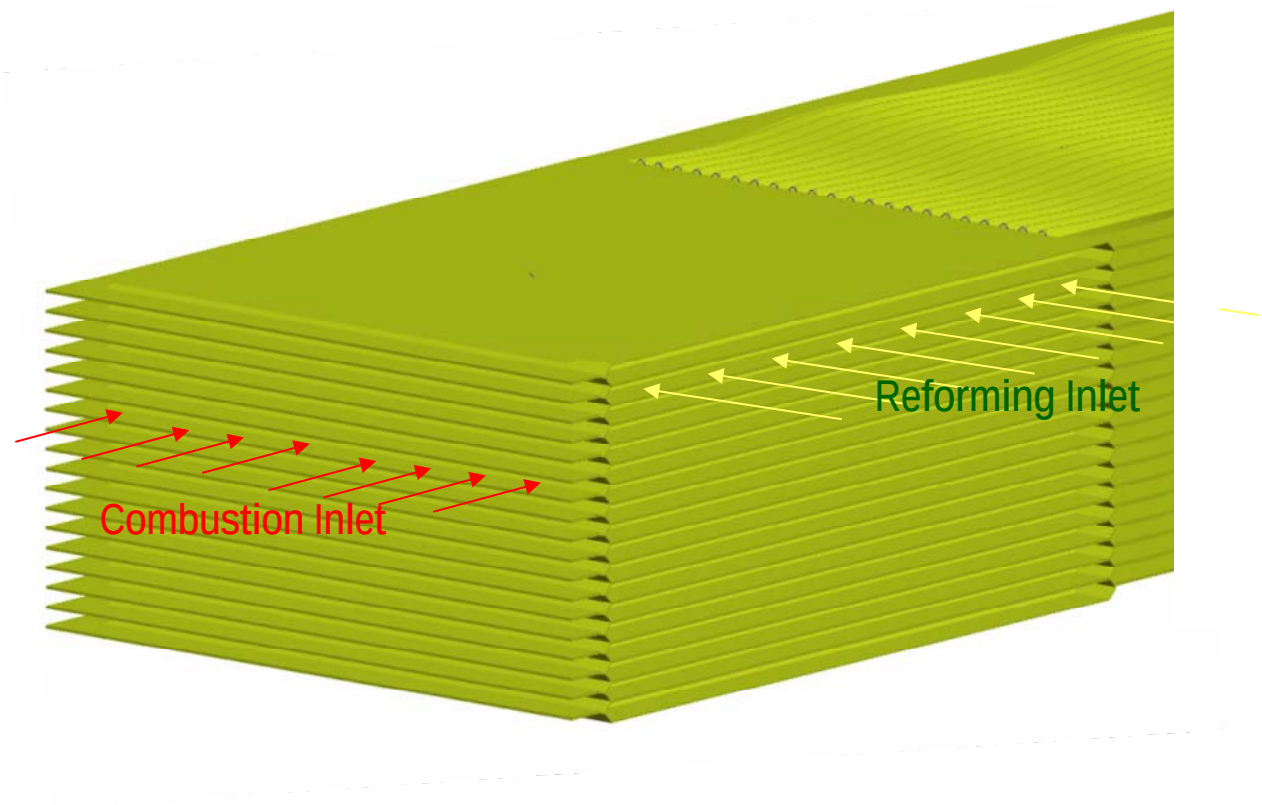

Figure 5.2.11. SP-2 plate stack: manifold system.

This ideal plate stack configuration came with a cost: the welding challenges became more complicated than the welders anticipated, and required extra work, expense and running changes in the stack design. Even though initial laser welding trials proved that the construction of this prototype was feasible, the laser welders required complete removal of the oxide layer. In order to accomplish this, CESI outsourced to professionally polishing company to clean the edges of the plates, using a proprietary technique. This oxide removing technique ended up not only removing the oxide, but a significant part of the foil as well, leaving the cleaned edges of the 0.002" foil, at a thickness of ~ 0.0015".

When the pieces were returned to the welders to start he assembly, they encountered another problem: the cleaned foils were so thin that the laser beam was breaking through the plates rather than welding the two plates together. The welder recommended the addition of extra material to the thinned areas to absorb part of the heat and reduce the likelihood of the laser beam breaking though the foil. CESI along with the welding specialists came up with the appropriate size of the add-on material that is shown in Figure 5.2.12.

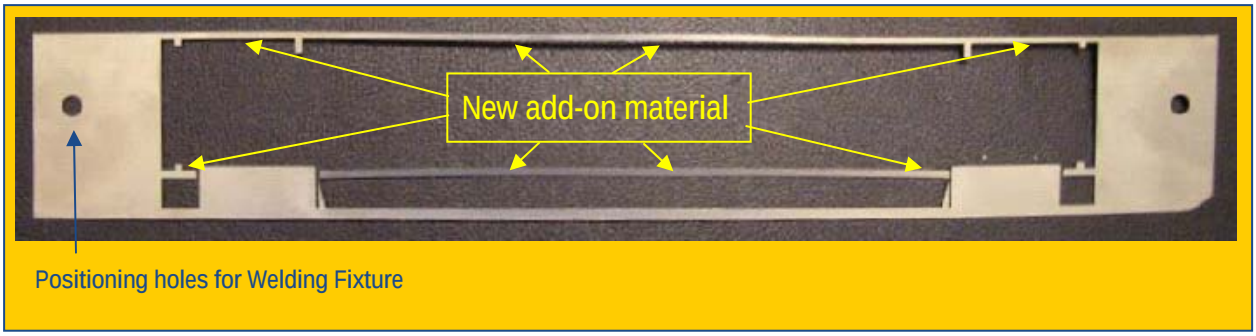

Figure 5.2.12. Added frame for SP-2 plates.

Figure 5.2.13 shows the finished plate pairs welded using this new added frame. This extra material resulted in successful welds, but added unwanted thermal mass (the reactor mass was increased by 117% from its original frameless configuration). The increased thermal mass would obviously result in a longer start-up time of the reactor and increasing the localizes stresses.

Figure 5.2.13. SP-2 plate with added frame.

The other welding challenge for SP-2 was the area of the plate stack where the foils form groves for the reforming reactants to enter and exit the reactor. As with the rest of the welded sections in the reactor, the reforming side must be completely isolated from the combustion side. The manifold area is especially critical because the shape of the foil and the immediate proximity to the combustion versus reforming manifold makes the welding difficult. Because of the problem that arose from thinner foil resulted from the cleaning process, a special insert (“gapper”) had to be designed and fabricated to provide the additional mass necessary to achieve an acceptable weld. Drawing of Figure 5.2.14 shows an exploded view of the area, and the shape and position of the insert needed to weld and seal all around it. Unfortunately, there was insufficient time and resources to complete a prototype using this process.

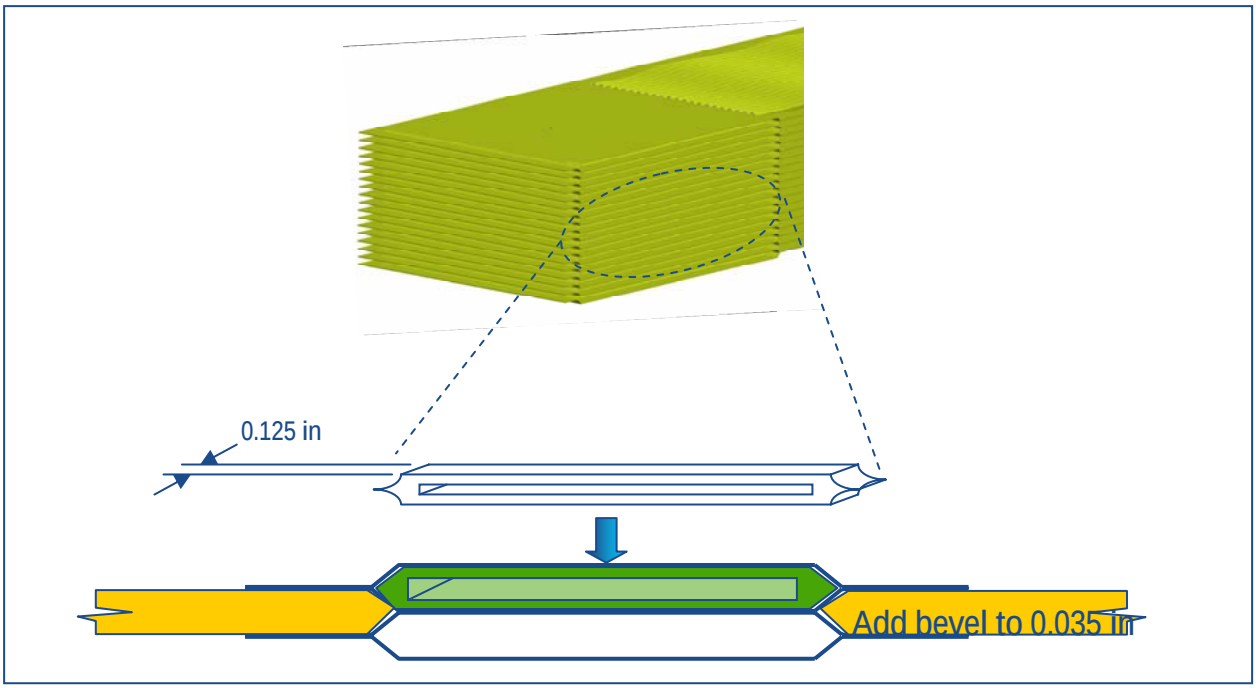

Figure 5.2.14. SP-2 manifold area with added "gapper" material.

With the changes that SP-2 had to go through in order to achieve welding the plate stack, the final design became a hybrid of AGT-2 and SP-1. With the added frames, SP-2 resulted in a plate stack with 20% more thermal mass than SP-1.

6 Market assessment

At the beginning of the program, UC Irvine's National Fuel Cell Research Center (NFCRC) was subcontracted to evaluate the potential market for a fuel processor system for the production of a hydrogen-containing stream for use in PEM fuel cells. The most significant finding of the study is the key role that fuel processing will play in the potential acceleration of fuel cell vehicle introduction into the marketplace at competitive prices. This scenario involves the development of superior fuel processing technology, enabling of the use of fuel cell technology together with current fueling infrastructure, early introduction of fuel cell technology into consumers' hands, and the introduction of hydrogen technologies facilitating the long-term development of the hydrogen economy. Thus, fuel processing technology will potentially accelerate fuel cell market entry and penetration leading to an increased incentive to develop H_2 infrastructure and establishing a potential long-term market for superior fuel processing technology within the H_2 economy.

The early introduction of fuel cell technology in the automotive sector will likely be accomplished by early introduction into the auxiliary power unit (APU) market in both long-haul trucks and passenger automobiles. This introduction will facilitate cost reduction of fuel cell technology as well as address the primary policy and regulatory hurdles facing the introduction of fuel cell technology into the automotive sector. This will offer the consumers the opportunity to grow comfortable with fuel cell technology

and begin to offer them the additional features and capabilities that fuel cell technology can offer (design flexibility, longer range, lower emissions, additional power and electrical features, etc.).

The plate-based fuel processing technology could also play a key role as a stationary power fuel processor (especially in developing countries where fuel infrastructure is scarce and the need for new installed power generating capacity is greatest). The need for CESI's fuel processing technology could be significant regardless of fuel cell type. Both PEMFC and solid oxide fuel cells (SOFC) will continue to require some type of fuel processor for cost effective early introduction to the marketplace (until there is a significant penetration of the hydrogen economy – perhaps 50-100 years off). These fuel processors will likely require significant integration with the fuel cell itself, leading to the need for CESI to work closely with fuel cell and fuel cell systems integrators in this near-term application area. The key factor to the success of CESI's fuel processor technology in this market sector is low life cycle cost. Additional factors include fuel flexibility, high efficiency, low emissions, low maintenance, and compact size.

NFCRC's analysis relied upon the prevalent industrial trends and infrastructure investment patterns that, although politically sensitive, forecast a longer schedule and more modest penetration rates than previously held. No major automotive or truck manufacturer can wager against fuel cells' eventual emergence, but the major automotive companies are consistently softening their time frames with public projections that, "mass-produced, affordable fuel cell vehicles are not expected to be available until at least 2010".[3] The current Administration and Congress' position on Corporate Average Fuel Economy (CAFE) standards decelerates rather than accelerates the urgency for fuel cells' introduction into the marketplace. The single greatest motivator for the transportation sector to maintain an aggressive fuel cell R&D fuel cell program is not regulation, government funding or fuel efficiency, but the potential for a single player, most notably Toyota, to make an unanticipated earlier and greater breakthrough.

7 Conclusions / Future direction

In this program, CESI took the initial steam reforming plate-reactor concept and advanced it towards an integrated fuel processing system. A substantial amount of modeling was performed to guide the catalyst development and prototype hardware design and fabrication efforts. The plate-reactor mechanical design was studied in detail to establish design guidelines which would help the plate reactor survive the stresses of repeated thermal cycles (from start-ups and shut-downs). Integrated system performance modeling was performed to predict system efficiencies and determine the parameters with the most significant impact on efficiency. In support of the system modeling, a single channel plate reactor model was created to better understand the intricacies of the steam-reforming plate reactor.

[3] Associated Press, "GM Presents Gas-Fed Fuel Cell Vehicle", May 1, 2002.

In conjunction with the modeling effort, a significant effort was directed towards catalyst development. CESI developed a highly active, sulfur tolerant, coke resistant, precious metal based reforming catalyst. CESI also developed its own non-precious metal based water-gas shift catalyst and demonstrated the catalyst's durability over several thousands of hours of testing. CESI also developed a unique preferential oxidation catalyst capable of reducing 1% CO to < 10 ppm CO over a 35°C operating window through a single pass plate-based reactor.

Finally, CESI combined the modeling results and steam reforming catalyst development efforts into prototype hardware. The first generation 3kW(e) prototype was fabricated from existing heat-exchanger plates to expedite the fabrication process. This prototype demonstrated steady state operation ranging from 5 to 100% load conditions. The prototype also demonstrated a 20:1 turndown ratio, 10:1 load transient operation and rapid start-up capability. Unfortunately, the prototype was not 100% effective in reforming the feed fuel. This was the result of pressure seals inherent to the plate's corrugation design. Furthermore, the plates 0.008" thick material limited its rapid start-up time potential.

To address the short-comings of the first generation prototype, CESI embarked on the design and fabrication of several second generation prototypes. These prototypes incorporated custom stamped plates and thinner 0.002" material. Having the second generation prototypes fabricated became a significant issue. The contracted vendors underestimated the difficulties in the final assembly process. New obstacles were encountered which resulted in repeated delays. CESI and DOE agreed that it was unlikely that the next generation prototypes could be fabricated and tested within the time and budget constraints of the contract. Therefore, it was mutually agreed to forgo the next generation fabrication/testing and simply close-out the program within 90-days of the contract expiration date of September 30, 2005.

If the resources were available for future development, CESI would consider an alternative plate reactor assembly process. The process that was developed for the generation 1 and 2 prototypes coated the plates *before* assembling the plate stack. An alternative process would involve coating the plates *after* assembling the plate stack. This would address many of the welding issues but create new issues in the catalyst coating process.